School of Civil, Environmental and Land Management Engineering

Master Degree in Civil Engineering – Structures

April 19, 2018

Analysis Of Submerged Floating Tunnel Resting On Flexible Soil Strata Subjected To Seaquake Excitation

Supervisor:

Prof. Luca Martinelli

Authors:

Sara Canziani 863167

Monica Pirozzi 872288

Contents

List of tables

List of Figures

List of Symbols

Greek letters

α	Coefficient of mass matrix
α_c	Parameter controlling coherence decay
β	Coefficient of stiffness matrix
β_t	Ratio of the amplitude envelope at t_{max}
γ	Coherency function
η	Deterministic envelope function
ζ_1	First damping ratio
ζ_2	Second damping ratio
ζ	Damping ratio
ζ_g	Ground damping
ζ_f	Filter damping
ξ_d	Horizontal separation distance
$\xi_d{}^L$	Projected horizontal distance
ρ	Water density
Γ	Fourier transform of the coherency function
φ	Random phase angles
ϕ	Velocity potential function of incident wave

w_1	First selected natural frequency
w_2	Second selected natural frequency
w_g	Ground frequency
w_f	Filter frequency
w	Circular frequency

Latin letters

A	Section area
c	Acoustic compressible wave velocity in water
C_D	Drag coefficient
C_M	Inertia coefficient
C_a	Added mass coefficient
$[C]$	Damping matrix
d	Depth of water;
D	Cylinder diameter
$E[\dot{x}^2]$	Mean square of the derivative of the process
g	Gravity acceleration
$(g),(s),(h)$	Superscript denoting respectively ground, structural and hydrodynamic contributions

$f(t,x)$	Time history
(f)	Subscript indicating free-field motion
f	Morison force
f_{water}	Wave resonance frequency
k	Wave number
$[K]$	Stiffness matrix
m_{add}	Added mass
$[M]$	Mass matrix
n	Numbers of resonance frequencies
p	Peak factor
Q	Generalized components of external loads vector
q	Displacements
R	Generalized non-linear restoring forces vector
S_0	Scale factor
$S_{CP}(w)$	Normalized Clough-Penzien spectrum
S	PSD
S_{max}	Peak value of the spectrum
s, c	Subscript indicating structural nodes and the ground-structure interface
t_{max}	Equivalent duration of the process
t_1, t_2	Ramp duration and decay starting time
$\dot{x}$	Structure move velocity

$\ddot{x}$	Structure move acceleration
$U_g(t)$	Vertical ground displacement at the sea bed
u	Water particle velocity
$\dot{u}$	Water particle acceleration;
$u - \dot{x}$	Relative velocity
$\dot{u} - \ddot{x}$	Relative acceleration
v_s	Shear wave velocity
v_{app}	Surface apparent velocity of wave
V	Section volume
$\text{var}[x]$	Variance (total power) of the process having PSD
w_{water}	Wave resonance circular frequency
z	Calculating structure location

List of Abbreviations

Submerged Floating Tunnels (SFTs)

The International Tunnel Association (ITA)

The Sino-Italian Joint Laboratory of Archimedes Bridges (SIJLAB)

Finite element (FE)

Bar finite element approach (NWB)

Co-rotational approach (CR)

Peak ground acceleration PGA

Soil structure interaction (SSI)

Power spectral density (PSD)

Fast Fourier Transformation (FFT)

Cross-power spectral density (CPSD)

Frequency-wave –number spectrum (F-K spectrum)

INTRODUCTION

Engineering is a field of study that always tries to find new challenges to face.

In the Civil Engineering field, a challenge that has become popular is to cross deep-water straits or rivers of some kilometres in length with a single span bridge. Consider that the longest single span bridge ever constructed on earth is the Akashi Kaikyō Bridge situated in Japan, Kobe with a central span of 1991km (nearly 2 km).

'2 km' has become the new record to beat, but it is not just a matter of overcoming records, the necessity of crossing bigger spans without intermediate pillars is a necessity when the seabed is too far from the water surface and the distance to be crossed is too long, causing great conceptual and execution problems.

This is exactly the case of the Messina Strait, a piece of sea of minimum length of 3 km separating the two regions of Sicily and Calabria in Italy.

The tricky points, in this case, become two, which are strictly connected. First of all, the span of the bridge is over 1 km the maximum one ever constructed, and only this brings a lot of uncertainties and problems from the constructional point of view, besides economical aspects because a bridge of this length will have enormous costs due to the giant dimensions of the structural elements, to be constructed by special firms right on the spot or with large prefabricated pieces very difficult to move. The second aspect is the depth of the seabed, that, in some points is of nearly 300m, making impossible to realize a multi-span bridge.

At this point, the idea of the Submerged Floating Tunnel was introduced for the first time in the '80 as an economical and convenient means to solve these types of problems, i.e. very long crossings in deep waters with a ratio cost/length quite efficient.
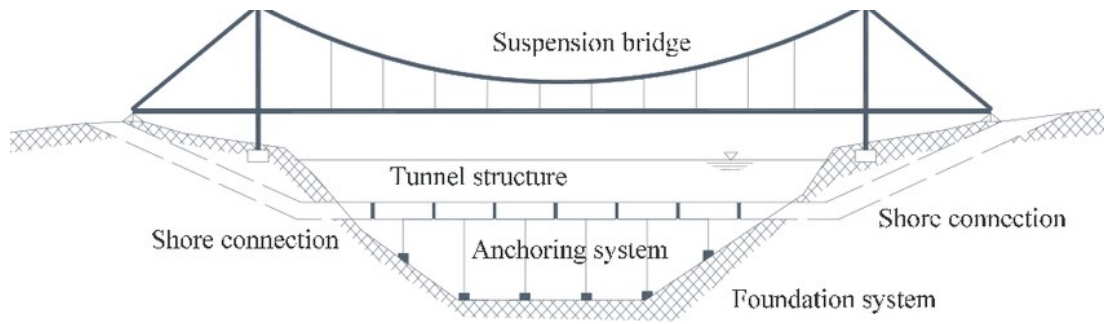
Figure 1 Typical Submerged Floating Tunnel and Suspension Bridge

The submerged floating structure is a new challenging idea still never realized that consists of a tunnel submerged in water and suspended in it or by floating islands at the sea surface or by anchoring bars at the seabed.

This type of structure is far away from the classical static structures since, being embebbed completely in water, it must exploit the effect of water, and so the Archimedes' Force, to be sustained and should face hydrodynamic effects of various kind in case of earthquake.

The point of this work of thesis will be exactly this one: to study a Submerged Floating Tunnel subjected to seaquake excitation, i.e. the effect of the shock waves generated in water by a seismic input at the seabed. We can well understand now that, in a seismic region like the South of Italy, this is a primary design action to be considered and the seism does not excite the structure directly but passing through the "filter" of water.

We will then also consider how the seismic signal is altered passing through different layers of flexible soil before reaching the supports of the structure.

So, this work of thesis will be essentially subdivided into two parts: one more theoretical, in which all equations and mathematical aspects, motivations and descriptions will be provided and a second part, we can say, much more practical, where the model of a real case study of an SFT over the Messina Strait will be presented, implemented and then analysed first under static loads and then in dynamical conditions under the excitations of earthquake and seaquake.

More in details we can say that:

1a) We will give a general technical explanation of what a submerged Floating Tunnel is, what are its historical developments and which are the various types of structures conceived up to this point.

1b) Then, we will focus on the seismic excitation, i.e. how to extend the given seismic input given in one point to a multiple support system, in order to be conveniently applied to the supports of our structure.

1c) Afterwards, we will introduce the concept of seaquake and its generation through the mathematical tools of transfer functions and Morison equation that enable us to transfer the seismic input from seabed to water and permitting a modelling of hydrodynamic seaquake forces on the tunnel.

Then we will apply all what we have seen above in a real analysis, i.e. we will implement a finite element model with the aid of the finite element software ANSYS. The models studied are two: first we will focus on a 2-D model of a single section of the tunnel, to have a model easily controllable and fast to analyse and then we will extend it to a 3-D model.

2a) So, in a first moment, we will test the goodness of our structural model under static conditions and determine the modes of vibration of the structure.

2b) In the end, we will apply the seismic and seaquake excitations in order to determine the response of the structure under these highly variable loads.

We hope you will enjoy this technical reading and we wish it will be of inspiration to you in order to produce new and interesting ideas for future developments of the problem.

Chapter 1: The Submerged Floating Tunnel (SFT): a new challenging infrastructure for crossing waterways

1.1 Introduction to SFTs

In modern civil engineering there are three conventional approaches to the solution of the water-crossing problem: bridges, underground tunnels and immersed tunnels. All of them are widely put into practice with mature design and construction technologies. Here, in this thesis, a challenging innovative structure, named Submerged Floating Tunnel (SFT) or Archimedes Bridge, is introduced as a promising alternative to cross sea-straits, lakes and waterways.
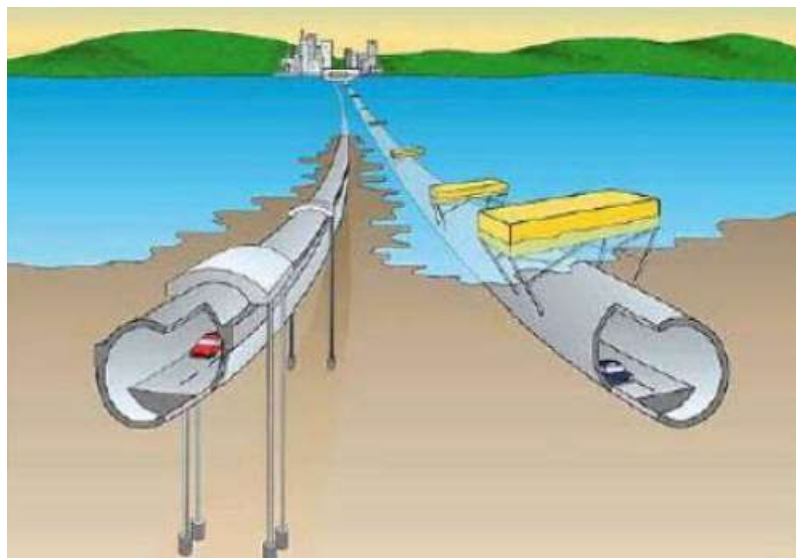
Figure 2 Example of a floating tunnel with different anchoring systems.

What are SFTs? A SFT, entirely immersed at some depth, serves all types of traffic by crossing a body of water between two shores. In most designs a circular cross section is adopted and the tunnel, subject to positive net buoyancy, is anchored at the seabed by suitable structural elements. The tunnel section is large enough to accommodate the road traffic and the related services. More generally SFTs can be fixed to the seabed, or to floating pontoons, by supporting structures spaced at intervals. Examples of these supporting structures, also called anchoring systems in this thesis,

are shown in Fig.2; they work in order to counteract the net buoyancy (Archimedes' force minus weight) and to limit the tunnel motion due to environmental and operational loads.
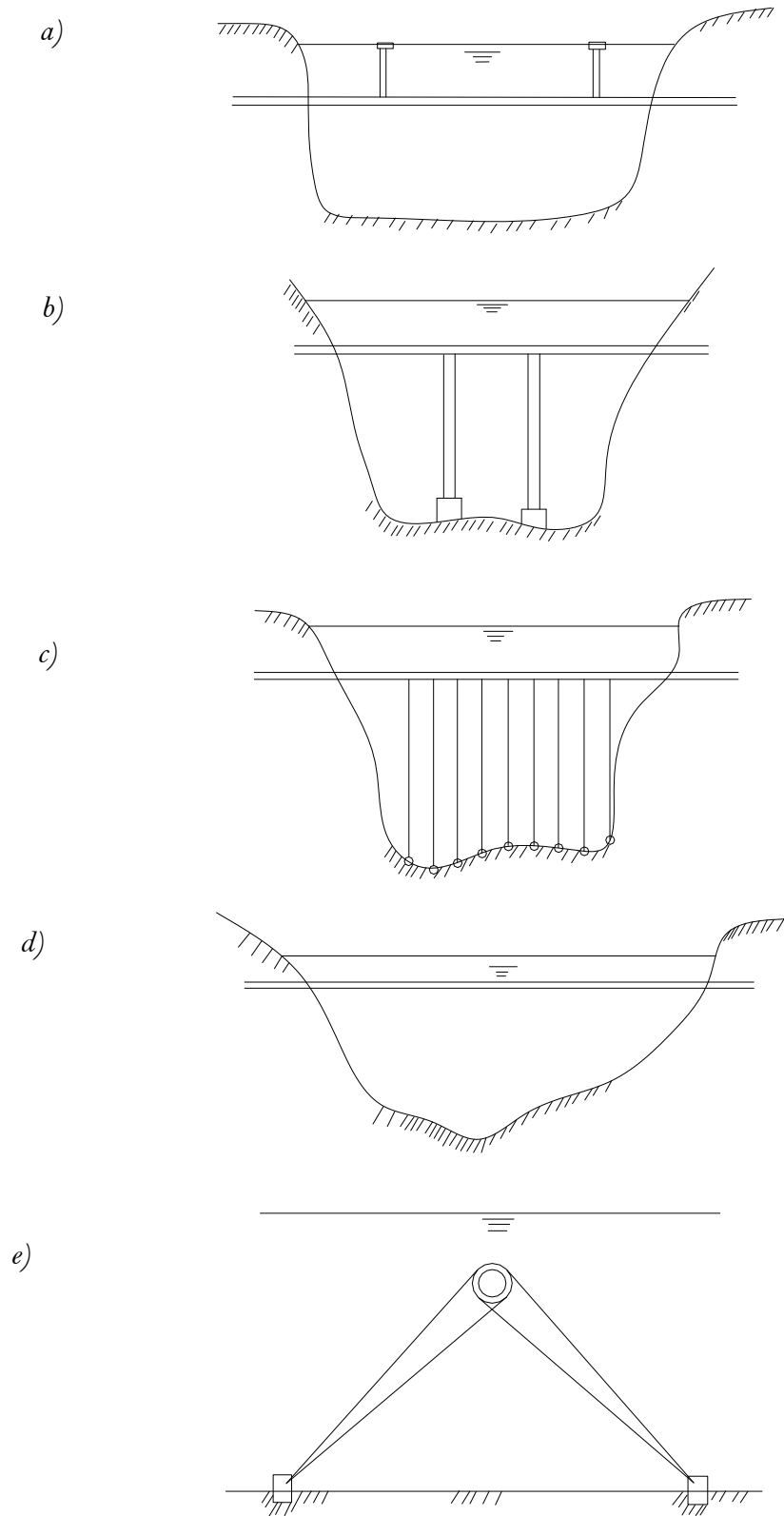
Figure 3 SFTs with different support systems: pontoons on the surface (a); columns to the seabed (b); tensioned anchoring bars/cables to the seabed (c); support at the abutments only (d); combinations of the above methods (e).

Analysis of SFT Resting on Flexible Soil Strata Subjected to Seaquake Excitation

SFTs are suitable for long distances and deep waters. The main conditions for its competitiveness are:

- where the water depth is larger than 50 m;
- where the crossing length is larger than 1 km;
- where the preservation of a scenic view or a natural habitat is considered highly important.

There are three main components in a Submerged Floating Tunnels:

- Tunnel body.

  It consists of one or several traffic lanes supported by a circular, elliptical or polygonal structural section; construction material is either steel, concrete or a composite combination. It is worth noting that the external diameter, and thus the volume, has a significant influence on the tunnel buoyancy.

- Anchoring system.

  Pontoons on the surface, columns or other support systems from the seabed, tensioned anchor bars or cables to the seabed, support at the abutments only or combinations of the above methods. In most research work, tension element anchoring has been the first choice. There are two types of tension anchoring elements: the cables and the bars, working as a tie connection between tunnel and sea ground. The differences between them are that the bars can bear some compressive load while the cables cannot; secondly hollow-section bars can reach a straight configuration under the combined action of weight and buoyancy (neutral condition), while the cables always show a catenary-type initial shape. Hollow sections are also efficient in terms of lateral stiffness; the steel material is suitable both for high strength requirements and for good resistance to fatigue. As to the cables, they have demonstrated high reliability in bridge and offshore engineering and can be easier to be put in operation. Tension resistance can be very high.

- Shore connections.

  They must satisfy two functional requirements; first, they must ensure water tightness to the joint between the floating tunnel and the onshore approaching tunnel. In structural term, the joint should be designed to allow

free longitudinal expansion and contraction to accommodate relative displacements between the two shores, with no vertical and transversal relative movements. The main problem for the shore connection is represented by longitudinal seismic actions; in fact, if one end is left axially free, large forces are imposed to the fixed end, also resulting in high axial forces in the tunnel section, which can be harmful for water tightness. In this work the adoption of elastic-plastic devices as longitudinal end-restraint elements has been considered, both for limiting the forces transmitted and for dissipating some of the kinetic energy developed in the tunnel. In a first design option the connection between the shore and the tunnel is left free, in axial direction, at one of the ends. At the other end a mechanical device is introduced, which should behave within the elastic range, showing high stiffness, when the axial force is smaller than the limit one. On the other hand, the device can suffer large plastic deformations when the tunnel axial force exceeds the limit value, giving rise to the hysteretic dissipative behaviour; this can be seen as an example of passive control device. In a second option, both ends are equipped with elastic-plastic devices; at one end, the device will be put in series with a shock-absorber element, allowing slow axial movements, but behaving as a rigid link when seismic actions occur.

1.2   History of SFTs

S. Preault first proposed the SFT idea in 1860. In 1923, the SFT was recognized as a realizable way to cross Norway fjords, whose depth is too high for bored tunnels; in fact, assuming a reasonable slope for approaching tunnel sections, a large depth results in excessive total length of the tunnel.

Then, a prize-winning proposal for a 5.3 km SFT between Calabria and Sicily over the 350 m deep Messina Strait in Italy, was proposed as an alternative to the suspended bridge. 20 years later, a remarkable time, it happened in 1989 that a working group for immersed and submerged floating tunnels was established by ITA (International Tunnel Association), which made it catch the world-wide attention [1-3], especially in Italy, Norway, China, Japan, USA and other countries.

After this notable historical moment, specialists started to work on this new topic not only on the theoretical and numerical fields but also on the design and construction aspects with growing interests. A large number of proposals were studied over the world.

In 2004, a Scientific and Technological Cooperation between the Peoples Republic of China and the Italian Republic was founded on the Sino-Italian Joint Laboratory of Archimedes Bridges (SIJLAB), which encouraged step further development on the SFTs and attracted new global interest in the topic [1-4].

Later, a prototype to be built in Qiandao Lake, an artificial lake located in Zhejiang Province, China, was proposed by SIJLAB. The prototype has a 100 m length and a 4.4 m external diameter; it was intended to be used for research purposes for some years, and then devoted to pedestrian usage and tourist attraction. Afterwards, much wider and deeper researches were based on this project. Although the project is now in a stand-by situation waiting for financial support, the obtained scientific achievements are profitable for further research or other SFTs' proposals.

Note that, owing to the special location of the SFT, several research fields must be covered to give a thorough view on the dynamic loading and the resulting structural behaviour, such as:

- seismic engineering analysis, studying both support-transmitted and fluid-transmitted loads;

- fluid-structure interaction, leading to the definition of forces due to sea waves and vortex shedding;

- vehicle-structure interaction, resulting in forces due to traffic loading;

- phenomenon related to impact and explosions, applied to both internal and external events.

- geotechnical engineering, for studying the determination of the transfer functions of the seismic signal thought different layers of flexible soil strata.

In seismic analysis, both the earthquake loads due to direct ground motion transmission to the structural supports and the so-called "seaquake" loading, due to the water transmission of compressive waves originated at the seabed, are worth more attention.

Oscillation due to dynamic interaction with moving vehicles is an aspect, which deserves investigation in relation to fatigue considerations and comfort requirements for people travelling through the tunnel. The latter aspect seems to be of utmost importance for an innovative infrastructure whose psychological acceptance from the community must be ensured by all technical means. There is nearly no related work on SFTs on this traffic problem, but there are similar works on other crossing solutions.

From the literature review, there is limited research effort focusing on the response of SFTs subjected to the seaquake forces, transmitted from the seabed vibration to the structure through water. More attention should be paid on this research area.

1.3 Reasons for Choosing Floating Tunnel

As an innovative structure to be taken as an alternative to traditional waterway crossing solutions, there are some pros and cons related to the SFT concept.

The pros are for SFTs:

- they ate invisible thanks to the submerged position in the water;
- take advantage of the water buoyancy;
- allow for very low gradient of the approaching lanes and thus for smaller overall tunnel length;
- provide space above the water surface for the ship traffic requirements and/or scenic view demand;
- are constructed away from densely populated areas and moved to the definite site;
- can be almost integrally removed at the end of the lifetime;
- have the possibilities of reuse or recycling;
- have a cost which is only linearly proportional to length;
- are theoretically feasible to surpass spans of any length;
- are not subjected to the wind actions;
- are subjected to water waves in a limited way, with a lower effect if compared to the wind acting on a bridge;
- are less dependent on the mechanical soil properties than underground tunnels or immersed tunnels.

On the contrary, some of the cons are listed below:

- a SFT is an unusual structure and little experience is available in practise;
- the abnormal location in the water needs more care in the safety assessment;
- new structures often receive much more challenges and tests;
- the environment is complex due to its position;
- there are difficulties in the construction to position the tunnel at a definite place;
- high expenses are necessary for preliminary researches and experiments;

- some accidental loading conditions involve very complex studies.

The pros shown seem to largely justify the interest on the SFT concept. On the other hand, SFTs deserves more comprehensive studies to solve some scientific and technical problems in order to convince the public of its safety. In order for the project come to fruition, various technical, economic, and social impact aspects must still be deeply investigated.

1.4 Design Features

The first step in the realization of a never-built structure is to have an all-round conceptual design; for a SFT this should cover the overall structural configuration, the cross-section and the supporting system of the tunnel. There are several aspects to be decided once the SFT proposal starts.

- Placement and length.

  The tunnel length mainly depends on the distance of shores, but also on its placement. SFTs are considered for long crossings and as the tunnel length increases, the SFT cost will proportionally decrease when compared to other solutions. For very long tunnels, the end connections to the shore are likely to become a critical aspect of the design, especially when high seismic forces must be considered.

- Depth.

  Since the SFT plays the role of 'underground bridge' with an anchoring system connecting it to the seabed, the water depth plays an important role. A hundred meter depth is considered a limit for column supported submerged tunnels; in deeper waters other solutions, as the one here considered, must be adopted. Another question is how deep should be placed the SFT tunnel in the water. The tunnel position in the water should leave enough space for the surface navigation; considering important sea-strait crossings, where large ships can navigate, a 30-40 m clear depth is deemed to be sufficient

Referring to the tunnel, the configuration of the tunnel cross-section and the choice of the material are the main aspects to be decided.

- Cross-section; circular.

  It has a marked effect on the hydrodynamic and structural behaviour. However, it is also decided based on functional requirements; for instance, the number of lanes for cars or railroad tracks and the various types of services to be considered. The internal diameter should be enough to accommodate them and to ensure the normal required operation. The external diameter, on the other hand, has the prominent influence on the ratio between the water

buoyancy and the tunnel weight, which is expected to be larger than one. It was detected that the increase of the ratio from 1.25 to 1.4 can lead to impressive improvements of the SFT response to extremely severe sea states. In general, a large ratio can improve the structural performance under severe environmental loadings; it is worth noting, however, that high net buoyancy forces can result in very high tension forces on the foundations under extreme loading, this being an aspect to be carefully considered in terms of feasibility and cost. Besides that, the cross-section must have enough strength to be always kept in the elastic region in any loading condition, to avoid any type of cracking in order to meet the water tightness requirement.

- Cross-section; other shapes.

  There are some different types, like circular, polygonal or elliptical, rectangular and circular tubes enclosed inside an external shell having a streamlined shape. The configuration depends on the traffic lanes and related facilities in a great measure.

- Material

  In FEHRL (1996), it is mentioned that the selection of the materials to be used to build a Submerged Floating Tunnel must be made according to the structural and functional performance which are intended to be ensured, but it has also to be a compromise among several factors such as the resistance to the marine environment, fabrication, assembly and maintenance issues, time needed for the supply, material and constructional cost, et cetera. The possible materials used in tunnel are steel, reinforced concrete, pre-stressed reinforced concrete, aluminium alloys and rubber foam. The most acceptable and reasonable material, having a large and experienced application in other immersed tunnels, is the steel-concrete composite one, which has higher strength and good resistance to fatigue from the steel material, and higher resistance to the corrosion and heavy beneficial weight (especially in SFTs) from the concrete material.

- *Selection of supporting system*

The tunnel body will move upward because of the positive net difference between water buoyancy and tunnel weight if there were no anchoring system. Or, as to the other supporting system (with pontoons floating on the water surface, see Fig 2), the tunnel will sink down to the seabed because of dead weight. As a result, the supporting system seems essential in the preliminary design. Two different load-carrying systems, the seabed anchoring system and the pontoon, can be seen as alternatives. The latter one is only accustomed to the very calm environment. More detailed proposals are based on the seabed anchoring system, which can be provided by means of anchoring bars or cables. Until now, the anchoring bar solution seem to be more competitive in complex environment, as it will be discussed in detail. When the anchoring bars are selected, the cross-section should be made in detail. Hollow sections seem to be the best choice, for they can have almost neutral buoyancy and higher lateral stiffness efficiency. The material for the bars is steel with high strength and good resistance to fatigue, which is of common usage in offshore engineering.

References in Chapter 1

[1-1] Ahmet Gursoy, Parsons Brinckerhoff International, Inc Tunnelling and Underground Space Technology 12, 83-86 (1997).

[1-2] Mariagrazia Di Pilato, Dynamic behaviour of Submerged Floating Tunnels (SFT) subjected to seismic and hydrodynamic excitation, Politecnico di Milano, Dipartimento di Ingegneria Strutturale PhD thesis (2006).

[1-3] Christian Ingerslev, Immersed and Floating Tunnels, Procedia Engineering 4, 51-59 (2010).

[1-4] Håvard Østlid, When is SFT competitive? Procedia Engineerin 4, 3-11 (2010).

[1-5] Federico Perotti, Gianluca Barbella, Mariagrazia Di Pilato, The dynamic behavior of Archimede's Bridges: Numerical simulation and design implications, Procedia Engineering 4, 91-98 (2010).

[1-5] Di Pilato, M., Feriani A., Perotti, F., Numerical models for the dynamic response of submerged floating tunnels under seismic loading, Earthquake Engineering and Structure Dynamics, (2008).

[1-6] Martinelli, L., Barbella, G., Feriani, A., A numerical procedure for simulating the multi-support seismic response of submerged floating tunnels anchored by cables, Engineering Structures 33, 2850-2860 (2011).

[1-7] Di Pilato, M., Perotti, F., Fogazzi, P, 3D dynamic response of submerged floating tunnels under seismic and hydrodynamic excitation, Engineering Structures, 30, 268-281 (2008).

[1-8] Youshi Hong, Fei Ge, Dynamic response and structural integrity of submerged floating tunnel due to hydrodynamic load and accidental load, Proceeding Engineering, 4, 35-50 (2010).

[1-9] Feriani A, Mulas MG and Lucchini G. Vehicle-bridge dynamic interaction: an uncoupled approach. Proc. of International Conference on Noise and Vibration ISMA 2008, Editors P. Sas, M. De Munck, Leuven, Belgium, Sept. 2008.

[1-10] Ahrens, D., Submerged floating tunnels: a concept whose time has arrived, Tunn. Undergr. Space Technol.11, 505-510 (1996).

[1-11] Brancaleoni F., Castellani A., D'Asdia P., The response of submerged tunnels to their environment, Engineering Structures, 11, 47-56 (1989).

[1-12] Giulio Martire, The development of Submerged Floating Tunnels as an innovative solution for waterway crossing, Facoltà di Ingegneria, Università degli Studi di Napoli Federico □, PhD thesis (2010)

Chapter 2: Multiple-support seismic excitation for the dynamic analysis of a SFT.

The problem that will be treated in this chapter deals with the seismic excitation to be applied to the supports of the structure.

If you consider a structure of moderate extension (we are talking about of order of meters), for example, a simple multi-story building used for residence purposes, we can study its dynamic behaviour exciting all its foundation with a single accelerogram. So we can make the approximation of having the same seismic motion for all the supports of the structure.

In the case of an SFT, due to the big distances crossed by such structure, we cannot use the same seismic input for all the supports because it is generated in a single point and then attenuated traveling from the epicentre to the point of interest. Having the supports a large distance between one another, we will have different intensity of the seismic motion in every point of the structure that we cannot neglect. Therefore, it is necessary to make reference to a non-synchronous input.

It is known that the response of an elastic structure subjected to a non-synchronous input can be obtained from the superimposition of two contributions: a dynamic component induced by the inertia forces and the so-called pseudo-static component, due to the difference in the support displacements. These latter can induce significant distortions in the structure, thus modifying the internal forces with respect to the case of synchronous input.

Therefore, the knowledge of the seismic motion time history at all the soil-structure interface nodes is required. A SFT has plan dimensions of the order of some kilometres; in this condition, a structural system must be considered to be subjected to partially correlate non-synchronous seismic input motion. In the work here described, this type of input has been introduced making use of artificial time histories.

2.1 Stochastic modelling of the ground motion

The stochastic modelling of the space-time variation of the seismic excitation is based on the Kanai-Tajimi power spectral density (PSD) modified by Ruiz and Penzien, which has been adopted to describe the seismic motion at a single point. In addition, the coherency model of Luco and Wong was introduced for representing the spatial variation of the ground motion. The resulting model is used for the generation of artificial time histories, which is made very efficient by introducing the Fast Fourier Transformation (FFT) method.

2.1.1 Coherency function for spatial variability: Luco and Wong model

In long structures, it cannot be assumed that the same input ground motion will be shaking all supports. In fact, in the seismic wave propagation process three effects are responsible for the variation of the local ground motion:

- the wave-passage effect, which is the difference in the arrival times of seismic waves at different locations;
- the incoherence effect or dispersion, resulting from reflections and refraction of waves through the soil during their propagation, as well as from the different superposition pattern for waves arriving from an extended source at various locations;
- the local effect, due to the difference in local soil conditions at each location.

The incoherence problem can be interpreted in terms of a random dispersion added to a reference acceleration input; the dispersion is a function of the distance between the point considered and the reference point, of the transmitting wave velocity and of a dispersion parameter. This aims to retain the acceleration response spectra of the ground motion. Due to the random character of the dispersion, the analyses are not exactly repeatable.

The coherency function is defined in terms of the cross-power spectral density (CPSD) of ground acceleration $S_{i,j}(\xi_d, w)$ between two stations i and j at a separation distance ξ_d.

$$\gamma(\xi_d, w) = \frac{S_{i,j}(\xi_d, w)}{\left[S_{i,i}(w) \cdot S_{j,j}(w) \right]^{1/2}} \tag{2.1}$$

where:

w = circular frequency;

$S_{i,i}(w)$, $S_{j,j}(w)$ = PSD at the station sites.

In this work, assume $S_{i,i}(w) = S_{i,i}(w) = S(w)$, there is no local effect considered, each station is the same PSD.

The coherency function can be changed into:

$$\gamma(\xi_d, w) = \frac{S_{i,j}(\xi_d, w)}{S(w)} \tag{2.2}$$

A suitable expression for the coherency function should reflect the phenomena. Some expressions are more designed-oriented, based on simplified methods to account for the effects of the correlation between the support motions. Luco and Wong 1986 model was here adopted in the form:

$$\gamma(\xi_d, w) = \exp\left[-\left(\frac{\alpha_c \omega \xi_d}{v_s} \right) \right] \exp\left[i \frac{\omega \xi_d^{L}}{v_{app}} \right] \tag{2.3}$$

where:

ξ_d = horizontal separation distance between two stations i and j ;

v_s = the shear wave velocity;

α_c = a parameter controlling coherence decay;

ξ_d^{L} = projected horizontal distance along the wave propagation direction;

v_{app} = the surface apparent velocity of wave.

The first term on the right-hand side decays exponentially with the frequency ω, with the horizontal separation distance ξ between the two stations i and j and through the shear waves velocity vs, with the inverse of the mechanical characteristics of the soil. The second term depends on the projected horizontal distance $\xi_d{}^L$ along the wave propagation direction and on the wave circular frequency ω, and it is a measure of the wave passage delay due to the surface apparent velocity of the waves.

The adopted model for the coherency function does not contain parameters describing the local effect, which should be accounted for in the local spectra $S_{ii}(\omega)$. Note that in this formulation the geometric incoherence effect is given an higher weight (square power) with respect to the wave passage effect.

2.1.2 PSD Function: Modified Kanai-Tajimi Spectum of Ground Acceleration

The adopted PSD function is the well-known modified Kanai-Tajimi spectrum of ground accelerations (Clough and Penzien 1975), expressed as (2.2)

$$\text{S(w)} = S_0 S_{CP} = S_0 \frac{w_g{}^4 + 4\varsigma_g{}^2 w_g{}^2 w^2}{(w_g{}^2 - w^2)^2 + 4\varsigma_g{}^2 w_g{}^2 w^2} \frac{w^4}{(w_f{}^2 - w^2)^2 + 4\varsigma_f{}^2 w_f{}^2 w^2} \tag{2.4}$$

where,

S_0 = intensity of the ideal white noise process modelling bedrock acceleration;

$S_{CP}(w)$ = normalized Clough-Penzien spectrum;

w_g, ζ_g = characteristic ground frequency and damping;

w_f, ζ_f = the parameters of an additional filter introduced to guarantee finite power for displacements.

In this equation, the scale factor S_0 depends on the peak ground acceleration (PGA) according to the following relation:

$$S_0 = \frac{\text{PG}^2}{\text{p}^2 \cdot \text{var}^*} \tag{2.5}$$

p = peak factor

$$p = \sqrt{2 \cdot \ln \frac{2.88 \cdot \Omega \cdot t_{max}}{2\pi}}$$ (2.6)

t_{max} = equivalent duration of the process;

$$\Omega = \sqrt{\frac{E[\dot{x}^2]}{var[x]}}$$ (2.7)

$E[\dot{x}^2]$ = mean square of the derivative of the process;

$$E[\dot{x}^2] = \int_{-\infty}^{\infty} \omega^2 S(\omega) d\omega$$ (2.8)

$var[x]$ = variance (total power) of the process having PSD, $S(\omega)$.

$$var[x] = \int_{-\infty}^{\infty} S(\omega) d\omega$$ (2.9)

$$var^*[x] = \int_{-\infty}^{\infty} S_{CP}(\omega) d\omega$$ (2.10)

2.1.3 FFT: Fast Fourier Transform Method

The Fourier Transform is an integral transform with a lot of practical applications that enables to transform a signal from the time-domain to the frequency-domain.

The general expressions of the direct F-T (from time to frequency) and the inverse F-T (from frequency to time) are the well-known formulae here below:

$$X(f) = \int_{-\infty}^{+\infty} x(t) * e^{-j2\pi f} \, dt$$ (2.11)

$$x(t) = \int_{-\infty}^{+\infty} X(f) * e^{+j2\pi} \, df$$ (2.12)

In other words, the F-T enables us to decompose a generic wave into many sub-components. More in details, the F-T allows to calculate the different components of the sinusoidal waves (amplitude, phase and frequency) that, if summed, give birth to the original signal.

This is very useful for different reasons:

1. Observing the sub-components of the wave we can filter the wave cancelling out the disturbing frequencies. After cleaning up the signal, we can bring it back to the time domain to obtain a better result.

2. In the frequency domain, a function of space and time can be decomposed in frequency, amplitude and phase of sinusoidal waves, so we have more information on which we can work on.

3. Working with many sinusoidal waves with different amplitude and phase is much better than working with a wave that is continuously varying in time, because in the first case we can perform the calculus with complex number that makes much easier to make certain operations that on the initial wave.

The Fourier Transform is a really complex operation from the computational point of view but, in the engineering field, we use the Fast Fourier Transform to reduce the computational effort of the overall procedure.

In 1965, an algorithm called FFT (Fast Fourier Transform) has been built that, with the mechanism '*divide et impera*', can reduce the complexity of the Fourier Transform from $O(n^2)$ to $O(n \log(n))$. Practically, the FFT algorithm simplified enormously the calculations and can be used also by small calculators. For example, if we want the Fourier Transform of 10^6 points, with the FFT you can reduce the calculation time from 2 weeks to 30 seconds.

So, with the classical transform, from time domain to frequency domain, the number of sums to be done was equal more or less to the number of points and the number of multiplications was equal to the square of the number of points. For this reason, the Fast version of the transform has been built, that enables to go to the frequency domain with much less operations, decomposing the wave into more sections and making the transform on each of them, in a fast way because the number of multiplications is drastically reduced.

The most common FFT algorithm is the Cooley-Tukey algorithm.

In our case, from the stochastic model described above, given the power spectral density and correlation function, artificial generation of time-histories has been performed by using the cosine series formula (2.13), which can be efficiently computed using the Fast Fourier Transform (FFT).

$$(x, t) = \sqrt{2} \sum_{\eta=\pm 1} \sum_{J=0}^{J-1} \sum_{n}^{N-1} \left[S(k_j, \omega_n) \Delta k \Delta \omega \right]^{1/2} \cdot \cos \left[\eta k_j x + \omega_n \left(t - \frac{x}{v_{app}} \right) + \right.$$

$$\left. \varphi^{(\eta)}_{jn} \right] \tag{2.13}$$

where:

$f(k, \omega)$ = the time history;

$S(k, \omega)$ = frequency-wave –number (F-K) spectrum;

k = wave number;

$\varphi^{(\eta)}_{jn}$ = two sets of independent random phase angles uniformly distributed in $(0, 2\pi]$.

To use the preceding equation, a discretization of the frequency-wave-number spectrum is to be performed. The F-K spectrum is obtained as follows:

$$S(k, \omega) = S(\omega) \cdot \Gamma(k, \omega) \tag{2.14}$$

$\Gamma(k, \omega)$ = the Fourier transform of the coherency function, which satisfies the condition

$$\int_{-\infty}^{\infty} \Gamma(k, \omega) dk = 1 \tag{2.15}$$

which implies

$$\int_{-\infty}^{\infty} S(k, \omega) dk = S(\omega) \tag{2.16}$$

That is, the power pertaining to a frequency is distributed among all the wave numbers. In the definition of Γ only the geometric incoherence term is included in the F-K spectrum.

$$|\gamma(\xi_d, w)| = \exp \left[- \left(\frac{\alpha_c \omega \xi_d}{v_s} \right)^2 \right] \tag{2.17}$$

So, we can get

$$\Gamma(k, \omega) = \frac{1}{2\pi} \int_{-\infty}^{\infty} |\gamma(\xi_d, w)| e^{-i\omega\xi_d} d\xi = \frac{1}{2\sqrt{\pi}} \exp \left[- \left(\frac{v_s k}{2\alpha\omega} \right)^2 \right] \frac{v_s}{\alpha_c |\omega|} \tag{2.18}$$

An advantage of equation is that the resulting F-K spectrum is quadrant symmetric

$$S(k, \omega) = S(-k, \omega) = S(k, -\omega) = S(-k, -\omega) \tag{2.19}$$

This permit simplifying the discretization of the spectrum. Vanmarcke (1983) first introduced the concept of quadrant symmetry. Note that coherency functions yielding quadrant-symmetric F-K spectra can depict only the incoherence of the seismic motions (Zerva 1992), and therefore the apparent propagation (wave-passage effect) of the seismic motions should be included explicitly in the equation of the simulated field, by means of the time-shift x / v_{app} .

The discretization is performed within the limits of an upper cut off wave number k_u and an upper cut-off frequency w_n, beyond which the contribution to the total power can be considered as negligible for practical purposes. On the regressions on the F, M and S spectra, these can be determined as follows:

$$\omega_u = 20 \cdot \omega_g \tag{2.20}$$

$$k_u = 6.65 \frac{\alpha}{v_s} \cdot \omega_f^{0.84} e^{0.047 w_g} \tag{2.21}$$

The upper cut-off frequency was determined by satisfying the following condition:

$$\frac{\int_0^{\omega_u} S(k,\omega) d\omega}{\int_0^{\omega_u + 2\pi} S(k,\omega) d\omega} - 1 = 10^{-5} \tag{2.22}$$

Whereas the upper cut -off wave number was determined by satisfying the following conditions:

$$S(k_u, \omega) = S_{max} \cdot 10^{-3}; \frac{\partial}{\partial \omega} S(k_u, \omega) = 0 \tag{2.23}$$

where $S_{max} \approx 2.218 \frac{v_s}{\alpha \omega_f}$ = peak value of the spectrum, which occurs at the point with coordinates (k=0, $\omega \approx 0.123 \omega_f$).

A way to check whether the upper cut-off frequency is correct for practical purposes is to make use of (3-a) as follows:

$$\sum_{k-k_u}^{k_u} S(k, \omega_n) \Delta k \approx S(w_n); \qquad w_n = 0, \dots, w_u \tag{2.24}$$

Once the cut-offs are determined, the discrete wave number and frequency are given by

$$k_j = j\Delta k; J = 0, \dots, M - 1, con\ M \geq 2J \tag{2.25}$$

$$w_n = n\Delta w; n = 0, \ldots, L - 1, con \ L \geq 2N \qquad (2.26)$$

M, L = powers of 2;

J,N = powers of 2;

J is larger or equal than the number of points for the discretization in space of the field (number of sites where the field is needed), $J\Delta k = k_u$

N is larger or equal than the number of points for the discretization in time of the field (number of points in the time histories) $N\Delta w = w_u$

The equation (4-11), can be rewritten to allow the usage of the fast Fourier transform (FFT) method, as

$$f\left(x_r, t_s, -\frac{x_r}{v_{app}}\right) =$$

$$\sqrt{2}\, Re\left[e^{-iwx,jv_{app}}\left(\sum_{\eta=\pm 1}\sum_{J=0}^{J-1}\sum_{n}^{N-1}\left\{[S(k_j, \omega_n)\Delta k\Delta\omega]^{1/2}e^{i\emptyset^{(\eta)}jn}\right\}e^{i\eta 2\pi /M}e^{i2\pi sn/L}\right)\right]$$

$$(2.27)$$

Where:

$$x_r = r\Delta x = r\frac{2\pi}{M\Delta k}; \qquad r = 0, \ldots, M - 1 \qquad (2.28)$$

$$t_s = s\Delta t = s\frac{2\pi}{L\Delta w}; \qquad s = 0, \ldots, L - 1 \qquad (2.29)$$

As a last remark, note that the period of the simulations is

$$T_0 = \frac{2\pi}{\Delta w} = L\Delta t \geq N_P\Delta t = t_{max} \qquad (2.30)$$

From the upper, the ground acceleration is expressed as a stationary process. Finally, we recall that we assumed the free-field ground acceleration to be a uniformly modulated non-stationary process. To account for the non-stationary characteristic of ground accelerations, the stationary time histories generated are modulated by means of a deterministic envelope function $\eta(t)$.

$$\eta(t) = \left(\frac{t}{t_1}\right)^2 \ per \ 0 \leq t \leq t_1$$

$$\eta(t) = 1 \quad per \ t_1 \leq t \leq t_2 \qquad (2.31)$$

$$\eta(t) = exp\left\{\frac{t-t_2}{t_{max}-t_2}ln\beta_t\right\} \quad per \; t_2 \leq t \leq t_{max}$$

where:

t_1, t_2 = ramp duration and decay starting time;

t_{max} = time-history duration;

β_t = ratio of the amplitude envelope at t_{max} to that during the stationary phase.

$$\eta(t) = exp\left\{\frac{t-t_2}{t_{max}-t_2}ln\beta_t\right\} \quad per \; t_2 \leq t \leq t_{max}$$

2.2 Seismic Motion Modelling Parameters

In the PSD equation, required parameters are adopted in the following:

$\omega_g = 10 \; rads^{-1}$, $\varsigma_g = 0.4$, $\omega_f = 1.0 \; rads^{-1}$, $\varsigma_f = 0.6$

In the coherency function (3-3), the related parameters are assumed:

$v_s = 3500 \; m/s$, $v_{app} = 4950 \; m/s$, $\alpha = 1$

In respect of the deterministic envelope function (3-31), the unknowns are given:

$$t_1 = 2s \, , t_2 = 5s, t_{max} = 40s, \beta_t = 0.25$$

For the transversal and vertical directions, peak ground acceleration PGA is 0.64 g while 85% of this value is taken for the longitudinal direction.

To take account of multiple-support excitation and soil structure interaction, displacement time histories and velocity time histories are required. Based on the frequency domain procedure, double integration to get time histories of ground velocity and displacement are described in chapter 5.

2.3 Conclusions

We have seen here how to generate non-synchronous seismic input motion that is needed to apply the dynamic loading to the supports of the SFT. In this way, we can take into account all the modifications that the seismic input undertakes traveling from the epicentre to the various points of the structure.

In Chapter 5, you will find generation and application of the time histories here theoretically derived.

References in Chapter 2

[2-1] Monti et al. - 1996 - Nonlinear response of bridges under multi-support excitation

[2-2] Shinozuka & Deodatis - 1996 - Simulation of multi-dimensional Gaussian stochastic fields by spectral representation

[2-3] Ray W. Clough, Joseph Penzien (1995), Dynamics of Structures, *Computers & Structures, Inc*.

[2.4] Fogazzi, P., Perotti, F. (2000), The dynamic response of seabed anchored floating tunnels under seismic excitation, *Earthquake Engng Struct. Dyn*. **29**, 273-295.

[2.5] Martinelli L., Barbella G., Feriani A. (2010), Multi-support seismic input and response of submerged floating tunnels anchored by cables, Technical Report N.6/2010, Università degli Studi di Brescia.

Chapter 3: The Concepts of Seaquake and Transfer Function

3.1 What is Seaquake

Seaquake is a hydrodynamic pressure propagating through water due to the seismic waves generated by an earthquake with epicentre beneath the sea. This phenomenon causes hydrodynamic excitations on the submerged structures.

The point is to understand If these forces provide a positive contribution to the overall behaviour of the structure, and so they tend to uplift the tunnel, or they provide a negative contribution, tending to make the tunnel sink.

3.1.1 Generalities

With the recent developing trend towards the exploitation and utilization of the ocean space, more and more projects involving floating structures are proposed and catch a lot of attention in the engineering research field. With regards to their special location, it is necessary and essential for the designers and researchers to ensure structural safety with respect to all types of hydrodynamic excitation, including the ones due to the so-called seaquake phenomenon. Actually, a number of cases call for attention to the effects of propagating seismic waves in water due to seaquakes and to the potential damaging effects that such waves may cause on the offshore structures and floating systems. These considerations hold for a new challenging structure as a SFT, submerged in the middle of the ocean. What is a seaquake will be the primary task to make it clear. It is defined as a hydrodynamic pressure due to shock waves consisting solely of compressional waves, since water cannot transmit a shear wave, traveling through the water and excited by the motion of the seabed during an earthquake.

As an environmental external accidental force acting on the structure, there were few studies on this topic. Rudolph (1887, 1895) was the first to study the phenomenon and gives an extensive list of occurrences. In 1957, Richter discussed further observations of the effects of earthquakes on the surface ships and submarines. In 1981, Hove

presented some cases of ships being severely shaken by seaquakes. One of them, considered as the most serious, concerned MT ' Ida Knudsen', a 32,500 ton Norwegian tanker that was struck by a magnitude 8.0 event on February 28, 1969 in the Atlantic Ocean approximately 450 km west of Gibraltar, and which damage was classified as total loss after an extreme shaking coming from beneath. Then, in 1983, Arochiasamy did some studies on the nonlinear transient response of floating platforms to the seaquake-induced excitation including cavitation effects. In 1988, Gin-show Liou proposed a systematic numerical approach for the response of tension-leg platforms, studied as rigid bodies under the forces due to vertically propagating waves caused by spatially varying seismic motion of the sea-bed. In the same period, Okamoto and Sakuta proposed a mathematical approach for studying seaquakes as a propagation phenomenon of acoustic waves in compressible fluids. In 1995, Tokuo Yamamoto worked on the stochastic fluid-structure interaction of large circular floating islands subject to wind waves and seaquakes and on the harmonic propagation of gravity waves and acoustic waves in the sea due to the vertical oscillation of the seabed. In 2002, Yoshiyuki built a realistic model of the seaquake effect in time domain, considering the sea bottom slope and soft sediments. It was noted that the maximum stress responses may exceed the admissible values due to the sea shock load. A very large floating structure placed in the shallow water was studied by Takamura et al, focusing on the resonance phenomena and considering the interrelationship between the vibration of the floating structure and the deformation of the seabed; the proposed procedure was based on a new boundary integral equation in which the seabed is a semi-infinite homogenous elastic solid.

Hereafter, we will discuss the concept of transfer function as a means to determine accelerations and velocities at the top of a series of flexible layers and in water. Then, the application of seaquake forces on a SFT is described with the aid of Morison equation.

3.2 The Concept of Transfer Function

In order to derive acceleration and velocities in every point of the soil and water above the rigid bedrock, it is necessary to introduce the concept of transfer function.

This function can be regarded as a sort of amplification factor of the movement at bedrock that can be used to amplify the base acceleration a_g and determine the dynamic characteristics of the means interested (flexible soil layers overlying the rigid bed and water).

To get an idea of the form that can assume this mathematical function, let's consider a soil layer over a semi-infinite bedrock domain. The aim is to derive a function that can be multiplied to the movement at the bedrock to obtain the one in layer 1.

The total displacement at a generic point of a semi-infinite domain in case of an incident harmonic wave can be obtained in the following way.

The problem is described by the classical 1D propagation wave equation:

$$\frac{\partial^2 u}{\partial x^2} = \frac{1}{\alpha^2} \frac{\partial^2 u}{\partial t^2}$$
(3.1)

where α is the speed of propagation of the wave, and the general solution has the form:

$$u(x,t) = f_1(x - \alpha t) + f_2(x + \alpha t)$$
(3.2)

i.e. it is composed by the sum of two differentiable functions, that represent the incident and the reflected waves.

If we assign a wave propagating with a finite speed c from $+\infty$ towards the origin, this wave is defined incident wave:

$$u(x,t) = f\left(t + \frac{x}{c}\right)$$
(3.3)

The stress-free boundary condition associated with the free surface of the domain, yields the following (von Neumann's type) condition named "free-surface":

$$\frac{\partial u(0,t)}{\partial x} = 0$$
(3.4)

Substituting the general solution of the wave equation

$$u(x,t) = f\left(t + \frac{x}{c}\right) - g\left(t - \frac{x}{c}\right) \tag{3.5}$$

Into the free surface boundary condition, we obtain:

$$f'(t) - g'(t) = 0 \tag{3.6}$$

from which g(t) = f(t) + constant. It is, however, immediate to see that the latter constant must vanish. It follows also that g(t – x/c) = f(t – x/c) represents the waveform u^r generated by the total reflection from the free surface and propagating in the opposite direction of the incident wave f(.). The total displacement at a generic point x is given by:

$$u(x,t) = u' + u' = f\left(t + \frac{x}{c}\right) + f\left(t - \frac{x}{c}\right) \tag{3.7}$$

i.e. the sum of an incident and a reflected wave.

From which it follows:

$$u(0,t) = 2f(t) = 2u' \tag{3.8}$$

That is the amplitude of the displacement at the free surface is twice that of the incident wave.

Equation (3.7), that expresses the total displacement at a generic point of the semi-infinite domain in case of incident harmonic wave, can also be written as follows:

$$u = \exp\left[i\omega\left(t + \frac{x}{c}\right)\right] + \exp\left[i\omega\left(t - \frac{x}{c}\right)\right] = 2\exp(i\omega t)\cos(Kx) \tag{3.9}$$

where

$$K = {}^{\omega}/_{c}$$

with

$$Re[u] = 2\cos(\omega t)\cos(Kx)$$

This equation shows that the half-space oscillates in stationary state of vibration for any value of the frequency of the incident wave.

If the semi-infinite domain is replaced by a layer of thickness H resting over an infinitely rigid base, and a sinusoidal motion of amplitude $e^{(i\Omega t)}$ is applied to the rigid base, the response of the elastic layer (which is a linear system) will also be sinusoidal with a frequency ω equal to the excitation frequency Ω. In general, this response can be expressed as the sum of two waveforms propagating in two opposite directions with amplitude A and B to be determined.

$$u = Aexp\left[i\Omega\left(t + \frac{x}{c}\right)\right] + Bexp\left[i\Omega\left(t - \frac{x}{c}\right)\right] \qquad (3.10)$$

From the free surface boundary condition, if follows immediately that A = B, and thus

$$u(x,t) = 2Acos\left(\frac{\Omega x}{c}\right)\exp(i\Omega t) \qquad (3.11)$$

For x = H, the displacement must be equal to the one prescribed, namely:

$$u(H,t) = 2Acos\left(\frac{\Omega H}{c}\right)\exp(i\Omega t) = \exp(i\Omega t) \qquad (3.12)$$

That yields:

$$A = \left[2\cos\left(\Omega H/c\right)\right]^{-1} \qquad (3.13)$$

That substituted in equation (3.12) gives:

$$u(x,t) = \frac{\cos\left(\frac{\Omega x}{c}\right)}{\cos\left(\frac{\Omega H}{c}\right)}\exp(i\Omega t) \qquad (3.14)$$

It follows from eq. (3.14) that:

$$u(0,t) = \frac{\exp(i\Omega t)}{\cos\left(\frac{\Omega H}{c}\right)} = \frac{u(H,t)}{\cos\left(\frac{\Omega H}{c}\right)} \qquad (3.15)$$

The expression

$$\frac{u(0)}{u(H)} = \frac{1}{\cos\left(\frac{\Omega H}{c}\right)} = H_1(\Omega)$$

represents the ratio between the displacement at the free surface and that at the bottom of the layer of arbitrary excitation frequency Ω; this ratio is called the *rigid base transfer function of the layer*.

In addition, we will now consider the case of stationary oscillations of an elastic layer of thickness H overlaying a semi-infinite domain that is also elastic. Let c_1 and c_2 denote the generic elastic propagation speeds in the layer and in the semi-infinite domain, respectively, ρ_1 and ρ_2, the corresponding mass densities, and $u_1(x,t)$, $u_2(\xi,t)$ the associated displacements.
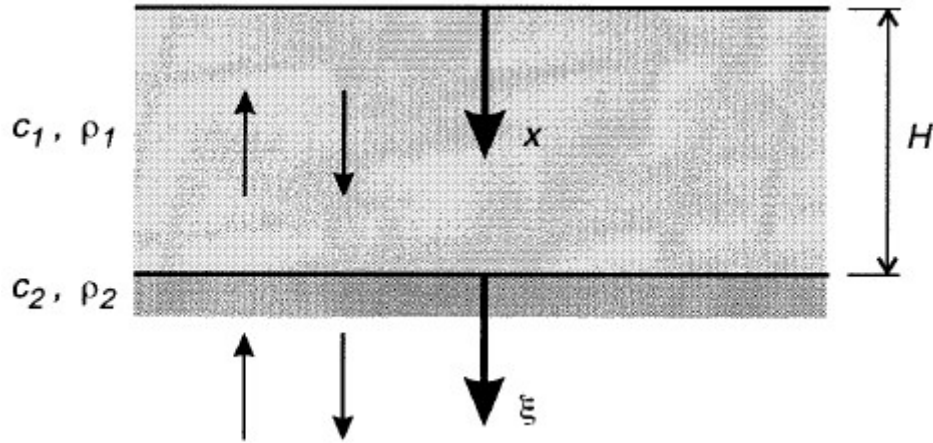
Figure 4 Flexible soil strata on semi-infinite flexible domain

In addition to the free surface boundary condition, the continuity of stress and displacement must hold at the layer interface, namely:

$$u_1(H,t) = u_2(0,t) \tag{3.16}$$

$$\rho_1 c_1^2 \frac{\partial u_1(H,t)}{\partial x} = \rho_2 c_2^2 \frac{\partial u_2(0,t)}{\partial \xi} \tag{3.17}$$

The motion in the lower domain will result from the superimposition of the incident harmonic wave, whose amplitude C is assumed known, and of a reflected wave, that is:

$$u_2 = C exp\left[i\omega\left(t + \frac{\xi}{c_2}\right)\right] + D exp\left[i\omega\left(t - \frac{\xi}{c_2}\right)\right] \tag{3.18}$$

In the same way, by introducing in the layer both an upward and a downward (reflected) wave of amplitude A and B, respectively, it is found in analogy with equation (3.14)

$$u_1 = 2A cos\left(\frac{\omega x}{c_1}\right) exp(i\omega t) \tag{3.19}$$

From equation (3.16) we derive

$$2A\cos\left(\frac{\omega H}{c_1}\right) = C + D \tag{3.20}$$

Whereas from equation (3.17) it follows

$$-2A\rho_1 c_1^2 \frac{\omega}{c_1}\sin\left(\frac{\omega H}{c_1}\right) = i\frac{\omega}{c_2}\rho_2 c_2^2(C - D) \tag{3.21}$$

From which, by setting $\eta = \rho_2 * c_2 / \rho_1 * c_1$ one obtains

$$i2A\sin\left(\frac{\omega H}{c_1}\right) = \eta(C - D) \tag{3.22}$$

Dividing the sides of (3.22) by η and summing up (3.20) and (3.21) gives

$$A = \frac{C}{\left[\cos\left(\frac{\omega H}{c_1}\right) + \frac{i}{\eta}\sin\left(\frac{\omega H}{c_1}\right)\right]} \tag{3.23}$$

Whence, substituting into eq. (3.21)

$$D = C\frac{\eta\cos\left(\frac{\omega H}{c_1}\right) - i\sin\left(\frac{\omega H}{c_1}\right)}{\eta\cos\left(\frac{\omega H}{c_1}\right) + i\sin\left(\frac{\omega H}{c_1}\right)} \tag{3.24}$$

Since the amplitude C of the incident wave is known (one could set C=1), we can compute the unknown amplitudes of the remaining waves in the layer and in the semi-infinite domain. Note that:

$$u_1(0, t) = 2A\exp(i\omega t)$$

$$u_1(H, t) = u_2(0, t) = (C + D)\exp(i\omega t) = 2A\cos\left(\frac{\omega H}{c_1}\right)\exp(i\omega t)$$

from which

$$H_1(\omega) = \frac{u_1(0,t)}{u_1(H,t)} = \frac{1}{\cos\left(\frac{\omega H}{c_1}\right)} \tag{3.25}$$

As for the previously treated case of the elastic layer over a rigid base.

If the layer didn't exist, the displacement u(0,t) at the surface of the outcropping base will be obtained from eq. (3.18) and by imposing the free surface boundary condition. The latter provides the equality C = D, from which

$$u_0(t) = 2C\exp(i\omega t)$$

Therefore, for any ω, the ratio between the displacement at the free surface of the layer and that of the outcropping half-space will be

$$H_2(\omega) = \frac{u_1(0,t)}{u_0(t)} = \frac{A}{C} = \frac{1}{co\left(\frac{\omega H}{c_1}\right) + \frac{i}{\eta}\sin\left(\frac{\omega H}{c_1}\right)} \tag{3.26}$$

Which is the *transfer function of the layer with respect to the elastic base.* By introducing the frequency f= ω/2π, the modulus of H_2, which is also called *amplification factor of the layer on elastic bedrock*, is given by:

$$A_2(f) = |H_2(f)| = \frac{1}{\left[\cos^2\left(2\pi\frac{H}{c_1}\right) + \left(\frac{\rho_1 c_1}{\rho_2 c_2}\right)^2 \sin^2\left(2\pi f\frac{H}{c_1}\right)\right]^{\frac{1}{2}}} \tag{3.27}$$

As plotted in the following graph:
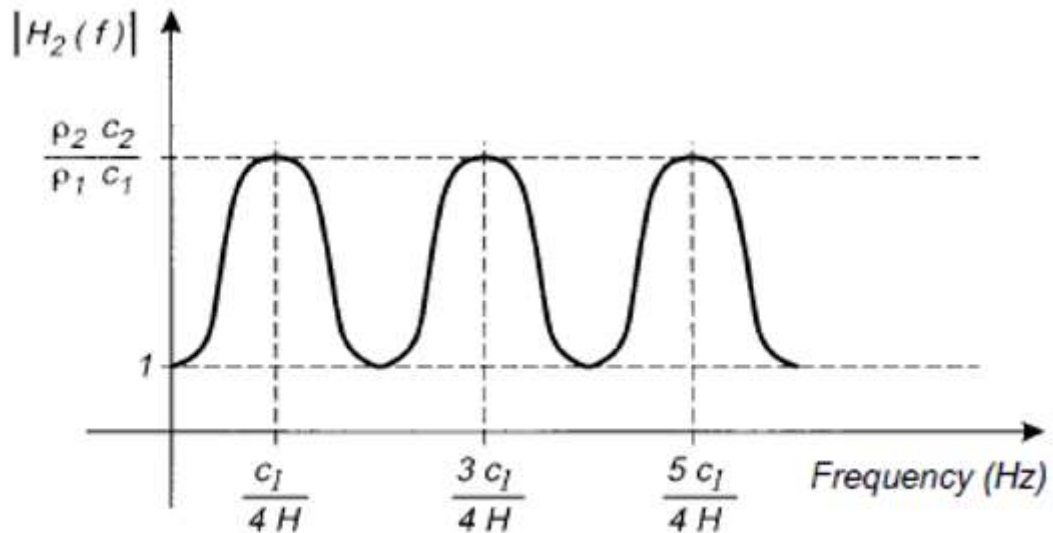
Figure 5 Amplification function of the layer overlying an elastic base

In the limit for η -> ∞ the previous rigid-base case is recovered.

These concepts were used to derived the transfer functions in the case of rigid bed, rigid bed and an elastic layer and rigid bed with multiple elastic layers.

3.2.1 Transfer Function for Rigid Seabed

The solution for the rigid seabed deals with the derivation of velocity and acceleration due to seaquake, being known the motion at the seabed. The problem will be solved

using the velocity potential that, due to the geometrical simplicity, can be solved in closed form.
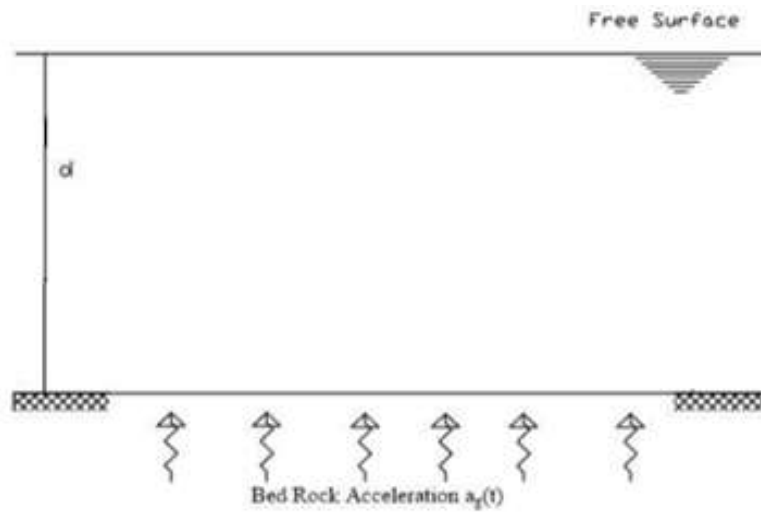
Figure 6 Schematization of rigid bedrock under a column of water d

Some assumptions are given in the following, which will be used in the deduction.

1. The hydrodynamic pressure due to the seaquake is associated with the water-transmitted seismic vibration from the sea bed to the floating structure. Neglecting the scattered wave, considering the solid structure here, the hydrodynamic pressure is related to incident waves;

2. the sea water is inviscid, incompressible and irrotational;3. the seaquake's velocity at the seabed is the same as the vertical ground velocity at this point without time lag;

3. the vertical ground motion refers to Chapter 2.

The linearized wave equation, as shown before, is given by

$$\nabla^2 \Phi = \frac{1}{c^2} \frac{\partial^2 \Phi}{\partial t^2}$$ (3.28)

where:

ϕ = velocity potential function of the incident wave;

Δ = Laplace operator;

c = acoustic compressible wave velocity in water with value of 1560 m/s.

The boundary conditions are given as follows:

55

Free surface boundary condition 1

$$\frac{\nabla \Phi}{\partial z} + \frac{1}{g}\frac{\partial^2 \Phi}{\partial t^2} = 0 \qquad \text{at z=d} \qquad\qquad (3.29)$$

This condition is obtained from three hypotheses:

1. Pressure is constant across the free surface.
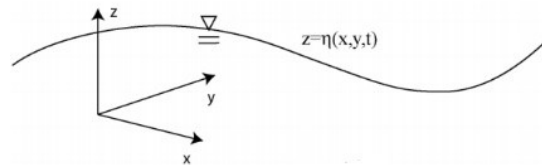
Figure 7 Reference system

The variable η is the free surface elevation, so z(x,y,t)=η(x,y,t). the pressure across the interface is equal to the atmospheric pressure $p = p_{atm}$ on z= η and from Bernoulli's equation at free surface we obtain:

$$p + \rho * \left(\frac{\partial \Phi}{\partial t} + \frac{1}{2}V^2 + gz\right) = c(t) \qquad\qquad (3.30)$$

$$p = -\rho * \left(\frac{\partial \Phi}{\partial t} + \frac{1}{2}V^2 + gz\right) + c(t) = p_{atm} \qquad\qquad (3.21)$$

Since c(t) is arbitrary we can choose a suitable constant that fits our needs, so in this case the equality between c(t), and atmospheric pressure is therefore imposed

$$c(t) = p_{atm}$$

The pressure boundary condition on z = µ becomes

$$\rho * \left(\frac{\partial \Phi}{\partial t} + \frac{1}{2}V^2 + g\eta\right) = 0 \qquad\qquad (3.22)$$

2. Once a particle on the free surface, it remains there always.

The normal velocity of a particle on the free surface follows the normal velocity of the surface itself: $\qquad z_p = \eta(x_p, t)$ z-position of particle

For small motion δz_p:

$$z_p + \delta z_p = \eta(x_p + \delta x_p, t + \delta t) = \eta(x_p, t) + \frac{\partial \eta}{\partial x}\delta x_p + \frac{\partial \eta}{\partial t}\delta t \qquad\qquad (3.23)$$

On the surface where $z_p = \eta$, this reduces to

$$\partial z_p = \frac{\partial \eta}{\partial x}\frac{\delta x_p}{\delta t}\delta t + \frac{\partial \eta}{\partial t}\delta t \qquad (3.24)$$

Where $\frac{\delta x_p}{\delta t} = u$ and $\frac{\delta z_p}{\delta t} = w$.

So finally we obtain:

$$w = u\frac{\partial \eta}{\partial x} + \frac{\partial \eta}{\partial t} \quad \text{on z=η} \qquad (3.25)$$

3. No flow through an impervious boundary or body.

If we consider Linear Plane Progressive Waves, the linear free-surface gravity waves can be characterized by their amplitude, a, wavelength, λ = 2π/k, and frequency, ω

$$\eta(x,t) = a * \cos(kx - \omega t) \qquad (3.26)$$
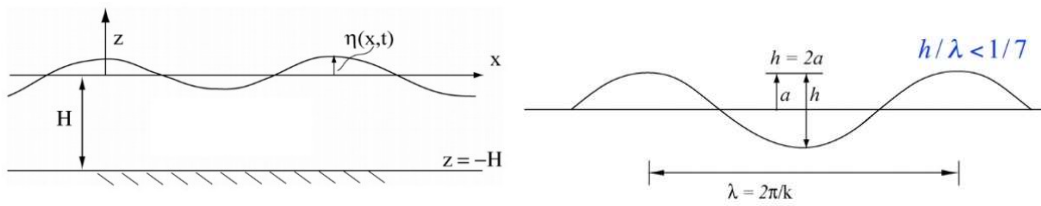
Figure 8 Characteristic parameters

- a is wave amplitude, h = 2a

- λ is wavelength, λ = 2π/k where k is wave number

- Waves will start to be non-linear (and then break) when h/λ > 1/7

Through this consideration, we can linearize the equation of the boundary condition.

1. Pressure is constant across the free surface.

$$\rho * \left(\frac{\partial \Phi}{\partial t} + \frac{1}{2}V^2 + g\eta\right) = 0 \qquad (3.27)$$

Compare $\frac{\partial \Phi}{\partial t}$ and $V^2 \sim \left(\frac{\partial \Phi}{\partial x}\right)^2$

$$\frac{\left(\frac{\partial \Phi}{\partial x}\right)^2}{\frac{\partial \Phi}{\partial t}} = \frac{a^2\omega^2 \frac{\partial \Phi^*}{\partial x^*}}{a\omega^2\lambda \frac{\partial \Phi^*}{\partial t^*}} = \frac{a}{\lambda}\frac{\frac{\partial \Phi^*}{\partial x^*}}{\frac{\partial \Phi^*}{\partial t^*}} \qquad (3.28)$$

If h/λ<<1/7 then a/λ<<1/14 since h=2a

$$\left(\frac{\partial \Phi}{\partial x}\right)^2 \ll \frac{\partial \Phi}{\partial t}$$

$\rho * \left(\frac{\partial \Phi}{\partial t} + \frac{1}{2}V^2 + g\eta\right) = 0$ becomes

$$\frac{\partial \Phi}{\partial t} + g\eta = 0 \quad \text{on z=η} \tag{3.29}$$

2. Once a particle on the free surface, it remains there always.

$$w = u\frac{\partial \eta}{\partial x} + \frac{\partial \eta}{\partial t} \tag{3.30}$$

Non-dimensionalize:

$$a\omega w^* = a\omega u^* \frac{a}{\lambda}\frac{\partial \eta^*}{\partial x^*} + a\omega \frac{\partial \eta^*}{\partial t^*} \tag{3.31}$$

If h/λ<<1/7 $\quad u\frac{\partial \eta}{\partial x} \ll \frac{\partial \eta}{\partial t}$ and $u\frac{\partial \eta}{\partial x} \ll$ w

Therefore $w = u\frac{\partial \eta}{\partial x} + \frac{\partial \eta}{\partial t}$ becomes

$$\frac{\partial \Phi}{\partial z} = \frac{\partial \eta}{\partial t} \quad \text{on z=η} \tag{3.32}$$

The non-dimensional variables used are: $\eta = a\eta^*; u = a\omega u^*; \omega t = t^*; \Phi = a\omega\lambda\Phi^*;$ $w = a\omega w^*; x = \lambda x^*; dt = \frac{1}{\omega} dt^*; d\Phi = a\omega\lambda d\Phi^*; dx = \lambda dx^*$

Since wave elevation, η, is proportional to wave amplitude, a, and a is small compared to the wavelength, λ, we can simplify our boundary conditions one step further to show that they can be taken at z = 0 versus z = η.

First take the Taylor's series expansion of ф(x, z=η, t) about z=0

$$\text{ф(x, z=η, t)=ф(x, 0, t)+}\frac{\partial \Phi}{\partial z}\eta + \cdots \tag{3.33}$$

It can be shown that the second order term and all subsequent HOTs are very small and can be neglected. Thus we can substitute ф(x, z=0, t) for ф(x, z=η, t) everywhere:

$$\frac{\partial \Phi}{\partial t} + g\eta = 0 \quad \rightarrow \quad \eta = -\frac{1}{g}\frac{\partial \Phi}{\partial t} \quad \rightarrow \quad \frac{\partial \eta}{\partial t} = -\frac{1}{g}\frac{\partial^2 \Phi}{\partial t^2}$$

$$\frac{\partial \Phi}{\partial z} = \frac{\partial \eta}{\partial t} \quad \rightarrow \quad \frac{\partial \Phi}{\partial z} + \frac{1}{g}\frac{\partial^2 \Phi}{\partial t^2} = 0 \quad \text{on z=0} \tag{3.34}$$

Seabed <u>boundary condition 2</u> imposes equality of acceleration between seabed and water

$$\frac{\nabla \Phi}{\partial z} = \frac{\partial U_g(t)}{\partial t} \quad \text{at z=0}$$

(3.35)

where:

g = gravity acceleration;

z = the calculating location;

d = depth;

$U_g(t)$ = the vertical ground displacement at the sea bed.

The derivation of the velocity potential can be found in Appendix A.

As a result, the velocity potential is written below in terms of a Fourier series expansion in space and time:

$$\Phi(z,t) =$$

$$\sum_{\eta=\pm 1} \sum_{j=0}^{J-1} \sum_{n}^{N-1} \sqrt{2S(w_n)\Gamma(k_j,w_n)\Delta k \Delta w} \frac{-c^2 w_n sin\frac{w_n}{c}(d-z)+cgco\frac{w_n}{c}(d-z)}{cw_n^3 cos\frac{w_n}{c}d+w_n^2 gsin\frac{w_n}{c}d} \left(sin \left[\eta k_j x + \right. \right.$$

$$\left. \left. w_n \left(t - \frac{x}{v_{app}} \right) + \Phi_{jn}^{(\eta)} \right] \right)$$

(3.36)

where the related symbols have been discussed in Chapter 2.

Once known the velocity potential, the seaquake velocity u, that is required in Morison equation (it will be discussed in the following paragraph) can be gained from the gradient of the scalar function ϕ. The seaquake acceleration can be therefore derived performing a derivation of the velocity.

So the seaquake velocity is:

$$u = \nabla \Phi = \frac{\partial \Phi}{\partial z}$$

(3.37)

and substituting:

$$u(z,t) =$$

$$\sum_{\eta=\pm1}\sum_{j=0}^{J-1}\sum_{n}^{N-1}\sqrt{2S(w_n)\Gamma(k_j,w_n)\Delta k\Delta w}\,\frac{cw_n\cos\frac{w_n}{c}(d-z)+g\sin\frac{w_n}{c}(d-z)}{cw_n^2\cos\frac{w_n}{c}d+w_n g\sin\frac{w_n}{c}d}\left(\sin\left[\eta k_j x+\right.\right.$$

$$\left.\left.w_n\left(t-\frac{x}{v_{app}}\right)+\Phi_{jn}^{(\eta)}\right]\right) \tag{3.38}$$

The seaquake acceleration in turn, is equal to:

$$\dot{u}=\frac{\partial u}{\partial t} \tag{3.39}$$

$$\dot{u}(z,t) =$$

$$\sum_{\eta=\pm1}\sum_{j=0}^{J-1}\sum_{n}^{N-1}\sqrt{2S(w_n)\Gamma(k_j,w_n)\Delta k\Delta w}\,\frac{cw_n\cos\frac{w_n}{c}(d-z)+g\sin\frac{w_n}{c}(d-z)}{cw_n\cos\frac{w_n}{c}d+g\sin\frac{w_n}{c}d}\left(\cos\left[\eta k_j x+\right.\right.$$

$$\left.\left.w_n\left(t-\frac{x}{v_{app}}\right)+\Phi_{jn}^{(\eta)}\right]\right) \tag{3.40}$$

3.2.2 Transfer Function for Rigid Seabed and a Flexible Layer

Next step is the derivation of the transfer function in the case of rigid seabed and a flexible layer.

The seismic waves propagate from its hypocentre to a given site through rocks and then vertically through soil deposits. Depending on soil properties, shape and thickness of soil deposits and ground motion characteristics, the seismic wave can either attenuate or amplify.

When there are no structures present, the ground motions are referred to as free-field motions. For example, when the foundation upon which the structure is situated is composed of solid rock, the high stiffness of the rock is little affected by the response of the structure so that the ground motions are approximately the same as the free-field motions. The response of these types of systems is a bit easier to compute compared with those where SSI have effects on the structural response, and they are regarded as fixed-base structures.

However, this is not the case if the ground is considered as soft soil. The motion of the foundation at the base of the structure will deviate from the free-field motion because the foundation is unable to adjust to the deformations of the free-field motion. Further on, the dynamic response of the structure to the ground motion will in turn cause deformations in the foundation.

The dynamic characteristics of an SFT system depend on the compressibility of fluid, the depth of seawater, the location of the tunnel structure in water, and energy absorption by a flexible seabed. All this influence the seismic responses of an SFT system substantially. Therefore, these effects must be considered rigorously for accurate and economical seismic designs of SFT systems.

In the Shi Chunxia PhD Program Thesis "Problems Related to the Seismic Behaviour of a Submerged Floating Tunnel", 2013, the dynamic characteristics of an SFT calculated by considering compressibility of fluid, the depth of seawater, the location of the tunnel structure in water and energy absorption of sea bed is not taken into consideration but an important factor to be considered in the analysis is the loss of energy during the propagation of waves. This phenomenon is usually referred as *material damping*. For the purposes of viscos-elastic wave propagation soils are usually modelled as materials whose resistance of shearing deformation is the sum of an elastic part and a viscous part.

In this section, we considered the sea bed as flexible and try to analyse the effects on the dynamic characteristics of an SFT.

Let's consider the response associated with the vertical propagation of shear waves through the linear viscoelastic system shown below figure (5-1). The system consists of horizontal layer which extend to infinity in the horizontal direction and has bed rock below. Layer is homogenous and isotropic and is characterized by the thickness, h_m, mass density, ρ, shear modulus, and damping factor, β.
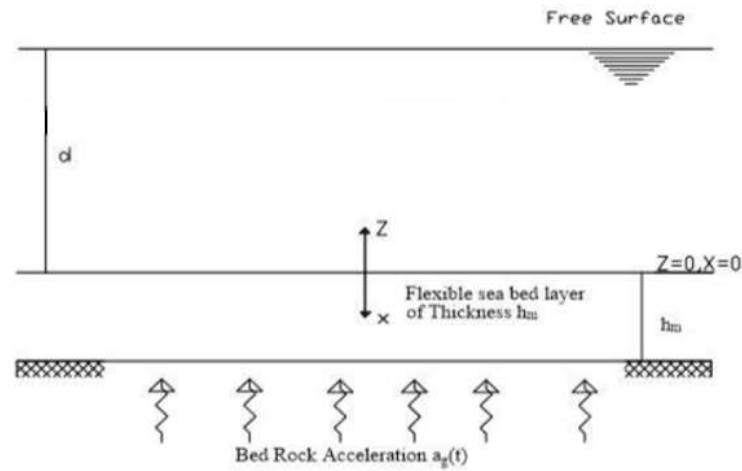
Figure 9 Schematic representation of flexible sea bed with one elastic layer

The 1D wave propagation equation through soil layers is given by the following equation:

$$\frac{\partial^2 u}{\partial x^2} = \frac{1}{\alpha^2}\frac{\partial^2 u}{\partial t^2} \tag{3.41}$$

where

$$\alpha = \left(\frac{\lambda+2\mu}{\rho_s}\right)^{1/2}$$

α has the dimensions of a speed, and depends exclusively on the elastic modulus and mass density of the material, it represents the velocity of propagation of the wave and must not be confused with the velocity of particle motion, which is instead a function of the position and of the instant of time considered.

ρ_s = Density of soil.

μ & λ = Lame's constants.

The boundary conditions are the following

B.c. 1: Compatibility between the motion of the elastic layer and bedrock acceleration

$a_g(t) = a_g * e^{(i\omega t)}$

$$a_g e^{i\omega t} + \frac{\partial^2 u}{\partial t^2} \quad \text{at x=h}_m \tag{3.42}$$

B.c. 2: Compatibility between flexible layer velocity and water velocity

$$\frac{du}{dt} + \frac{d\Phi}{dz} = 0 \text{ at x=0 and z=0} \tag{3.43}$$

B.c. 3: Equilibrium equation at the interface between water and soil layer

$$\frac{\rho_s\left(\frac{\partial u}{\partial x}\right)\omega^2}{k_s^2} - \rho_w \frac{\partial \Phi}{\partial t} = 0 \text{ at x=0 and z=0} \tag{3.44}$$

where:

ρ_w = Density of water

ϕ = Velocity Potential

$k_s = \rho_s\omega^2 / E^*$

$E^* = (\lambda + 2\mu) + i\omega\,\eta$ the complex modulus.

η = viscosity constant.

u = ground displacement.

By solving equation (3.41) with the three boundary conditions, we obtain the velocity potential for motion of water as follows:

$$\Phi = \frac{-e^{i\omega t}2a_ge^{ik_sx}\left[M\left(cg\cos\left(\frac{(d-z)\omega}{c}\right)-c^2\omega\sin\left(\frac{(d-z)\omega}{c}\right)\right)\right]}{\omega\left[N\omega\sin\left(\frac{d\omega}{c}\right)+P\cos\left(\frac{d\omega}{c}\right)\right]\left(g\omega^2\sin\left(\frac{d\omega}{c}\right)+c\omega^3\cos\left(\frac{d\omega}{c}\right)\right)} \tag{3.45}$$

where

$$M = g\rho_s\omega^2\sin\left(\frac{d\omega}{c}\right) + c\rho_s\omega^3\cos\left(\frac{d\omega}{c}\right)$$

$$N = \left(c^2k_se^{2ik_sx} - c^2k_s\right)\rho_w + \left(-ige^{2ik_sx} - ig\right)\rho_s$$

$$P = \left(-ice^{2ik_sx} - ic\right)\rho_s\omega^2 + \left(ck_sg - cgk_se^{2ik_sx}\right)\rho_w$$

$$k_s = \frac{\rho_s\omega^2}{E^*}$$

$$E^* = (\lambda + 2\mu) + i\omega\eta 0$$

And the viscosity is given by the following equation

$$\eta = \frac{2\beta(\lambda+2\mu)}{\omega}$$

λ and μ are the lame's constant, these are derived from elastic-waves velocities:

$$\lambda = \rho_s(VP^2 - 2VS^2)$$

$$\mu = \rho_s VS^2$$

where:

VP = Compressional -wave (P-wave) Velocity

VS = Shear-wave (S-wave) Velocity

ρ_s = Density of soil layer

C = Compressional wave velocity.1560 m/s^2

As for the velocity potential for rigid bed, we can derive the expression of the velocity of water deriving with respect to z the velocity potential and the acceleration deriving the velocity. The expressions are as follows.

Velocity

$$u = \nabla \Phi = \frac{\partial \Phi}{\partial z} \tag{3.46}$$

$$u = \frac{-e^{i\omega t}2a_g e^{ik_s x}\left[M\left(\omega g \sin\left(\frac{(d-z)\omega}{c}\right) - c\omega^2 \sin\left(\frac{(d-z)\omega}{c}\right)\right)\right]}{\omega\left[N\omega \sin\left(\frac{d\omega}{c}\right) + P\cos\left(\frac{d\omega}{c}\right)\right]\left(g\omega^2 \sin\left(\frac{d\omega}{c}\right) + c\omega^3 \cos\left(\frac{d\omega}{c}\right)\right)} \tag{3.47}$$

Acceleration

$$\dot{u} = \frac{\partial u}{\partial t} \tag{3.48}$$

$$\dot{u} = \frac{-e^{i\omega t}2\omega a_g e^{ik_s x}\left[M\left(\omega g \sin\left(\frac{(d-z)\omega}{c}\right) - c\omega^2 \sin\left(\frac{(d-z)\omega}{c}\right)\right)\right]}{\omega\left[N\omega \sin\left(\frac{d\omega}{c}\right) + P\cos\left(\frac{d\omega}{c}\right)\right]\left(g\omega^2 \sin\left(\frac{d\omega}{c}\right) + c\omega^3 \cos\left(\frac{d\omega}{c}\right)\right)} \tag{3.49}$$

The detailed mathematical derivation of these functions is described in Appendix B.

3.2.3 Transfer Function for Rigid Seabed and Two Flexible Layers
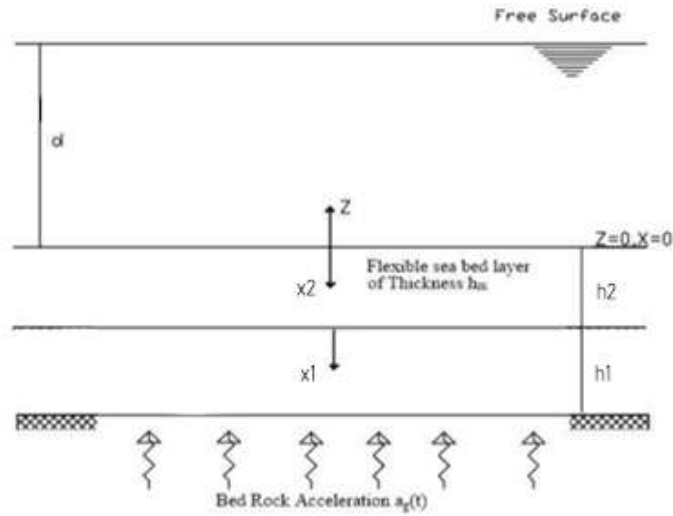
Figure 10 Schematic representation of flexible sea bed with two elastic layers

With respect to the case of a single flexible layer, we need to add the boundary condition related to the compatibility of velocity at the interface between the two different soil strata, from which we obtain the expression of the transfer function.

Bc1: compatibility between the motion of the second layer with the first one

$$\frac{d^2 u_2}{dt^2} + \frac{d^2 u_1}{dt^2} = 0 \text{ at x=h}_2 \tag{3.50}$$

Bc2: compatibility of water velocity and ground layer 2 velocity

$$\frac{du_2}{dt} + \frac{d\Phi}{dz} = 0 \text{ at z=0 and x=0} \tag{3.51}$$

Bc3: equilibrium in the vertical direction at water soil layer

$$\frac{\rho_{s2}\left(\frac{\partial u_2}{\partial x}\right)\omega^2}{k_{s2}^2} - \rho_w \frac{\partial \Phi}{\partial t} = 0 \text{ at z=0 and x=0} \tag{3.52}$$

Where:

ρ_w - Density of water

ϕ - Velocity Potential

$k_s = \rho_s \omega^2 / E^*$

$k_{s2} = \rho_{s2}\omega^2\,/E_2{}^*$

$E^* = (\lambda + 2\mu) + i\omega\,\eta$ The complex modulus.

$E_2{}^* = (\lambda_2 + 2\mu_2) + i\omega\,\eta_2$ The complex modulus.

η - viscosity constant.

u2 - Ground displacement of layer 2

u1 - Ground displacement of layer 1

By solving equation (3.41) with the three boundary conditions, we obtain the velocity potential for motion of water as follows:

$$
\Phi = \Bigg\{ (g\cos(\mu(d-z))
$$

$$
- c^2\mu\sin(\mu(d-z))\,e^{it\omega}2a_g e^{ih_2 k_2}\left\{N\omega\sin\left(\frac{d\omega}{c}\right) + M\cos(d\mu)\right\}\Bigg\}
$$

$$
/\Bigg\{ (gsin(d\mu) + c^2\mu\cos(d\mu))\Big\{P\rho_w^2 + [Q\rho_{s2} + R\rho_1]\rho_w
$$

$$
+ S\omega\sin\left(\frac{d\omega}{c}\right)
$$

$$
+ [[T\rho_{s1}\rho_w + U\rho_{s1}\rho_{s2}]\omega^2 + V\rho_w^2 + Z\rho_{s2}\rho_w]\cos(d\mu)\Big\}\Bigg\}
$$

With:

$$
N = \big[(c^2 g k_1(e^{2ih_1 k_1} - 1)\sin(d\mu)
$$
$$
+ c^4 k_1(e^{2ih_1 k_1} - 1)\mu\cos(d\mu))\rho_{s2}\rho_w - (ig^2(e^{2ih_1 k_1} + 1)\sin(d\mu)
$$
$$
+ ic^2 g(e^{2ih_1 k_1} + 1)\mu\cos(d\mu))\,\rho_{s1}\,\rho_{s2}\big]
$$

$$
M = -\big(icg(e^{2ih_1 k_1} + 1)\sin(d\mu) + ic^3(e^{2ih_1 k_1} + 1)\mu\cos(d\mu)\big)\rho_{s1}\rho_{s2}\omega^2
$$
$$
+ (g^2 k_1(1 - e^{2ih_1 k_1})\sin(d\mu)
$$
$$
+ c^3 g k_1(1 - e^{2ih_1 k_1})\mu\cos(d\mu))\rho_{s2}\rho_w
$$

$$
P = \Big[k_2\left(c^4 k_1(e^{2ih_1 k_1} - 1)e^{2ih_2 k_2} + c^4 k_1(1 - e^{2ih_1 k_1})\right)\mu\sin(d\mu)
$$
$$
+ (c^2 g k_1(e^{2ih_1 k_1} + 1)e^{2ih_2 k_2}
$$
$$
+ c^2 g k_1(1 - e^{2ih_1 k_1})e^{2ih_2 k_2})\cos(d\mu)\Big]
$$

$$
Q = \Big[(ic^2 g k_1(1 - e^{2ih_1 k_1})e^{2ih_2 k_2} + ic^2 g k_1(1 - e^{2ih_1 k_1}))\mu\sin(d\mu)
$$
$$
+ (ic^4 k_1(1 - e^{2ih_1 k_1})e^{2ih_2 k_2} + ic^4 k_1(1 - e^{2ih_1 k_1}))\mu^2\cos(d\mu)\Big]
$$

$$R = k_2\left(-ic^2g\left(e^{2ih_1k_1}+1\right)e^{2ih_2k_2}+ic^2g\left(e^{2ih_1k_1}+1\right)\right)\mu\sin(d\mu)$$
$$+ k_2\left(-ig^2\left(e^{2ih_1k_1}+1\right)e^{2ih_2k_2}-ic^2g\left(e^{2ih_1k_1}+1\right)\right)\cos(d\mu)$$

$$S = \left[\left[\left(-g^2\left(e^{2ih_1k_1}+1\right)e^{2ih_2k_2}-g^2\left(e^{2ih_1k_1}+1\right)\right)\mu\sin(d\mu)\right.\right.$$
$$+\left(-c^2g\left(e^{2ih_1k_1}+1\right)e^{2ih_2k_2}\right.$$
$$\left.\left.\left.-c^2g\left(e^{2ih_1k_1}+1\right)\right)\mu^2\cos(d\mu)\right]\rho_{s1}\rho_{s2}\right]$$

$$T = \left[k_2\left(-ic^3\left(e^{2ih_1k_1}+1\right)e^{2ih_2k_2}+ic^3\left(e^{2ih_1k_1}+1\right)\right)\mu\sin(d\mu)\right.$$
$$+\left(k_2\left(icg\left(e^{2ih_1k_1}+1\right)e^{2ih_2k_2}-icg\left(e^{2ih_1k_1}+1\right)\right)\cos(d\mu)\right]\rho_1\rho_w$$
$$\left.-k_2cg\left(e^{2ih_1k_1}+1\right)\left(1+e^{2ih_2k_2}\right)\cos(d\mu)\right]$$

$$U = \left[-cg\left(\left(e^{2ih_1k_1}+1\right)e^{2ih_2k_2}+\left(e^{2ih_1k_1}+1\right)\right)\mu\sin(d\mu)\right.$$
$$\left.-c^3\left(\left(e^{2ih_1k_1}+1\right)e^{2ih_2k_2}+\left(e^{2ih_1k_1}+1\right)\right)\mu^2\cos(d\mu)\right]$$

$$V = \left[c^3gk_1k_2\left(\left(1-e^{2ih_1k_1}\right)e^{2ih_2k_2}+\left(e^{2ih_1k_1}+1\right)\right)\mu\sin(d\mu)\right.$$
$$\left.+cg^2k_1k_2\left(\left(e^{2ih_1k_1}-1\right)e^{2ih_2k_2}+\left(1-e^{2ih_1k_1}\right)\right)\cos(d\mu)\right]$$

$$Z = icg^2k_1\left(\left(e^{2ih_1k_1}-1\right)e^{2ih_2k_2}+\left(e^{2ih_1k_1}-1\right)\right)\mu\sin(d\mu)$$
$$+ic^3gk_1\left(\left(e^{2ih_1k_1}-1\right)e^{2ih_2k_2}+\left(e^{2ih_1k_1}-1\right)\right)\mu^2\cos(d\mu)$$

As for the velocity potential for the other two cases, we can derive the expression of the velocity of water deriving with respect to z the velocity potential and the acceleration deriving the velocity.

The velocity u has the following expression:

$$u = \left\{ \left(\mu g \sin(\mu(d-z)) \right) \right.$$

$$- c^2 \mu^2 \cos\left(\mu(d-z)\right) e^{it\omega} 2a_g e^{ih_2 k_2} \left\{ N\omega \sin\left(\frac{d\omega}{c}\right) + M \cos(d\mu) \right\} \right\}$$

$$\left/ \left\{ (g\sin(d\mu) + c^2 \mu \cos(d\mu)) \left\{ P\rho_w^2 + [Q\rho_{s2} + R\rho_1]\rho_w \right. \right. \right.$$

$$+ S\omega \sin\left(\frac{d\omega}{c}\right)$$

$$\left. + \left[[T\rho_{s1}\rho_w + U\rho_{s1}\rho_{s2}]\omega^2 + V\rho_w^2 + Z\rho_{s2}\rho_w \right] \cos(d\mu) \right\} \right\}$$

Using these formulas and based on the artificial generation procedures for the multiple support seismic motion (Chapter 2), a numerical procedure has been coded for the generation of the time histories of seaquake fluid velocities and forces on the tunnel.

3.3 Seaquake Forces on a SFT

For the application of the seaquake forces to the tunnel, the fluid-structure interaction must be taken into account. To this purpose, we will explain the Morison equation and we will use it as a means to derive the hydrodynamic forces acting on the tunnel based on water acceleration and velocity.

3.3.1 Fluid Forces on Bodies: Generalities

In order to design offshore structures, surface vessels and underwater vehicles, an understanding of the basic fluid forces acting on a body is needed. In the case of *steady* viscous flow, these forces are straightforward. *Lift* force, perpendicular to the velocity, and *Drag* force, in line with the flow, can be calculated based on the fluid velocity, U, force coefficients, C_D and C_L , the object's dimensions or area, A, and fluid density, ρ. For viscous flows the drag and lift on a body are defined as follows:

$$F_{Drag} = \frac{1}{2}\rho U^2 A C_p \tag{C.1}$$

$$F_{lift} = \frac{1}{2}\rho U^2 A C_L \tag{C.2}$$

The drag force arises due to viscous rubbing of the fluid. The fluid may be thought of as comprised of several "layers" which move relative to one another. The layer at the surface of the body "sticks" to the surface due to the *no-slip condition*. The next layer of fluid away from the surface rubs against the layer below, and this rubbing requires a certain amount of force because of viscosity. One would expect that in the absence of viscosity, the force would go to zero (D'Alambert's Paradox).

Beyond steady flow, especially in the presence of free surface waves, we must consider *unsteady*, time dependent motions of both the fluid and the body and the fluid inertial forces arise, adding to the total forcing on a body.
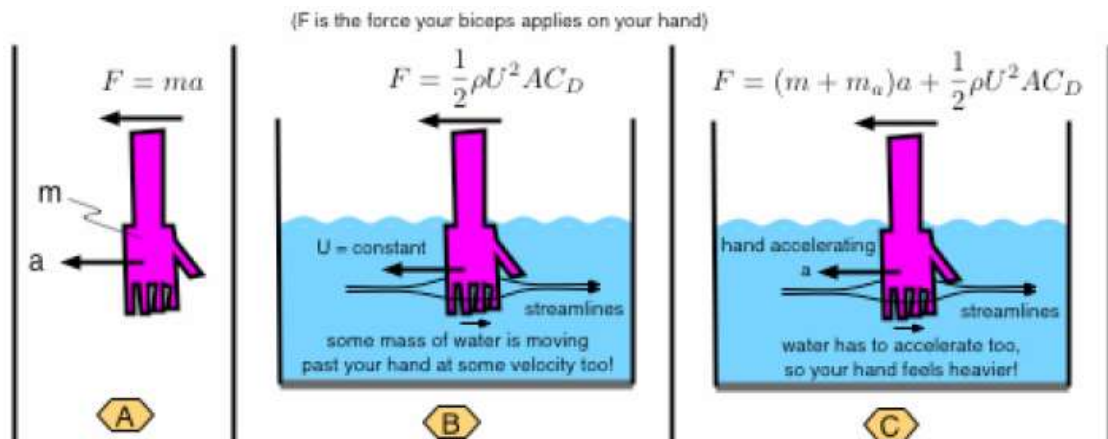
Figure 11 Fluid forces on a body

We can do the following experiment:

A) Wave your hand in the air. Feel the force it takes to accelerate your hand. F=ma.

B) Fill your bathtub with water. Run your hand through (with the palm facing forward) at a slow, constant speed. Feel the drag on your hand. Notice that the water must move to flow around your hand.

B1.5) Run your hand through at another constant, faster speed. Notice that it takes more force. Recall the drag force is proportional to U^2. Notice that the water now moves at some constant, faster speed around your hand.

C) Try and accelerate your hand from the slow speed to the fast speed. It's hard, huh?! Notice that the water flowing past your hand has to accelerate as your hand accelerates. Since some mass of water must accelerate, your hand feels heavier.

We capture this idea with the concept of *added mass*.

3.3.2 The Concept of Added Mass

Take the case of an unsteady moving body, $U_b(t)$, in an unbounded inviscid, irrotational fluid ($\mu=0$) with zero velocity, $U_f = 0$. The time-dependent force on the body is directly proportional to the body acceleration:

$$F(t) = -m_a \frac{dU_b(t)}{dt} \tag{C.3}$$

70

Where m_a, is the system added mass, depends on the body geometry and direction of motion. This is an *added* inertial force or *added mass* force on the body. By comparison, in an inviscid steady flow, by D'Alembert's Paradox, the force on the body would be zero.

1) Unsteady Moving Body Stationary Fluid: Force on a sphere (radius *a*) accelerating in an unbounded quiescent (non-moving) fluid. *U* =*U*(*t*) is the unsteady body velocity.
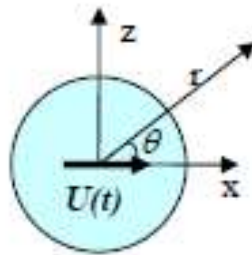
Figure 12 Unsteady moving body stationary fluid

It can be demonstrated that:

$$F_x = -\dot{U}(t)\left(\tfrac{1}{2}\rho\forall_s\right)$$
(C.4)

V_s = Volume of the sphere

$m_a = 1/2\rho\forall_s$ is the added mass

2) Unsteady Moving Fluid Stationary Body: Force on a sphere (radius *a*) in an unbounded unsteady moving fluid. Uf(t) =*U(t)* is the unsteady fluid velocity.

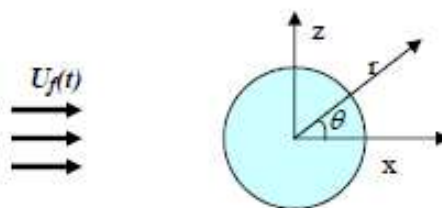*Figure 13 Unsteady moving body stationary fluid*

Thus, we obtain:

$$F_x = \dot{U}_f(\rho\forall + m_a)$$
(C.5)

Where the non-added mass term is due to the pressure gradient necessary to accelerate the fluid around the sphere.

3) Unsteady Moving Fluid; Unsteady Moving Body: Force on a moving sphere (radius *a*) in an unbounded moving fluid. $U_f=U_f(t)$ is the unsteady fluid velocity and $U_b(t) =U(t)$ is the body velocity.
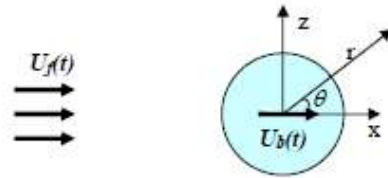

Figure 14 Unsteady moving body stationary fluid

The case of the unsteady moving body and fluid can be determined by combining the results from the previous two cases.

$$F_x = -\dot{U}_b \left(\frac{1}{2}\rho\forall_s\right) \text{ (moving body still fluid)} \qquad (C.6)$$

$$F_x = \dot{U}_f(\rho\forall + m_a) \text{ (moving fluid still body)} \qquad (C.7)$$

Moving Body & Moving Fluid

$$F_x - \dot{U}_b(m_a) + \dot{U}_f(\rho\forall + m_a) = \dot{U}_f\rho\forall + m_a(\dot{U}_f - \dot{U}_b) \qquad (C.8)$$

For the case of unsteady motion of bodies underwater or unsteady flow around objects, we must consider the additional effect (force) resulting from the fluid acting on the structure:

$$m\ddot{x} + b\dot{x} + kx = f(t) - m_a\ddot{x} \qquad (C.9)$$

In a physical sense the added mass can be regarded as the weight added to a system due to the fact that an accelerating or decelerating body (i.e. unsteady motion: $dU/dt \neq 0$) must move some volume of surrounding fluid with it as it moves.

Added mass forces can arise in one direction due to motion in a different direction, and thus we can end up with a 6 x 6 matrix of added mass coefficients.

A good way to think of the added mass components, m_{ij}, is to think of each term as mass associated with a force on the body in the ith direction due to a *unit* acceleration in the jth direction.

3.3.3 Morison Equation

After the premise about the forces that arise on a body that interacts with a fluid, we are ready to introduce Morison equation, that is our means to apply seaquake excitation to the tunnel.

Morison equation, popular in the condition when circular section's diameter divided by the wavelength is smaller than 0.2, here is largely justified for the structure given the tunnel section diameter. So, it is introduced to simulate the hydrodynamic loading in the simplified approach, based on beam elements, to the structural modelling. With the large-scale dimension of SFT, spatial distribution of structural response cannot be simply expected as a rigid body motion because of the significant structural deformation. The extended approach given by Chakrabarti for the case of oscillating cylinders in waves is used. The wave force f on a moving cylinder is written in terms of the normal components of the relative velocity and acceleration with single coefficients:

$$f = \frac{1}{2}C_D \rho D |u - \dot{x}|(u - \dot{x}) + C_M \rho \frac{\pi}{4} D^2 (\dot{u} - \ddot{x}) + \rho \frac{\pi}{4} D^2 \ddot{x} \qquad \text{(C.10)}$$

Or, in another form:

$$f = \frac{1}{2}C_D \rho D |u - \dot{x}|(u - \dot{x}) + C_A \rho \frac{\pi}{4} D^2 (\dot{u} - \ddot{x}) + \rho \frac{\pi}{4} D^2 \dot{u} \qquad \text{(C.11)}$$

where:

C_D , C_M = drag coefficient and inertia coefficient, $C_M = C_A + 1$;

C_A = added mass coefficient;

ρ = water density;

D = cylinder diameter;

u , $\dot{u}$ = instantaneous water particle velocity and acceleration;

$\dot{x}$, $\ddot{x}$ = structure move velocity and acceleration;

$u - \dot{x}$, $\dot{u} - \ddot{x}$ = relative velocity and acceleration.

In equation (C.10), the first part is the drag force, the second is the hydrodynamic inertia force, and the third is Froude-Krylov force which is used in fluid dynamics to describe the non-viscous forces on the floating body in regular waves.

Parameters C_D and C_M are experimentally derived; here, C_D =1.2 and C_M = C_A +1, where added mass coefficient C_A is equal to 2.

3.4 Conclusions

In this chapter we introduced the concept of seaquake and a way of applying it on our SFT structure.

The aim was to find a way to model the dynamic forces generated by the seaquake phenomenon on the tunnel. The means used was the Morison equation, that is an empirical formulation that takes into account the added mass that moves along with the body in unsteady motion.

The velocities and accelerations of water to be introduce in Morison equation depend on the soil on which the structure is built. Here arose the necessity to derive the transfer functions, in order to find a correlation between the motion at the rigid seabed, that has been stochastically extended to multiple supports in Chapter 2, and the velocity in water considering the presence of only rigid rock or of additional flexible layers in between.

To make it more clear, you can refer to the following graph that schematically explains all the procedure and concepts seen till now related to the effect of an earthquake on an underwater structure.

MODELLING OF EARTHQUAKE & SEAQUAKE ON SFT RESTIG ON FLEXIBLE LAYER OVER RIGID ROCK

Movement at FOUNDATIONS ← Action of EARTHQUAKE on SFT → Movement of WATER on the tunnel (SEAQUAKE)

MORISON EQUATION
Idrodinamic Forces

Transfer Function of seismic movement from bedrock to flexible layer → TRANSFER FUNCTION ← Acceleration & velocity derived from transfer function from bedrock to water

Ratio between dispacements at top and bottom of layer (Amplification Factor of design seismic motion at 1 point represented by accelerogram of ECs)

SEISMIC MOVEMENTS AT MULTIPLE SUPPORT: Stochastic modelling of motion at bedrock

Starting Point: PSD Function of Ruiz & Penzien (sesmic motion at 1 point)

Coherency Function of Luco & Wong (spatial variation of ground motion)

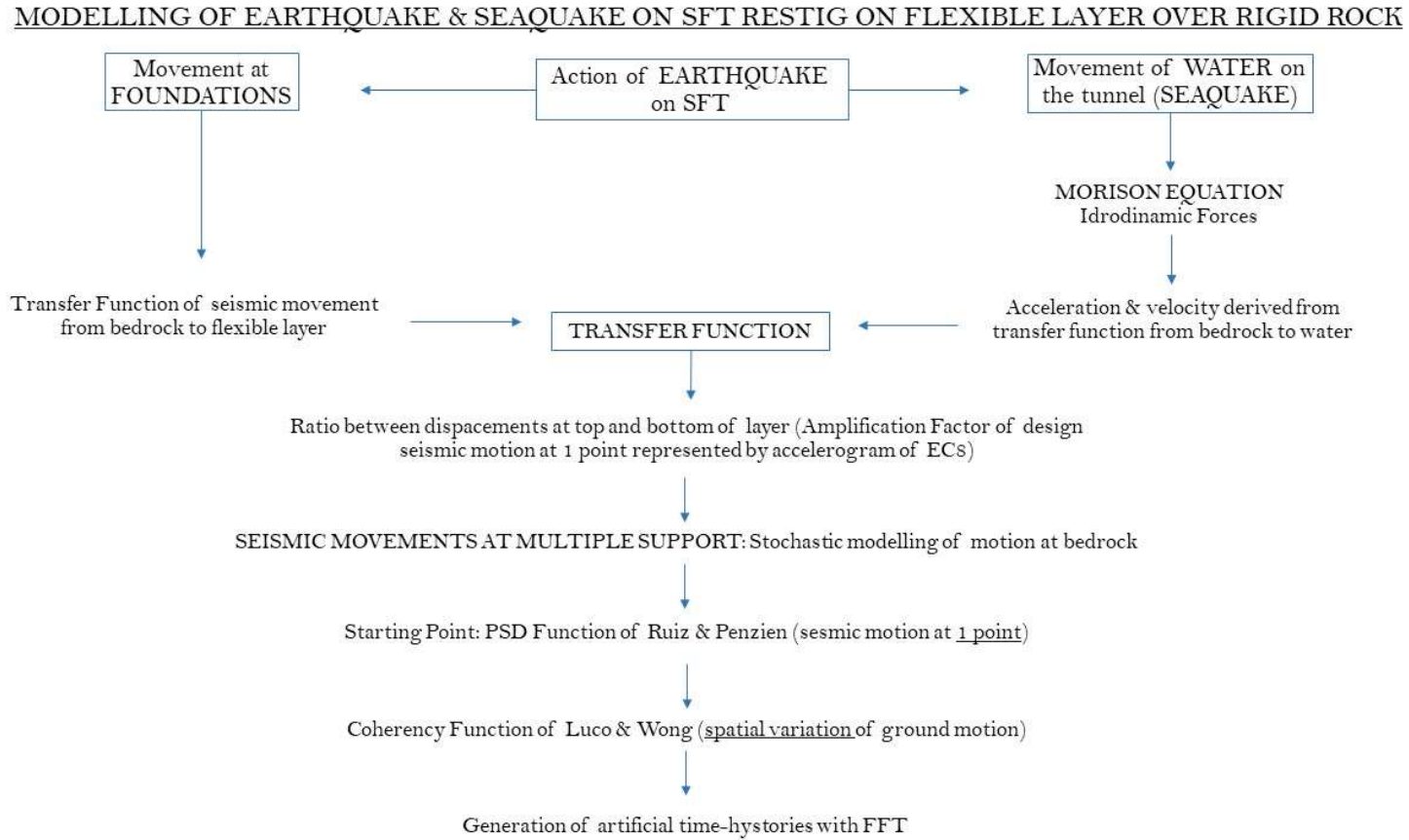Generation of artificial time-hystories with FFT

Figure 15 Modelling of earthquake and seaquake of SFT resting on flexible layer over rigid bedrock

References in Chapter 3

[3-1] Faccioli e Paolucci - Seismic Wave Propagation

[3-2] Hydrodynamics – Prof. A. H. Techet

[3-3] Handbook of Offshore Engineering – Subrata K. Chakrabarti, Offshore Structure Analysis, Inc.

[3-4] Chakrabarti, S.K. (1987), Hydrodynamics of offshore structures, *Computational Mechanical Publication*, Southampton Boston.

[3-5] Takuji Hamamoto (1995), Stochastic fluid-structure interaction of large circular floating islands during wind waves and seaquakes, *Probabilistic Engineering Mechanics*, **10**, 209-224.

[5.6] Takuji Hamamoto (1995), Stochastic fluid-structure interaction of large circular floating islands during wind waves and seaquakes, *Probabilistic engineering mechanics,* **10**, 209-224.

Chapter 4: Case Study – Modelling of a SFT over the Messina Strait

The aim of this thesis is to use all the theoretical information presented above to study a real case, or better a project, that consists in a proposal for the crossing of the well-known Messina Strait in the south of Italy, a piece of sea of width that goes from a minimum of 3km to a maximum of 16km. The strategic and economical importance of this infrastructure has drawn attention from the '80, also because, due to the extension of the crossing, it is a very challenging structure from the engineering point of view that pushes engineers to find innovative and new solutions for the resolution of the problem.

Here comes the concept of Submerged Floating Tunnel that is regarded as the best solution of such type of problem due to the fact that it enables to cross distances much higher than a bridge can do and its cost is proportional to its length (unlike bridges whose cost is proportional to the square of their length, due to its great dependence from the bending moment diagram). Last, but not the least, due to the fact that these innovative structures have a cost not proportional to their spatial extension, we can choose the best strategic points for the construction on both shores, regardless of the two nearest points. This will bring a more functional structure both for traffic and dislocation of vehicles and for feasibility.

Our model consists of a 4680 km underwater tunnel, made up of two separated tunnels connected by linkages, anchored to the seabed by anchoring bars and running from the town of Catona on the Calabria coast, to the town of Punta S. Ranieri on the Sicily coast.

The geological model of Messina Strait is shown in the following figure and in particular we made reference to the section of the Calabria slope, desumed by the studies of the Stretto di Messina Society, that only reports the presence of normal faults (thick lines).
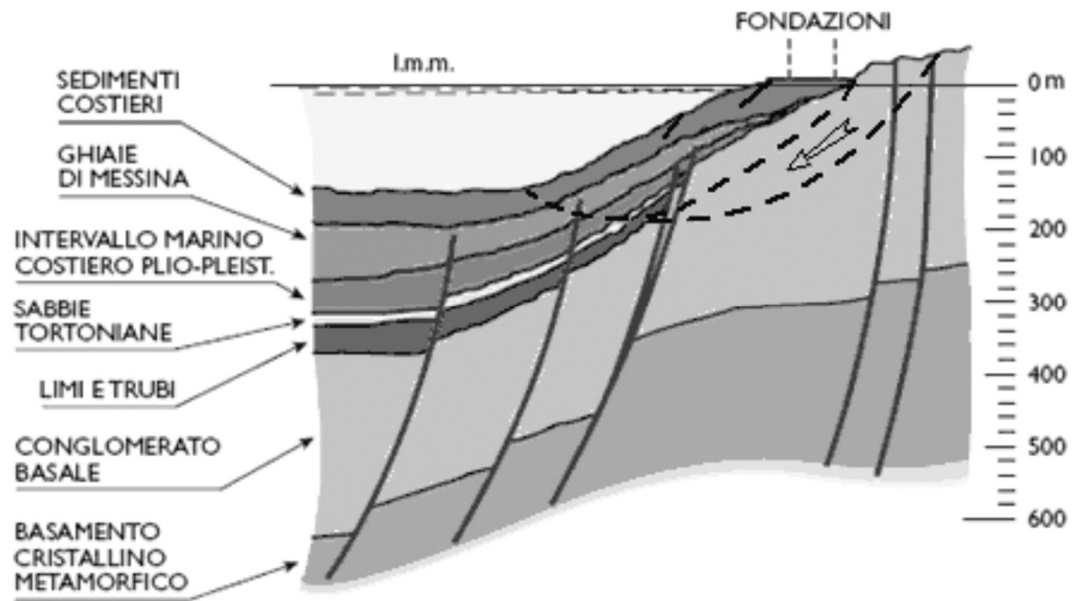
Figure 16 Geological model

Since there is not enough available information, we considered only the first two layers, the first composed of terraced deposits, with a constant thickness of 42 m and the second layer composed of "Messina" gravel, with a constant thickness of 107 m.

The details to obtain the model and the different analysis that we have done will be discussed in details in this chapter.

4.1 General scheme of the Model in ANSYS

The software used for the analysis is ANSYS, a sophisticated engineering finite element simulation software. The aim was to construct a 2D model first, considering only a section of the tunnel and in order to have a simple model to be easily controlled and rapidly analysed, and then to extend this model in 3D to have a better understanding of the overall behaviour of the structure.

To get an idea of what we are talking about you can refer to the figure below, which shows a preliminary sketch of the tunnel in transversal and longitudinal planes.
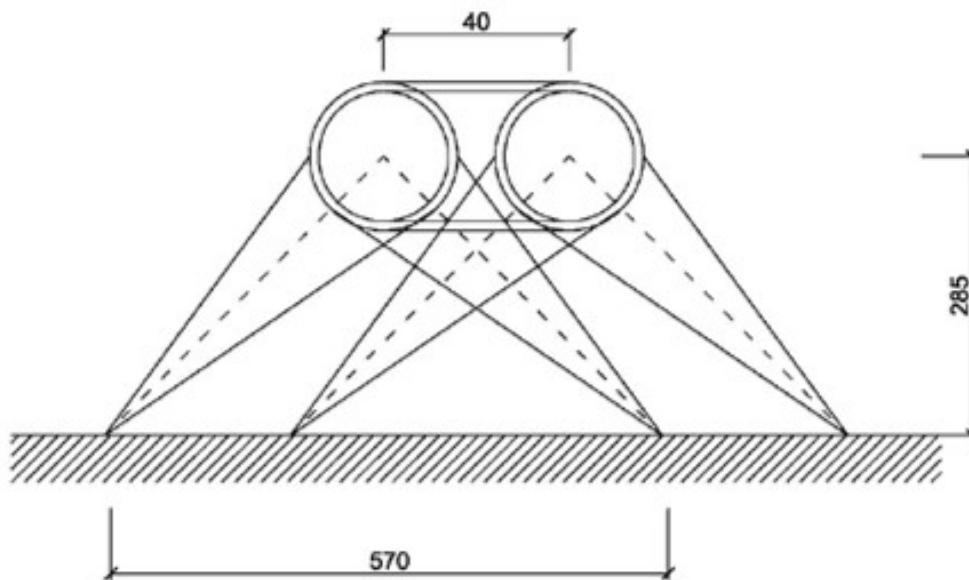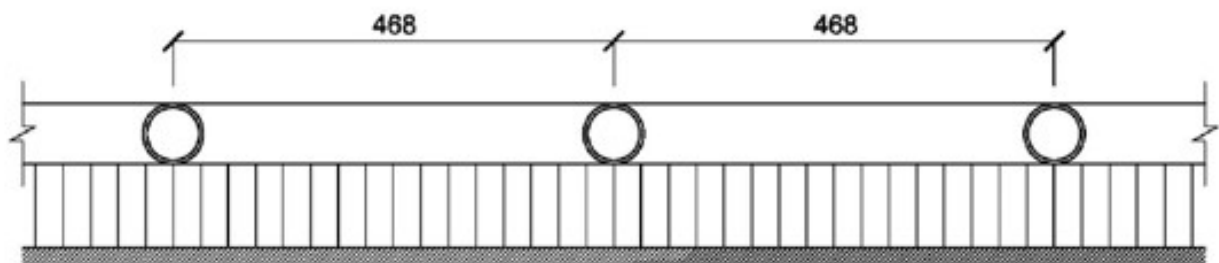

Figure 17 Transversal section of the model

Figure 18 Longitudinal section of the model

For the crossing of the Italian strait between Sicily and Calabria, a solution composed of two tunnels separated by 40m of water, and anchored to the ground by 4 anchorage

bars for each tunnel that converge into two anchorage points to the ground which distance is 570m has been proposed. The tunnels are submerged in water for 40m and, in the deepest point, they are 285m above the seabed.

The section of the tunnel and of the linkage is a circular, hollow section with external diameter of 15.95m and internal diameter of 13.95m with a total thickness of 2m.

The section of the bars, of 3 different types to accommodate the changing of the internal actions along the length, is also an empty tube of dimensions 0.933 for the external diameter, 0.871 for the internal diameter, with total thickness of 60mm for bars type A, 0.975 for the external diameter, 0.91 for the internal diameter, with total thickness of 65mm for bars type B, and 1.029 for the external diameter, 0.961 for the internal diameter, with total thickness of 68mm for bars type C.

4.1.1 Material Properties

The materials used for the construction of the structure are the two basic materials commonly used in civil engineering practice: steel and concrete.

The tunnel is a composite section composed of two sheets of steel of 20mm, one external and the other internal, and an internal filling of concrete. The section is therefore treated in the analysis as an homogenized section of area A = 58.24 m^2, equivalent elastic modulus E of 2.943×10^7 kN/m^2, and self-weigh W = 1200 kN/m. The geometrical and mechanical characteristics are summarized in the table below:

D_{est} [m]	D_{int} [m]	Area [m^2]	I [m^4]	W [kN/m]	E [kN/m^2]
15.95	13.95	58.24	1637	1200	2.934×10^7

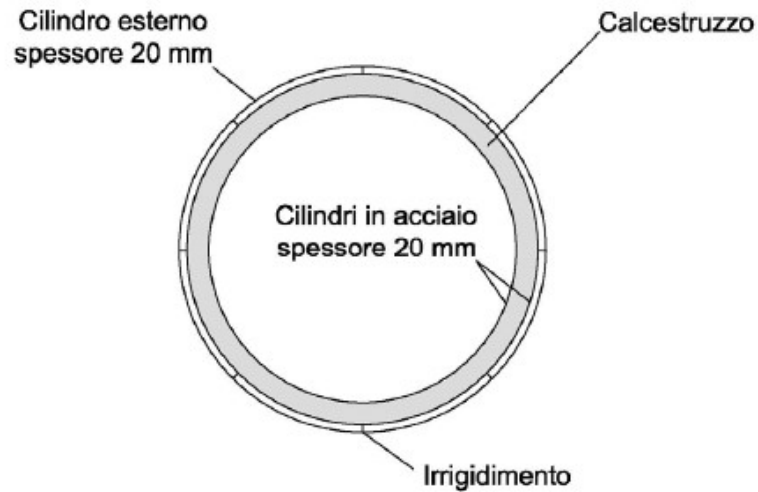*Table 1 Geometrical and mechanical characteristic of the tunnel section*

Figure 19 Tunnel section

For the anchorage system, composed entirely in steel, the elastic modulus is assumed to be E = 2.06*10^8 kN/m^2, while the yielding stress is s = 210*106 kN/m^2 and the hardening ratio is taken as m = 0.02. The bars are of three different sections, A, B and C, that, as we will see discussing about the 3-D model, will be distributed all along the length of the model for optimization purposes.
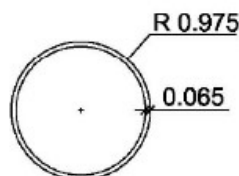
Section	R_{est} [m]	R_{int} [m]	Area [m^2]	I [m^4]	E [kN/m^2]	s [kN/m^2]	m [-]
A	0.993	0.871	0.351	0.139	2.06*10^8	210*10^6	0.02
B	0.975	0.91	0.385	0.171	2.06*10^8	210*10^6	0.02
C	1.029	0.961	0.425	0.211	2.06*10^8	210*10^6	0.02

Table 2 Geometrical and mechanical characteristic of the tunnel bars
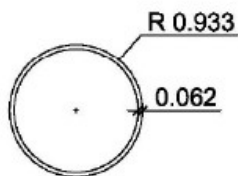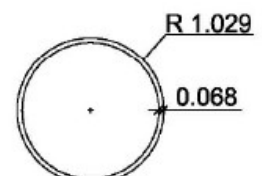

Figure 20 Geometry of bars section

4.1.2 How to Build a 2D Model

Now, we will explain in details how to obtain the model of this structure in ANSYS.

We considered three different sections along the span of the tunnel:

Midspan (section 35) at z = 2484 m with bars type A

Quarter-span (section 15) at z = 1044 m with bars type B

End of tunnel (section 5) at z = 324 m with bars type C

We will explain here how to obtain the model for the section at midspan, the same passages can be followed to construct the other two sections.

The files where written in .txt format and then launched into the program. The language used is the programming language proper of ANSYS Mechanical APDL and a detailed guide of all the commands can be found in the Help Section of the program.

The first step is to define the geometry of the structure, i.e. define the coordinates of the nodes, using the command '*N,Xcoord,Ycoord,Zcoord*'. The file 'master.txt' contains all the definition of such nodes and it is also the main file, containing all the secondary files, that should be launched in the program to run the analysis.

Remember that we considered only a piece of the tunnel of 72 m of length. The two tunnels where modelled with 5 nodes each separated by a distance of 18 m. For tunnel 1 the nodes numbering goes from 18139 to 18143 and for tunnel 2 from 118139 to 118143, in order to promptly identify to which part of the structure each node belongs.

Then we have to create the 4 points of the section of the tunnels from which anchorage bars depart, and these are identified with numbers:

Tunnel 1: 1293 – 1311 – 1312 – 1330

Tunnel 2: 31293 – 31311 – 31312 – 31330

Then we generate the nodes in which we will apply the constraints at the base of the anchoring bars into the ground:

Tunnel 1: 1302 - 1321

Tunnel 2: 31302 - 31321

Now, with the command 'FILL', we define the nodes of the anchoring bars. These are composed of 10 nodes which extremes are:

Tunnel 1: 1293-1302, 1302-1311, 1312-1321, 1321-1330

Tunnel 2: 31293-31302, 31302-31311, 31312-31321, 31321-31330

In the end, we add a linkage between the nodes 18141 and 118141 (central nodes) of the two tunnels, which nodes are 5001-5008.

To make a schematic summary you can refer to the table below:

	Tunnel Longitudinal	Tunnel Section	Base Constraints	Anchoring Bars	Linkage
Tunnel 1 Nodes	18139-18143	1293 1311 1312 1330	1302 1321	1293-1302, 1302-1311, 1312-1321, 1321-1330	5001-5008
Tunnel 2 Nodes	118139-118143	31293 31311 31312 31330	31302 31321	31293-31302, 31302-31311, 31312-31321, 31321-31330	5001-5008

Table 3 Nodes of the 2-D model midspan section

Then we have to create the elements that will be assigned to the tunnel and the anchoring bars with all the mechanical characteristics described before. The type of elements chosen by ANSYS library are presented in the table below:

No.	Component of SFT	Elements in ANSYS	Description
1	Tunnel	BEAM4	3-D Elastic
2	Anchoring bar	BEAM188	3-D Inelastic

Table 4 ANSYS type element used in the 2-D model

For a detailed description of the characteristics of BEAM4 and BEAM188, you can refer to APPENDIX D.

An example of ANSYS code for the definition of the elements is:

```
!!! CREATE ELEMENTS OF BARS SECTION (TYPE A) !!!

et,1,beam188
sectype,1,beam,ctube
secdata,0.871,0.933
mp,ex,1,2.06e11
mp,nuxy,1,0.3
mp,dens,1,5220/0.696


!!! CREATE ELEMENT OF THE TUNNEL !!!

et,2,beam4
sectype,2,beam,ctube
r,2,58.24,1637,1637,,2
mp,ex,2,2.943e10
mp,dens,2,1560000/9.81/58.24
mp,gxy,2,1.131923077e10
!mp,gxy,2,ex/2.6
```

Figure 21 Code definition of the ANSYS elements used in the 2.D model

Then, we proceed creating the elements with the command '*E,node1,node2*' and assigning the element's characteristics before created to each element.

With the command 'ACEL,,9.81' ANSYS considers automatically the self-weight of the elements in the analysis. So, in the next step of the definition of the forces, you DON'T have to input the forces related to the self-weight of the structure.

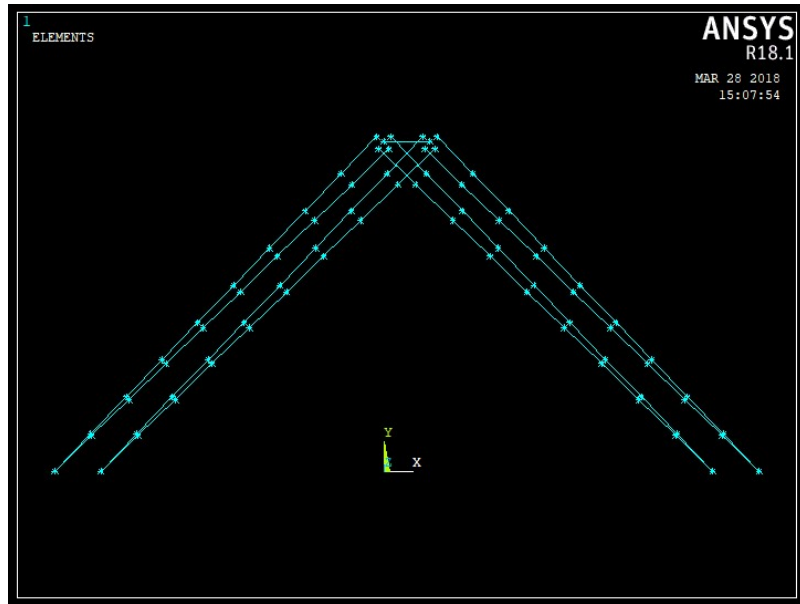At this point, the model as the aspect shown below and geometrically is fully defined.

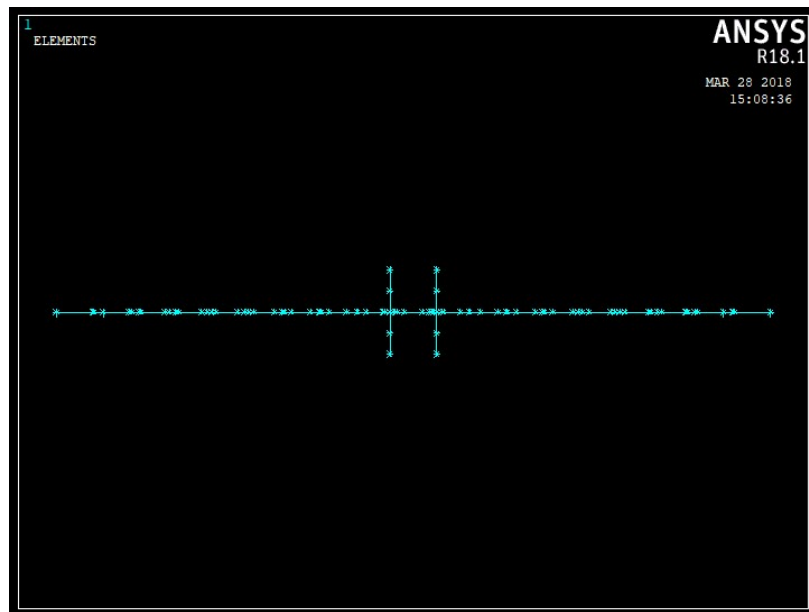*Figure 22 Frontal view of elements of the ANSYS 2-D model midspan section*

Figure 23 Upper view of elements of the ANSYS 2-D model midspan section

Figure 24 Nodes number of the ANSYS 2-D model

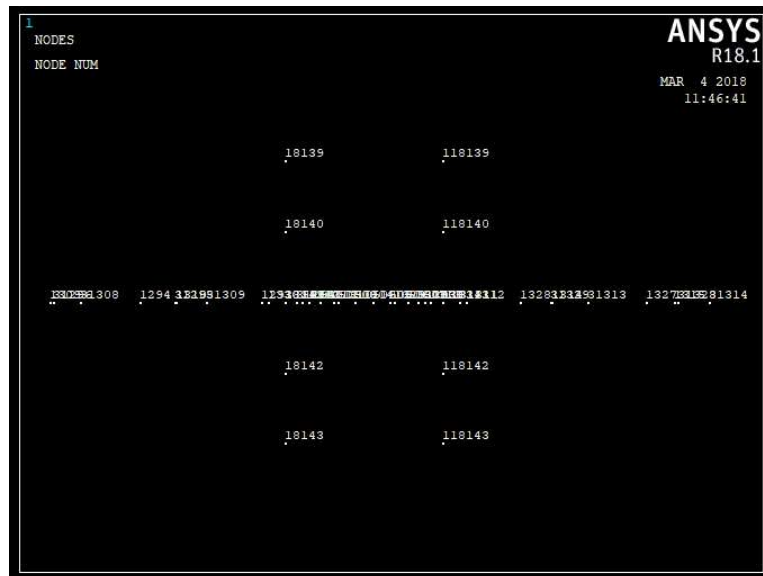*Figure 25 Nodes number of the ANSYS 2-D model*

For the section at a quarter span, with bars type B at z = 1044m, you can refer to the following table for nodes numbering:

	Tunnel Longitudinal	Tunnel Section	Base Constraints	Anchoring Bars	Linkage
Tunnel 1 Nodes	18059-18063	533 552 551 570	542 561	533-542, 542-550, 553-561, 561-570	5001-5008
Tunnel 2 Nodes	118059-118063	30533 30552 30551 30570	30542 30561	30533-30542, 30542-30550, 30553-30561, 30561-30570	5001-5008

Table 5 Nodes for the generation of ANSYS model of quarter span section
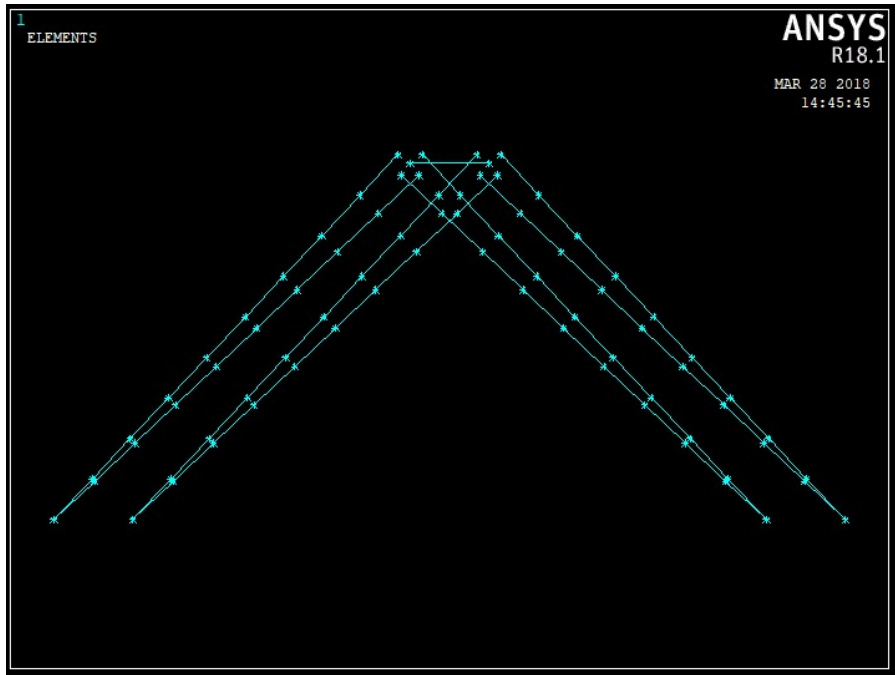
The model is has shown below:

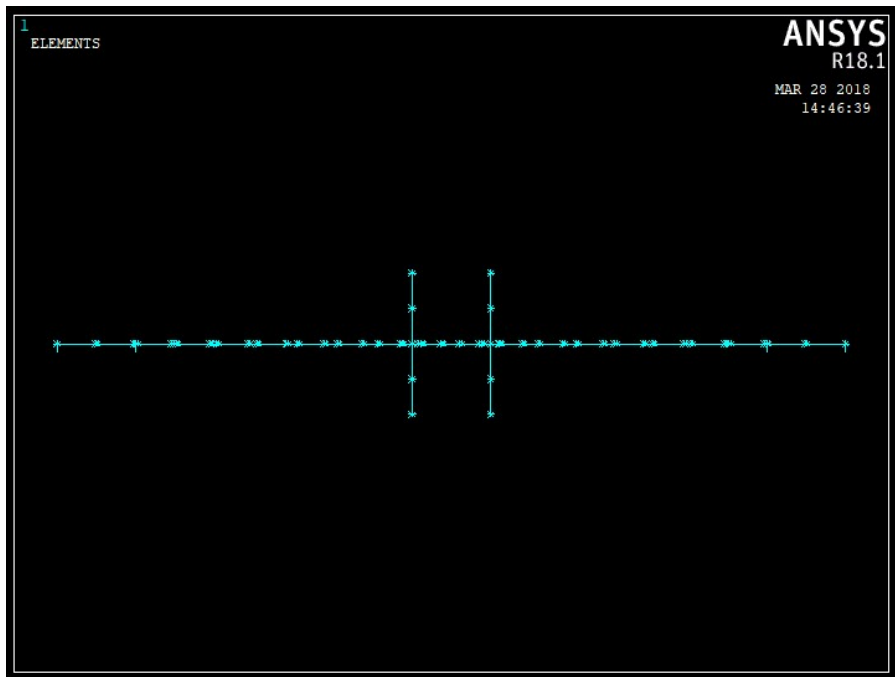*Figure 26 Transversal view of elements of quarter-span section*

Figure 27 Upper view of elements of quarter section

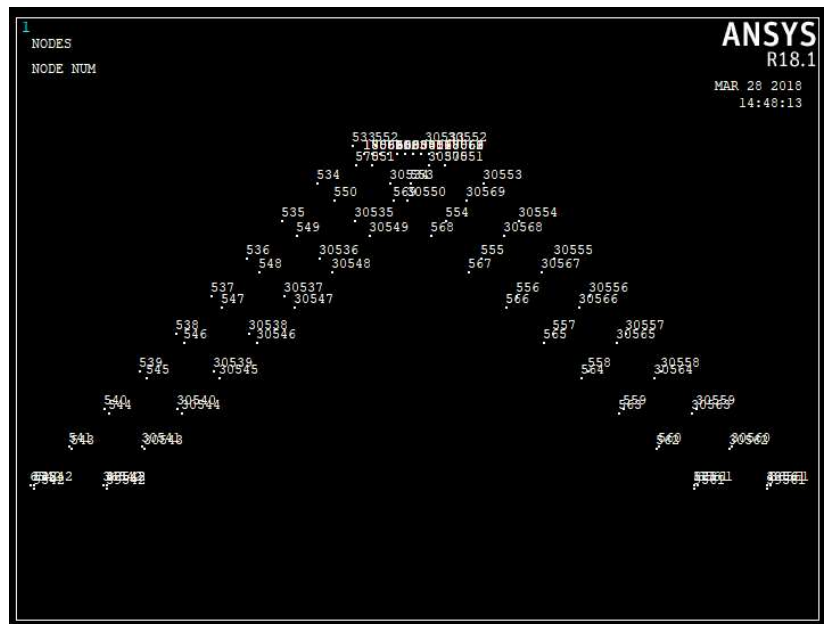*Figure 28 Upper view of nodes of quarter span section*

Figure 29 Transversal view of nodes of quarter span section

The nodes of the section at the end of the tunnel with bars type C at z=324m can be found in the table below:

	Tunnel Longitudinal	Tunnel Section	Base Constraints	Anchoring Bars	Linkage
Tunnel 1 Nodes	18019-18023	153 172 171 190	162 181	153-162, 162-170, 173-181, 181-190	5001-5008
Tunnel 2 Nodes	118019-118023	30153 30172 30171 30190	30162 30181	30153-30162, 30162-30170, 30173-30181, 30181-30190	5001-5008

Table 6 Nodes for the generation of ANSYS model of end section

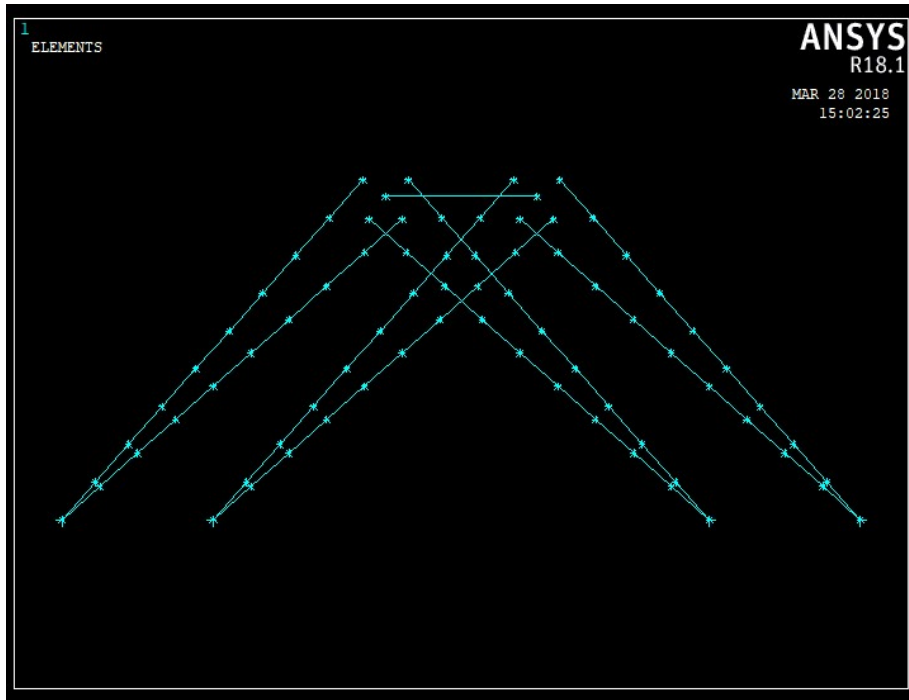Below you can find the scheme of the model in ANSYS:
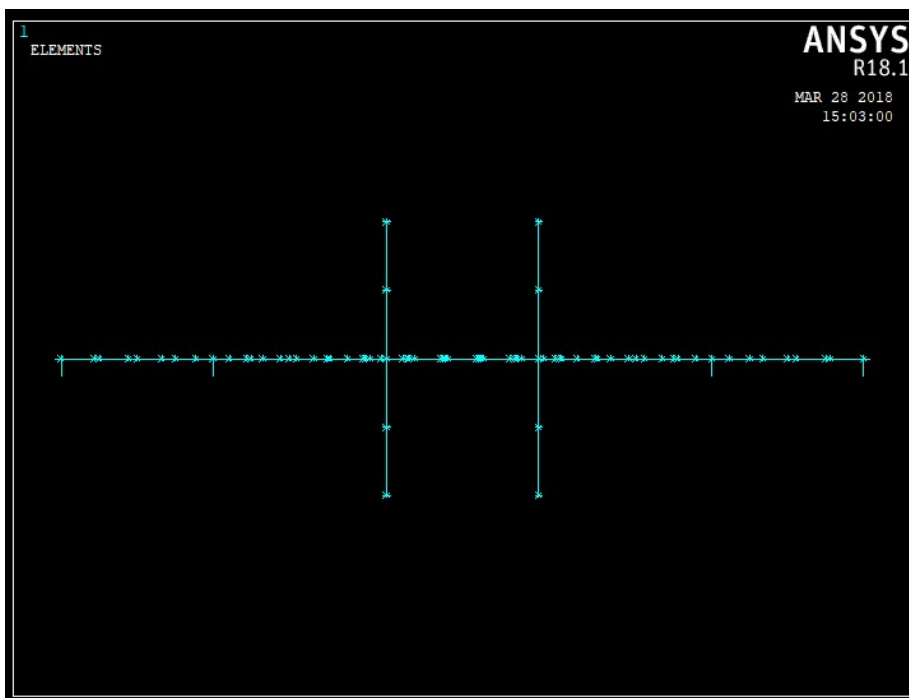
Figure 30Transversal view of elements of end section

Figure 31 Upper view of elements of end section

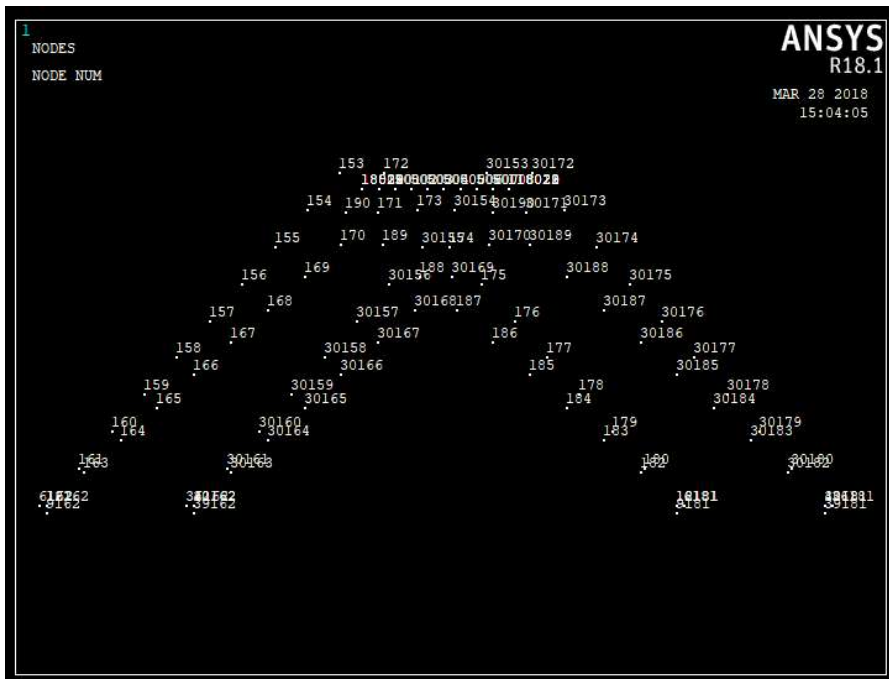*Figure 32 Upper view of nodes of end section*

Figure 33 Transversal view of nodes of end section

4.1.3 Extending the 2D model: The 3D Model

In the 3-D model, we basically extend our 72m tunnel to its entire length of 4680 km.

Respect the other model in this case there are three different type of anchorage bars that are described in the same way.

The type of elements chosen by ANSYS library are presented in the table below:

No.	Component of SFT	Elements in ANSYS	Description
1	Tunnel	BEAM4	3-D Elastic
2	Anchoring bar A	BEAM188	3-D Inelastic
3	Anchoring bar B	BEAM188	3-D Inelastic
4	Anchoring bar C	BEAM188	3-D Inelastic

Table 7 ANSYS type element used in the 3-D model

The ANSYS code definition for these elements is:

```
!!! CREATE ELEMENTS OF BARS SECTION (TYPE A)

et,1,beam188
sectype,1,beam,ctube
secdata,0.871,0.933
mp,ex,1,2.06e11
mp,nuxy,1,0.3
mp,dens,1,5220/0.696

!!! CREATE ELEMENTS OF BARS SECTION (TYPE B)

et,3,beam188
sectype,3,beam,ctube
secdata,0.91,0.975
mp,ex,3,2.06e11
mp,nuxy,3,0.3
mp,dens,3,5775/0.770

!!! CREATE ELEMENTS OF BARS SECTION (TYPE C)

et,4,beam188
sectype,4,beam,ctube
secdata,0.961,1.029
mp,ex,4,2.06e11
mp,nuxy,4,0.3
mp,dens,4,6375/0.850

!!! CREATE ELEMENT OF THE TUNNEL !!!

et,2,beam4
sectype,2,beam,ctube
r,2,58.24,1637,1637,,2
mp,ex,2,2.943e10
mp,dens,2,1560000/9.81/58.24
mp,gxy,2,1.131923077e10
!mp,gxy,2,ex/2.6
```

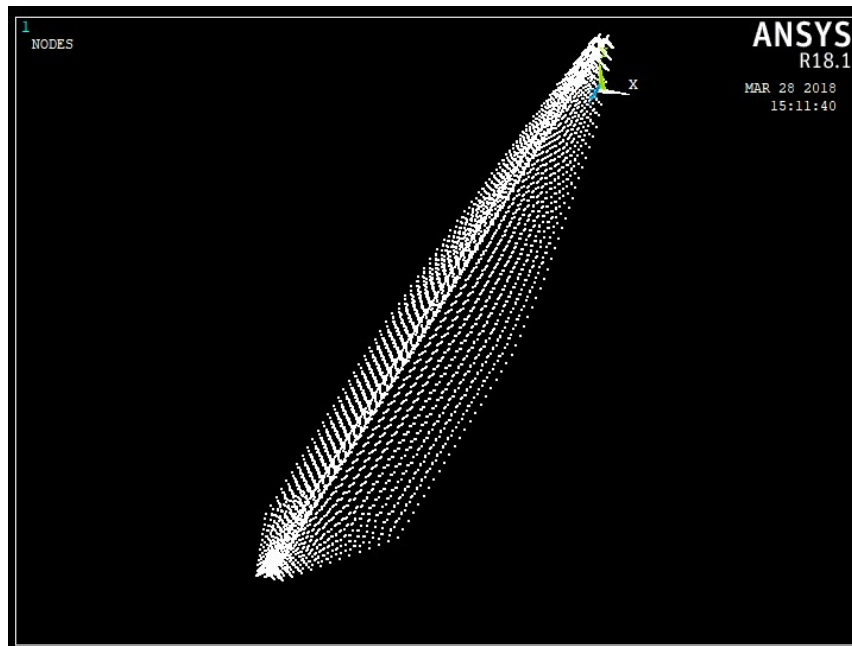*Figure 34 Code definition of the ANSYS elements used in the 2.D model*

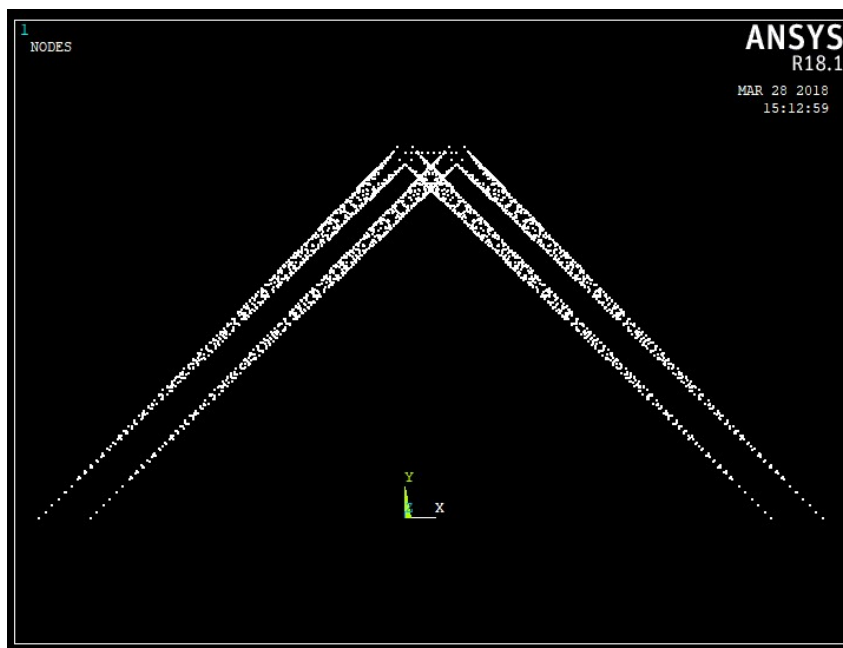*Figure 35 View of the nodes of the 3-D model*

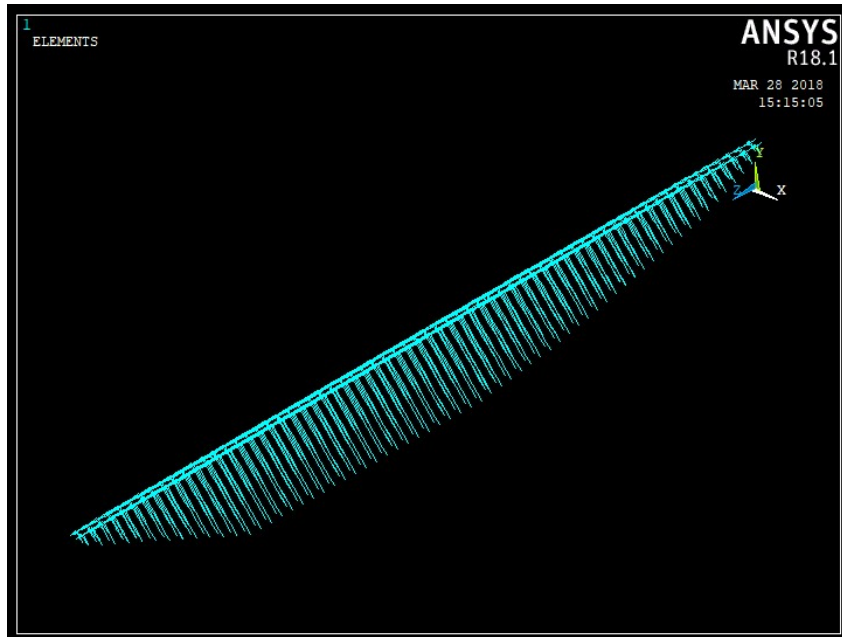*Figure 36 Sectional view of the nodes of the 3-D model*

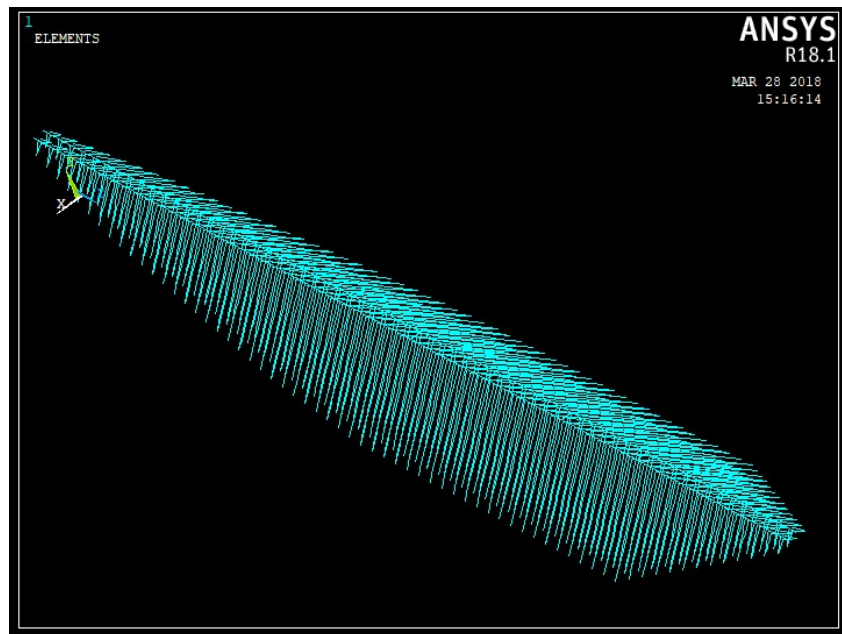*Figure 37 View of elements of 3-D model*

Figure 38 View of elements of 3-D Model

4.2 Static and Modal Analyses

4.2.1 Constraints

For both the 2-D model and 3D model, the application of the constraints deals with the creation of a rigid region for the section of the tunnel, and assigning constraints to the anchorage points to the ground and to the extremes of the tunnels.

Creating a rigid region for the section of the tunnel practically means to constraint all the degrees of freedom of the nodes of the section be equal to the master node of the section that, in case of section (35) at midspan, for tunnel 1 (in 2D analysis) is 18141 and for tunnel 2 (in 2D analysis) is 118141. This can be made using the command 'CERIG'.

For the application of constraints to a single node, you can use the command '*D,node,dof,0*'. For the anchorage points, we put a clamp, for the extremes of the tunnels instead, we constraint only the displacement in the transversal direction X (Z is the longitudinal axis of the tunnel and Y is the vertical one), so UX = 0 and the rotation around the Z axis, so ROZ = 0.

4.2.2 Loading Conditions: Self-Weight & Buoyancy Force

The loading conditions, for the purpose of the static and modal analyses that we are going to undertake in this Chapter, we have to consider only the static forces due to self-weight of the structural elements and the buoyancy force, for the fact that the tunnel is completely submerged in water.

Due to the location in deep water, the SFT model takes the fluid modelling fully into account. The static buoyancy force has a twofold effect on the behaviour of the anchoring system; first, the net buoyancy acting on the anchoring bars is very small (close to the neutral conditions), so that they are almost straight under normal static loading. This avoids catenary effects that can result in significant stiffness reduction when small oscillations due to the serviceability dynamic loading are considered.

Secondly, the net buoyancy acting on the tunnel results in a pre-stressing state for the anchoring bars, which are designed to be always tensioned under service loads.

The force per unit meter to be applied to the tunnel due to self-weight is the weight per unit length of the tunnel of 1200 kN/m increase of 30% to take into account the non-structural and variable loads. For the anchoring bars, the force due to self-weight have been calculated multiplying the density of steel that has a value of 7500 kg/m^3 by the net area of the section.

For the buoyance forces, instead, the Archimede's Principle for Buoyancy was used, that states:

"The upward buoyant force that is exerted on a body immersed in a fluid, whether fully or partially submerged, is equal to the weight of the fluid that the body displaces and acts in the upward direction at the centre of mass of the displaced fluid."

Translated in mathematical form:

$$S_A = (\rho_a * g * V_{tot})$$

Where:

g – gravity acceleration

ρ_a – desity of water equal to 1020 kN/m^3

V_{tot} – total volume of water displaced by the element.

The values obtained are shown in the following table:

	Self-Weight [kN/m]	Buoyancy Force [kN/m]	Total Length [m]	Buoyancy Ratio [-]
Tunnel	1560	1999.31	72	-
Bar Type A	25.85	27.36	403	1.06
Bar Type B	28.32	29.88	238	1.06
Bar Type C	31.28	33.29	117	1.06

Table 8 Values of the self-weight and buoyancy forces

For the application of the forces in ANSYS, we have to consider only the buoyancy force, since, as discussed, the self-weight is considered automatically by the program.

For the tunnel the function SFBEAM is used, that assigns a weight per unit length to the elements of the tunnel.

For the bars, instead, the command F is used, which enables to add a force in a single node. So the values of the buoyancy forces of the table must be multiplied by the length of the bar and divided by 9, that are the elements composing each bar. In this way you obtain the value of the force to be applied in each internal node (in which two bars converge). For the two extreme nodes, you have to divide this force by 2, since in that nodes only one bar converges.

Last step is to set ANTYPE to STATIC and then MODAL and run the analysis. The results are discussed in the following paragraph.

4.2.3 Results of Static Analysis

The static analysis was done to validate our model and see if all the properties and forces were assigned in the correct way. We want to design a SFT that, under static condition, will float a little bit upwards in order to put in tension the anchoring bars and avoid buckling effects of these ones.

2-D Model

For the 2-D model, we obtained the deformed shape shown in the following figures:
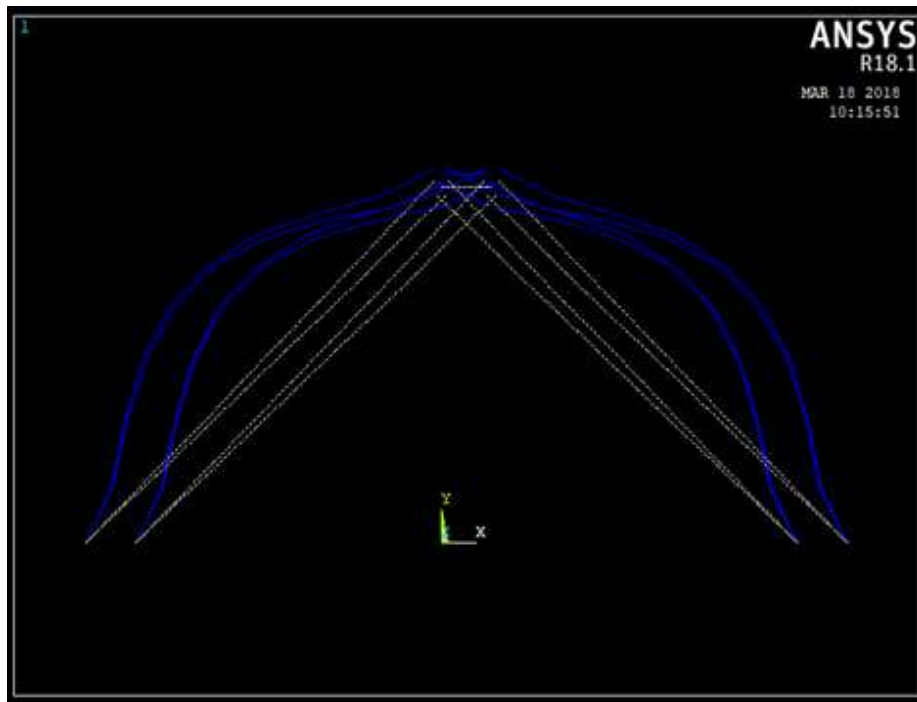
Figure 39 Deformed shape of the section in the 2-D model (frontal view) midspan section
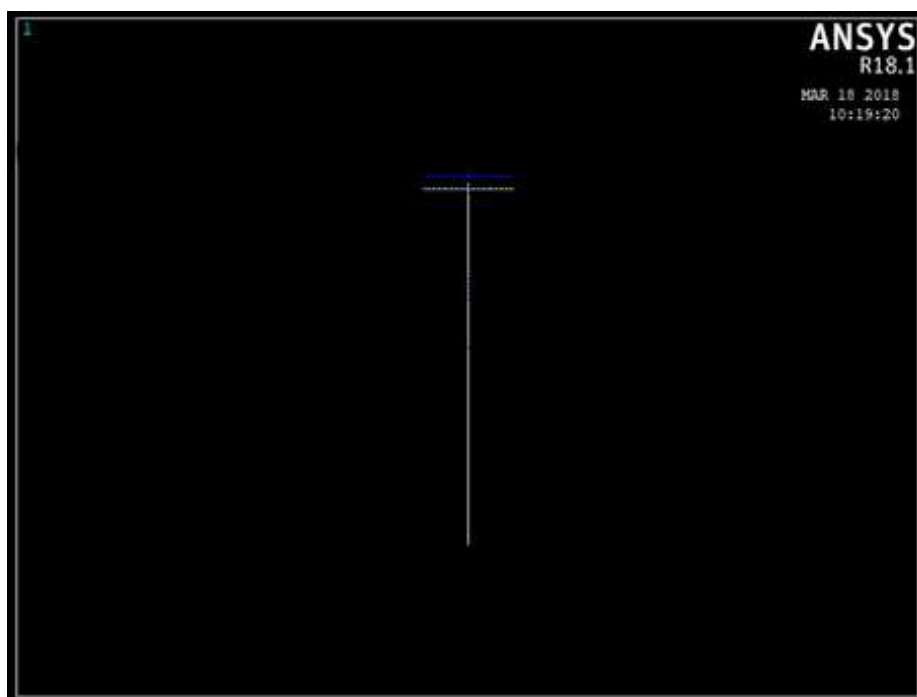

Figure 40 Deformed shape of the section in the 2-D model (upper view midspan section)
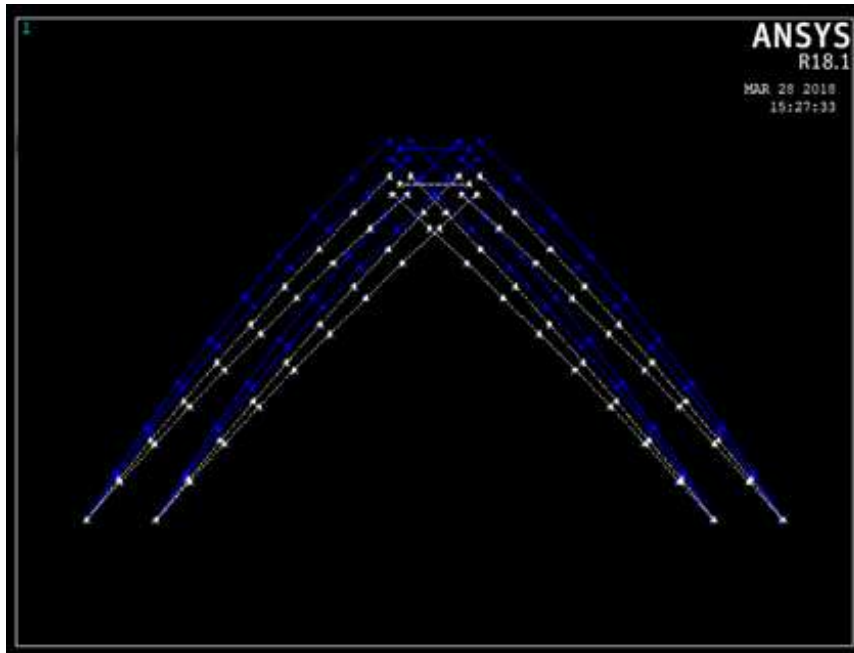
Figure 41 Deformed shape of the section in the 2-D model (frontal view) quarter span section
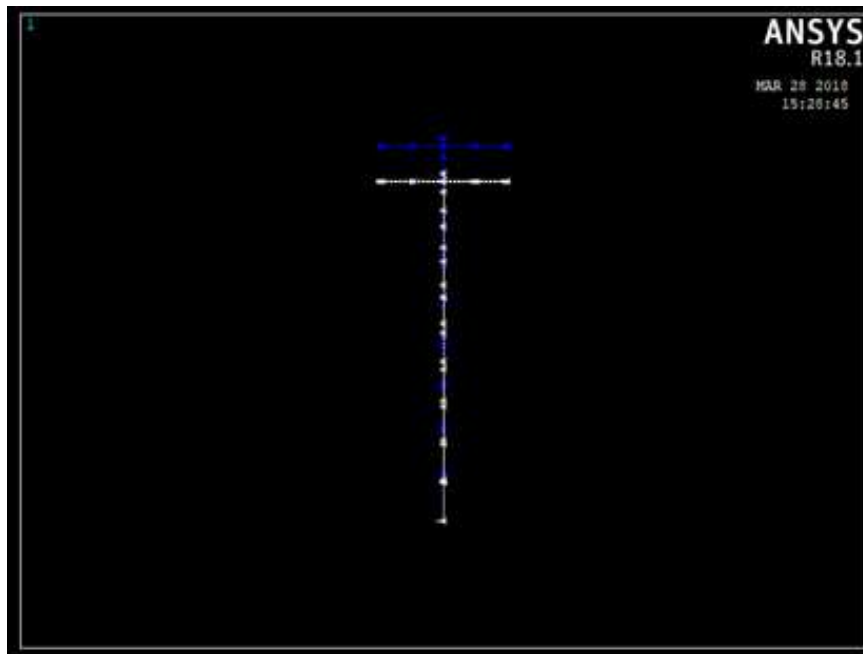

Figure 42 Deformed shape of the section in the 2-D model (upper view quarter span section)
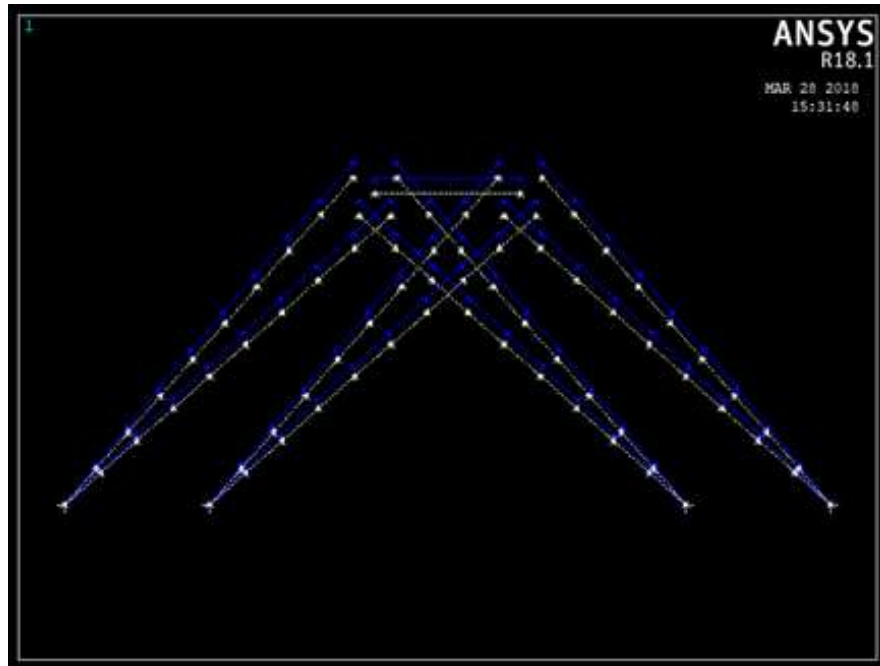
Figure 43 Deformed shape of the section in the 2-D model (frontal view) end section
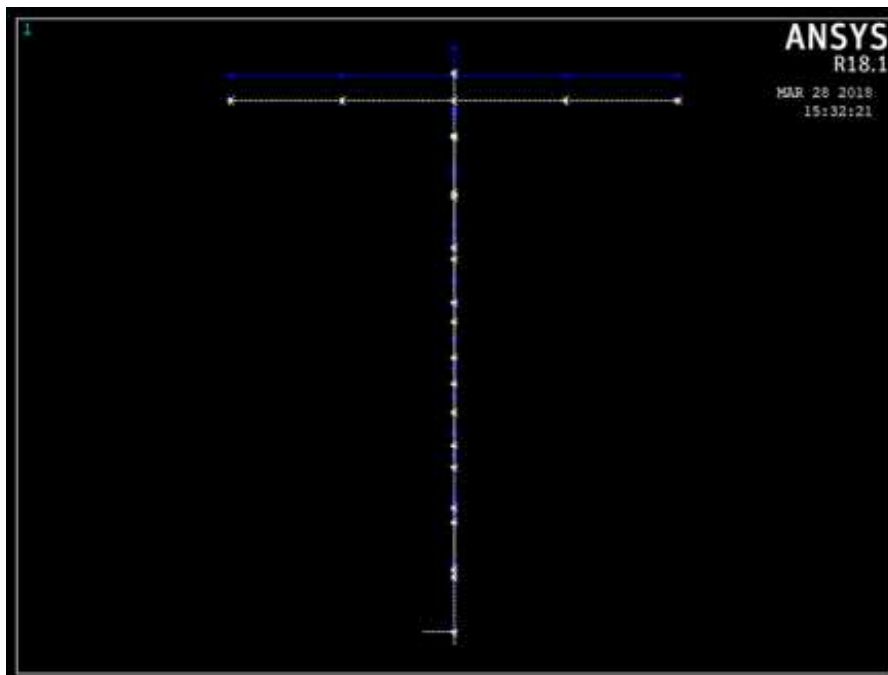
Figure 44 Deformed shape of the section in the 2-D model (upper view end section)

Analysis of SFT Resting on Flexible Soil Strata Subjected to Seaquake Excitation

We can see how the tunnel is subjected to a prevailing buoyancy force that tends to push it upwards, with a displacement of the two tunnels can be found in the following table.

Section	Maximum Displacement in Vertical Direction [cm]
Midspan (35 – Bars A)	89.57
Quarter-span (15 – Bars B)	65.02
End of Tunnel (5 – Bars C)	34.76

Table 9 Results of static analysis for 2-D Model

We can notice how the displacement is more pronounced at midspan and decreases moving towards the end of the tunnel.

Extending to the 3-D Model, we obtained the same deformed shape as shown above, but with a more rigid behaviour due to the interaction between the various sections of the tunnel. The displacement of the two tunnels is the correspondence of the section that was used for the 2D analysis is 89.04 cm.

Figure 45 Deformed shape of the section in the 3-D model (upper view)

Figure 46 Deformed shape of the section in the 3-D model (upper view)

105

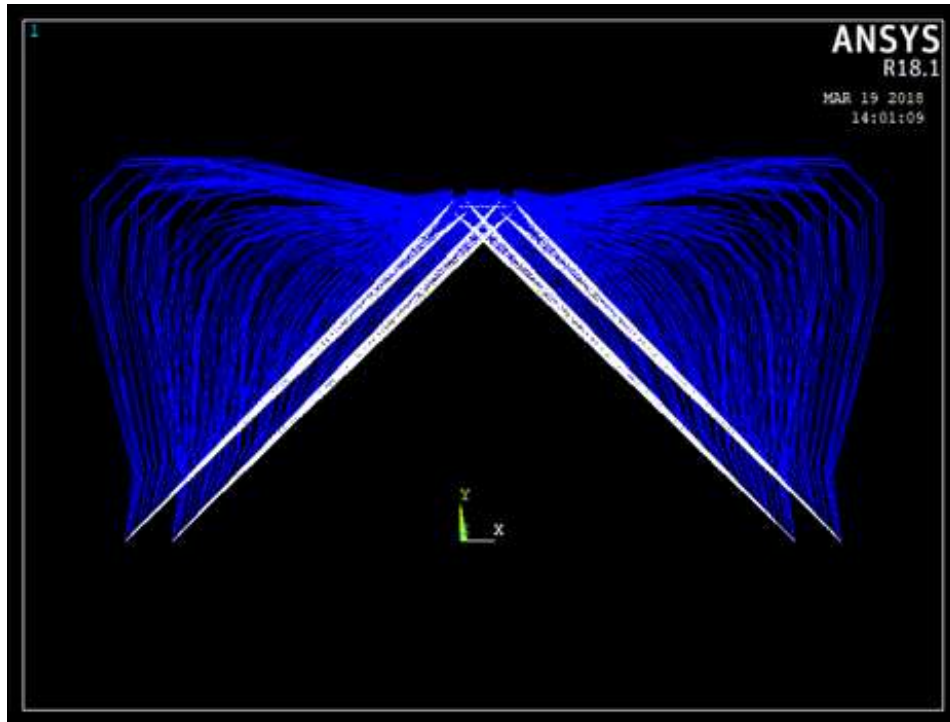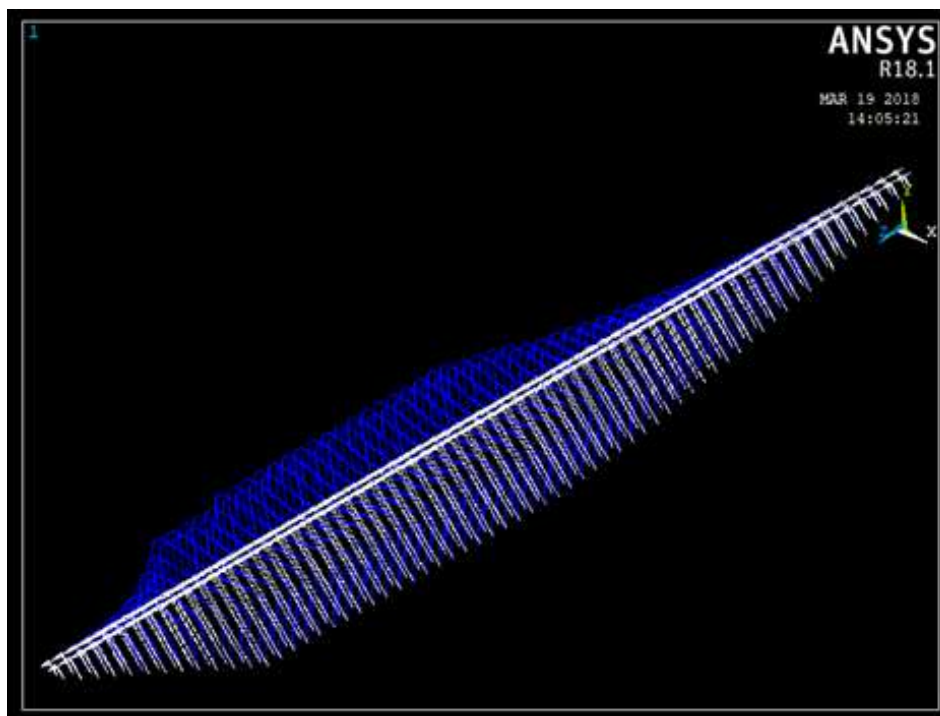## 4.2.4 Results of Modal Analysis: Modal Shapes

4.2.4.1 Modal Analysis of 2-D Model

Here you can find the results of the modal analysis on the 2-D Model. The modes are of different types. We can distinguish between in-plane modes, which refer to the transversal movement of the cables, and out-of-plane modes, which refer to the longitudinal motion of the cables. The former can be furthermore subdivided in symmetric and anti-symmetric modes.

In the following tables, the natural periods and frequencies derived from the analysis in ANSYS (that will be therefore labelled as Experimental) are reported:

	Experimental Period T_{ANSYS}		
Mode	In Plane Sym	In Plane AntiSym	Out Plane
1	13,47836049	-	13,18339
2	-	4,542357484	4,521818
3	2,138259884	-	2,120081
4	-	1,315356791	1,14321
5	0,662427133	-	0,662383
6	-	0,402933355	0,403047

Table 10 Experimental period obtain from ANSYS (T_{ANSYS})

	Experimental Frequencies T_{ANSYS}		
Mode	In Plane Sym	In Plane AntiSym	Out Plane
1	0,074193	-	0,075853
2	-	0,22015	0,22115
3	0,46767	-	0,47168
4	-	0,76025	0,87473
5	1,5096	-	1,5097

6	-	2,4818	2,4811

Table 11 Experimental frequencies obtain from ANSYS (TANSYS)

In order to check our model, we calculated the natural periods of the bars with a theoretical approach based on the theory of dynamics of suspended cables (Irvine – Cable Structures). The results obtained can be found in the following table. As we can observe, the periods, especially for the first modes, are quite similar to what we theoretically expected. So we can say that our anchoring bars have a behaviour similar to that of a cable.

	Theoretical Period T_{th}		
Mode	In Plane Sym	In Plane AntiSym	Out Plane
1	14,28571429	-	14,09915
2	-	3,524786733	7,049573
3	3,174603175	-	4,699716
4	-	1,762393366	3,524787
5	0,403225806	-	2,819829
6	-	1,174928911	2,349858

Table 12 Theoretical period (T_{th})

According to Irvine book, we consider a uniform flat-sag suspended cable anchored on supports at the same level. If we give a slight disturbance to this cable, we can write its equation of motion.

Out-of-Plane Modes

From the solution of the equation of motion by separation of variables, we can derive the natural frequencies of the out-of-plane motion as:

$$\omega_n = \frac{n\pi}{l}\left(\frac{H}{m}\right)^{1/2} \tag{4.1}$$

and the associated modes:

$$\widetilde{v_n} = A_n sin\frac{n\pi x}{l} \tag{4.2}$$

where n=1,2,3... signify the first, second, third modes, respectively and so on. H is the thrust of the cable, m is the mass per unit length and l is the distance between the two supports of the cable.

The frequency of the first out-of-plane mode is the lowest of any given flat-sag suspended cable.

In-Plane Modes

Regarding the in-plane motion, we should distinguish between symmetric and anti-symmetric in plane modes.

A symmetric in-plane mode is defined as one in which the vertical component of the mode is symmetric. And, vice versa, an anti-symmetric in-plane mode is defined as one in which the vertical component of the mode is anti-symmetric.

Anti-Symmetric

For the anti-symmetric in plane modes, the equation to find the natural frequencies is the following one, where the meaning of the terms is the same as the previous equation:

$$\omega_n = \frac{n\pi}{l}\left(\frac{H}{m}\right)^{1/2}$$

and the vertical modal components are given by:

$$\widetilde{w_n} = A_n \sin\frac{2n\pi x}{l}, \quad \text{n=1,2,3,...}$$ (4.3)

Symmetric

In the case of symmetric in-plane modes, additional tension is induced and the problem becomes more complicated. To find the natural frequencies, the following transcendental equation should be solved:

$$\tan\frac{\omega}{2} = \frac{\omega}{2} - \frac{4}{\lambda^2}\left(\frac{\omega}{2}\right)^3$$ (4.4)

The solution of this equation and the natural frequencies of the first modes can be found in tables provided by the author.

For more details about the derivation of the above equations, you can refer to the book *Cable Structure* by Irvine.

Here you can find the representation of the modal shapes of the in-plane and out-of-plane modes.
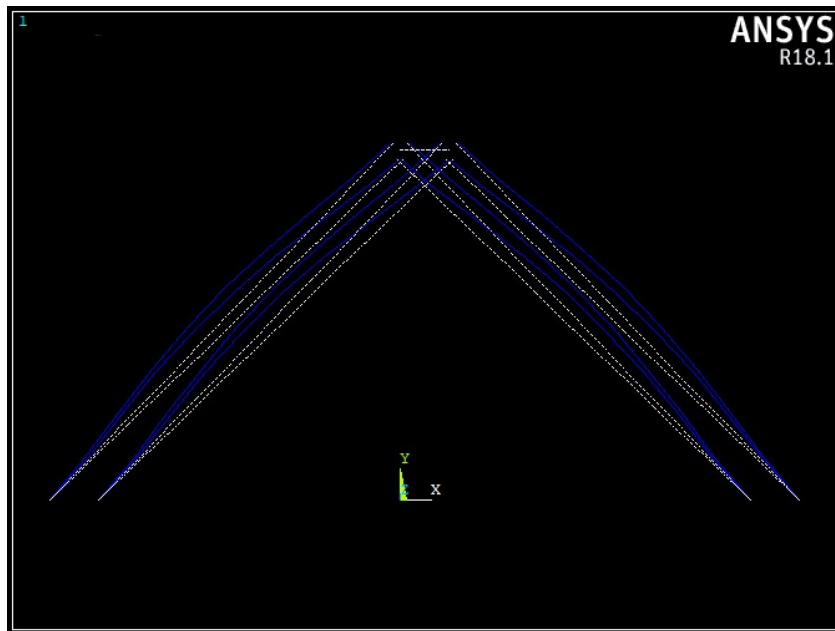
1) In plane symmetric

Figure 47 First in plane symmetric mode
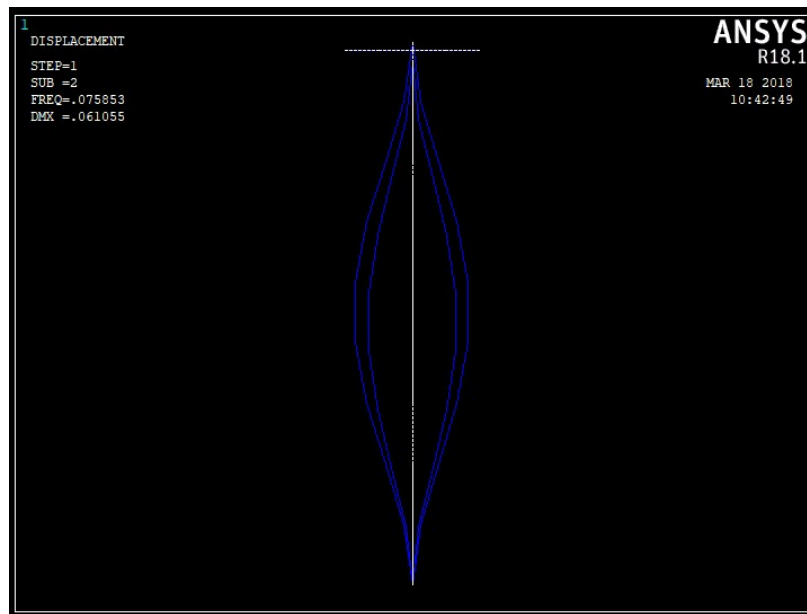
Out of Plane

Figure 48 First out of plane mode

2) In plane anti-symmetric

Figure 49 Second in plane anti-symmetric mode

Out of Plane

Figure 50 Second out of plane mode

3) In plane symmetric

Figure 51 Third in plane anti-symmetric mode

Out of plane

Figure 52 Third out of plane mode

4) In plane anti-symmetric

Figure 53 Fourth in plane anti-symmetric mode

Out of plane

Figure 54 Fourth out of plane mode

5) In plane symmetric
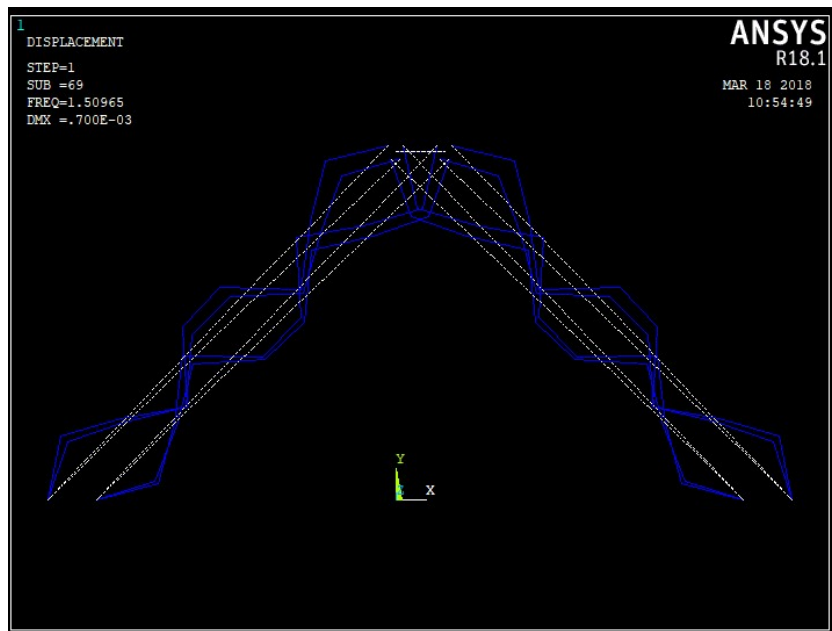
Figure 55 Fifth in plane symmetric mode
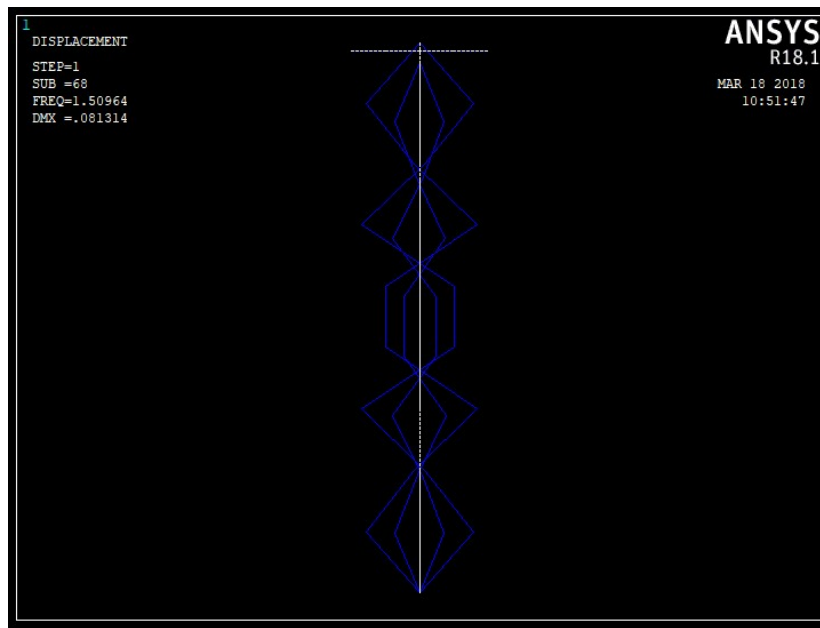
Out of Plane

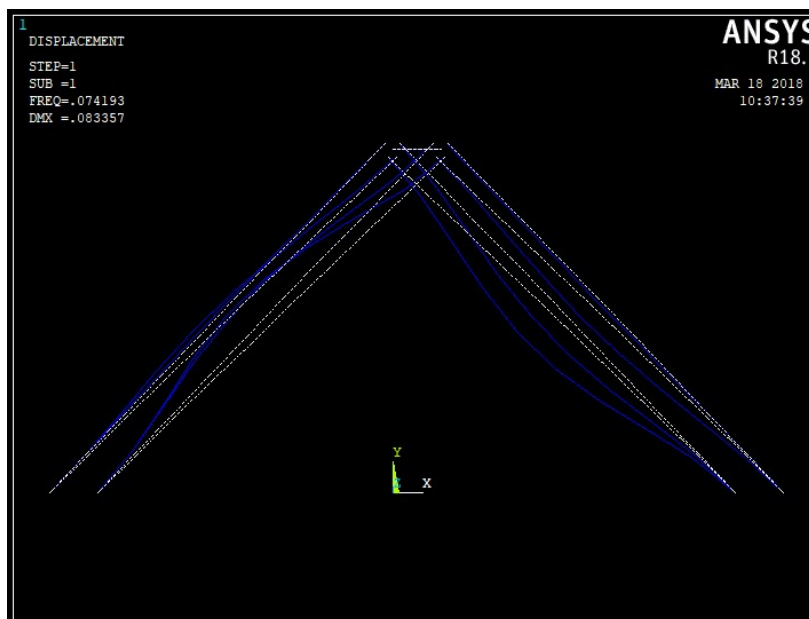*Figure 56 Fifth out of plane mode*

6) In plane anti-symmetric

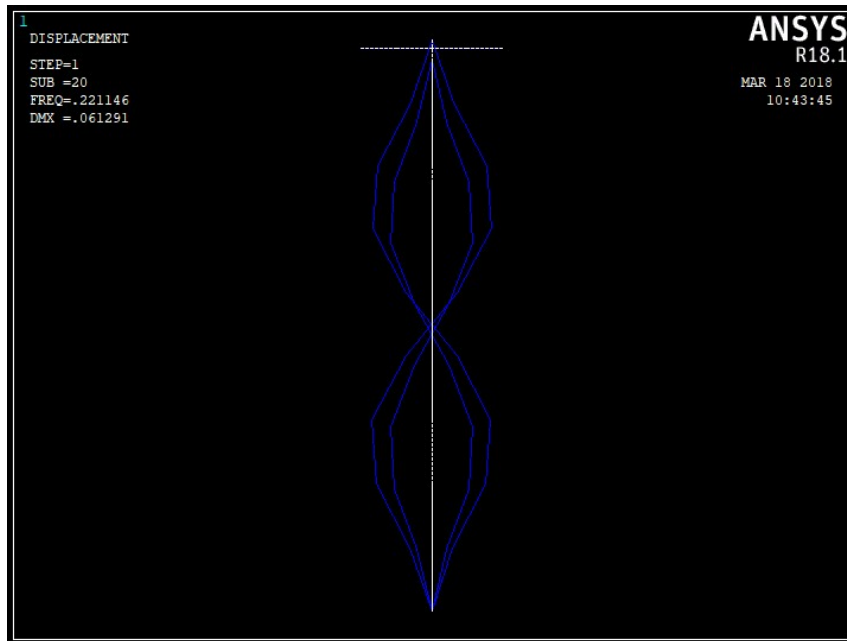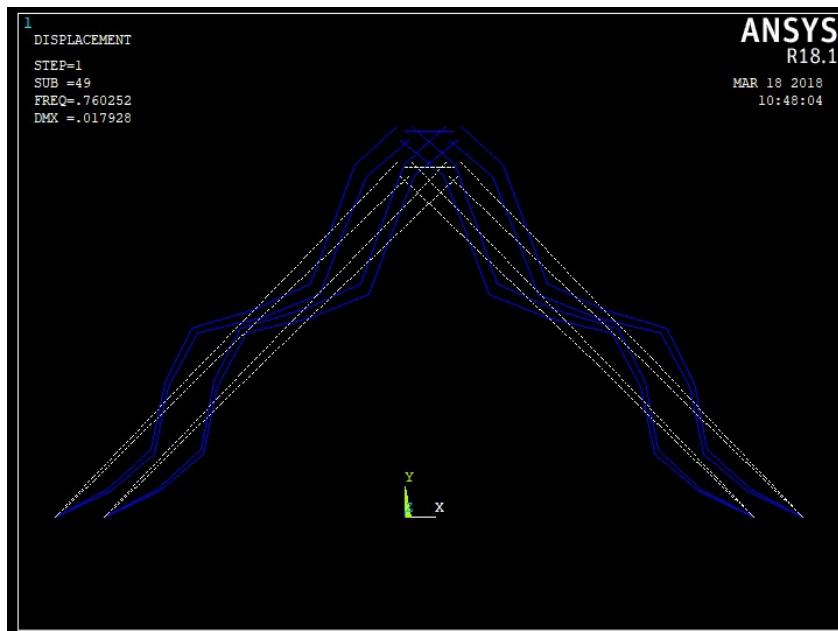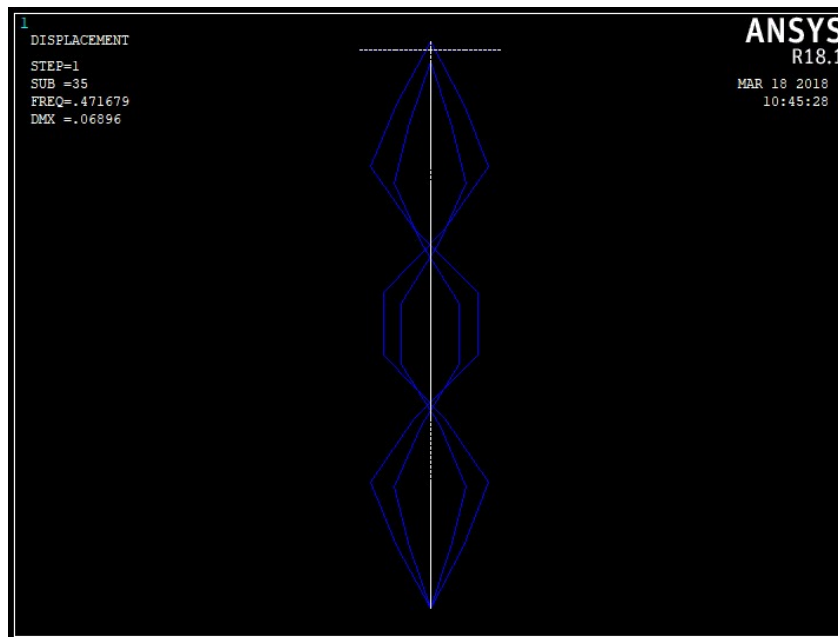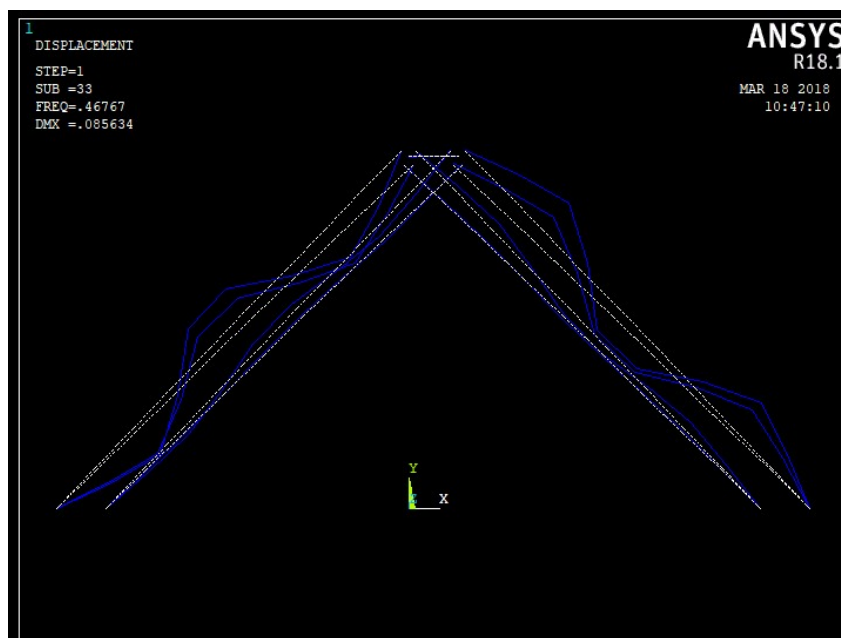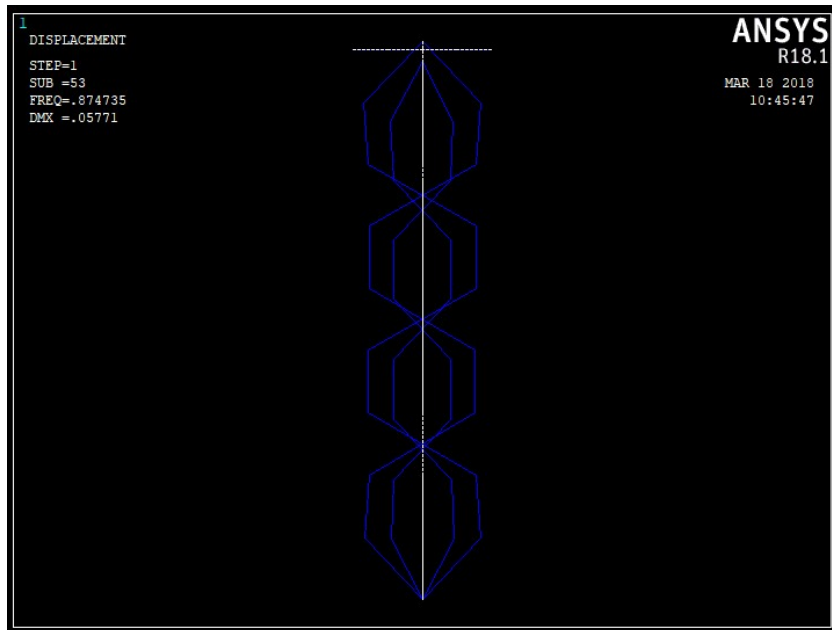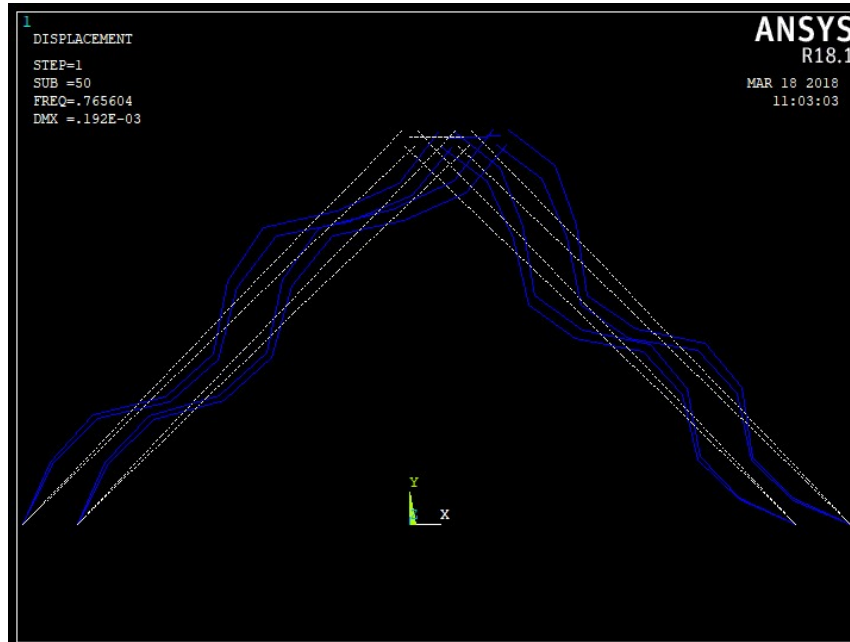*Figure 57 Sixth in plane anti-symmetric mode*
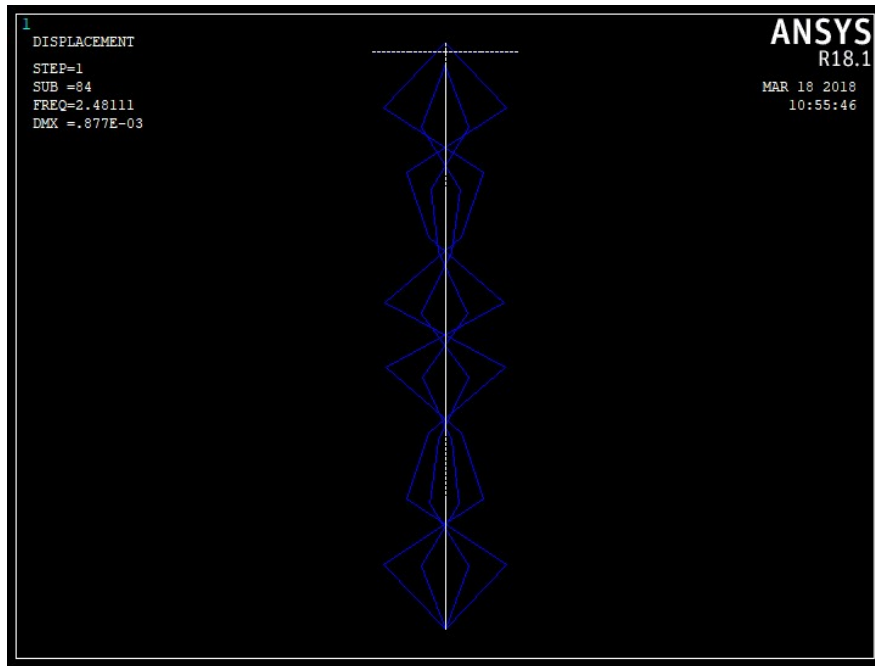
Out of Plane

Figure 58 Sixth out of plane mode

4.2.4.2 Modal Analysis of 3-D Model

The modal analysis of the whole SFT structure is based on the static configuration. As a result, the modal analysis results shows a large number of bars' local mode shapes, leading to a very complex picture of the vibration modes in which the tunnel behaviour is partially hidden. To solve this problem and get a clearer image of tunnel vibrations, a simplified model where the anchor bars inertia is concentrated only at the ends was set, in order to override the bars' local modes.

The results of the real 3-D modal analyses are reported in the following table.

Mode	Description	Natural frequencies [Hz]
1	Tunnel first longitudinal vibration mode	0.196
2	Tunnel second longitudinal vibration mode	0.391
3	Tunnel first transversal vibration mode	0.580
4	Tunnel first vertical vibration mode	0.580
5	Tunnel second transversal vibration mode	0.585
6	Tunnel second vertical vibration mode	0.585

Table 13 Natural frequencies of the 3-D model obtain from ANSYS

1) Tunnel first longitudinal vibration mode
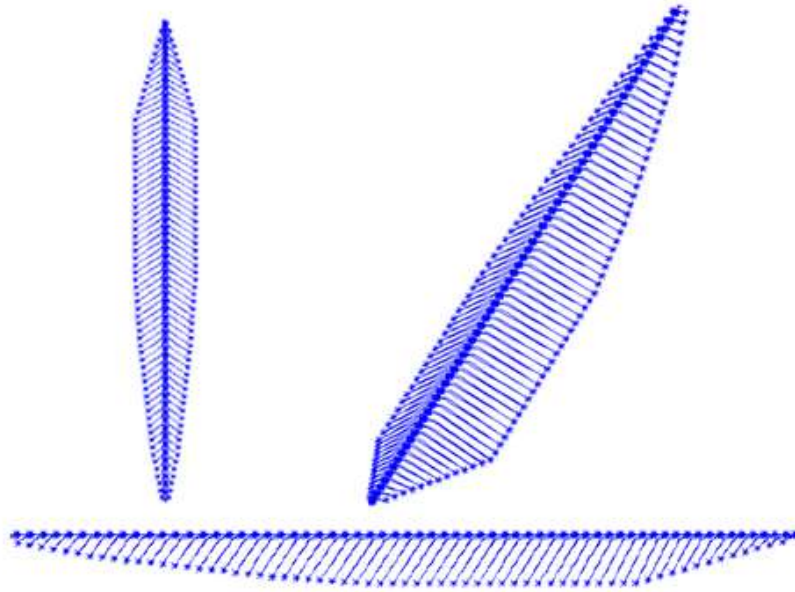
Figure 59 First mode of the 3-D model

2) Tunnel second longitudinal vibration mode
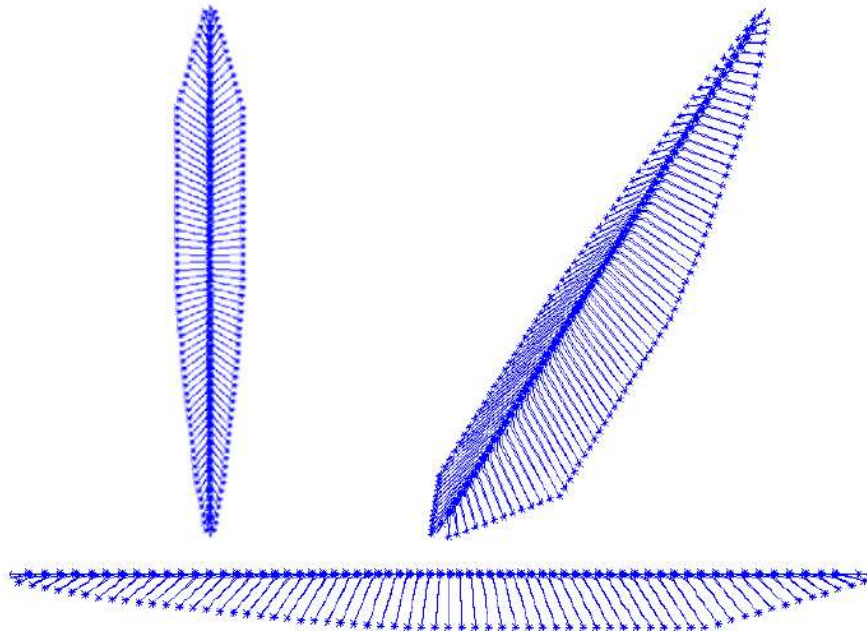
Figure 60 Second mode of the 3-D model

3) Tunnel first transversal vibration mode
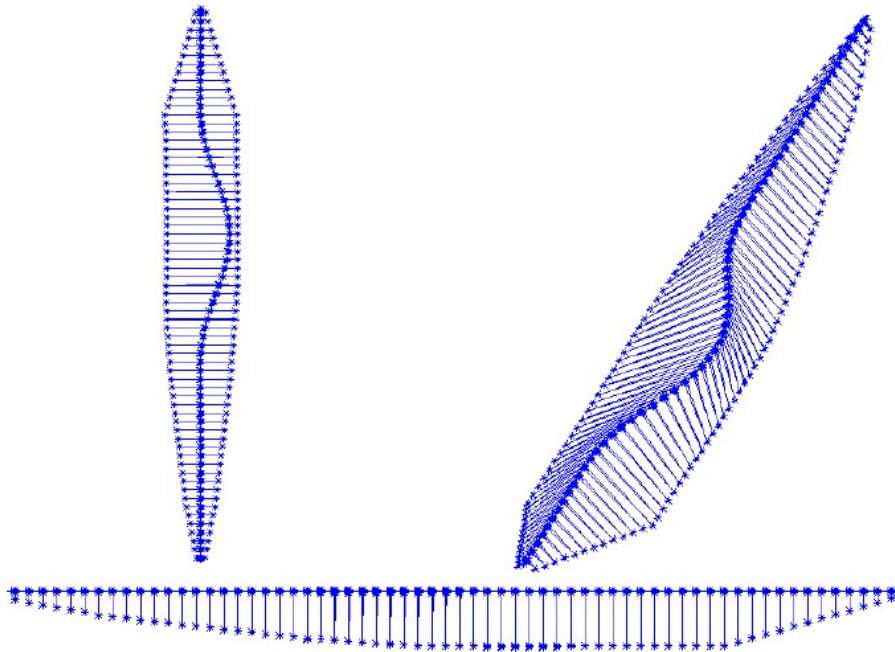
Figure 61 Third mode of the 3-D model

4) Tunnel first vertical vibration mode
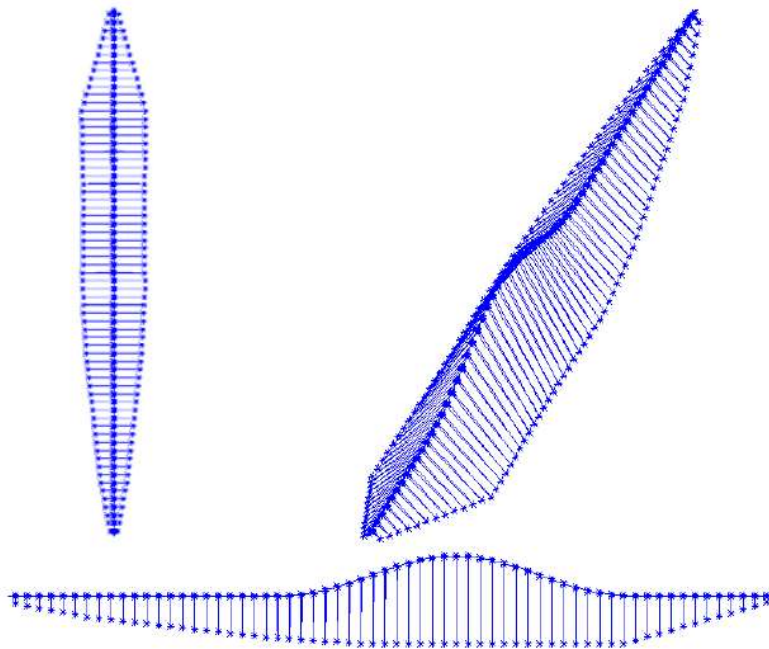
Figure 62 Fourth mode of the 3-D model

5) Tunnel second transversal vibration mode
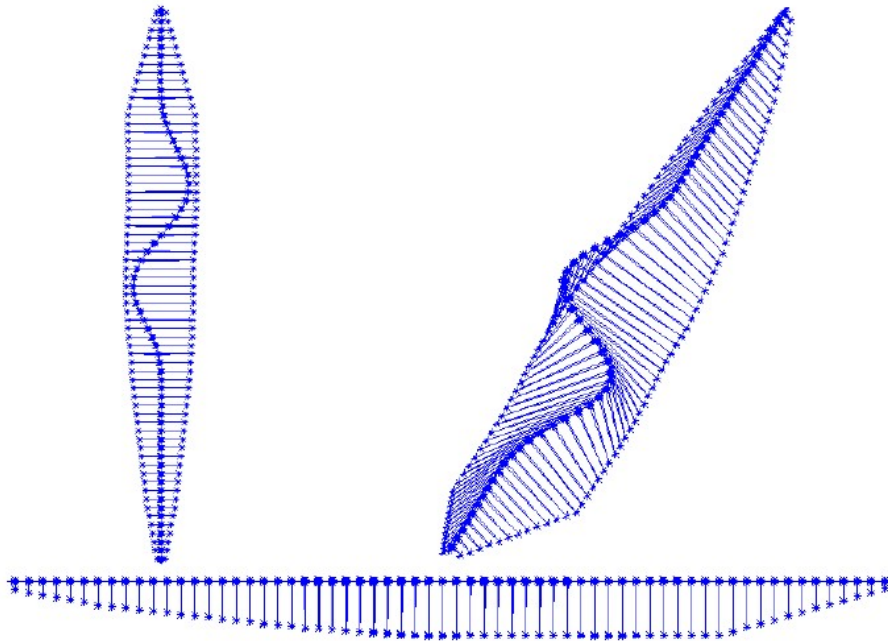
Figure 63 Fifth mode of the 3-D model

6) Tunnel second vertical vibration mode
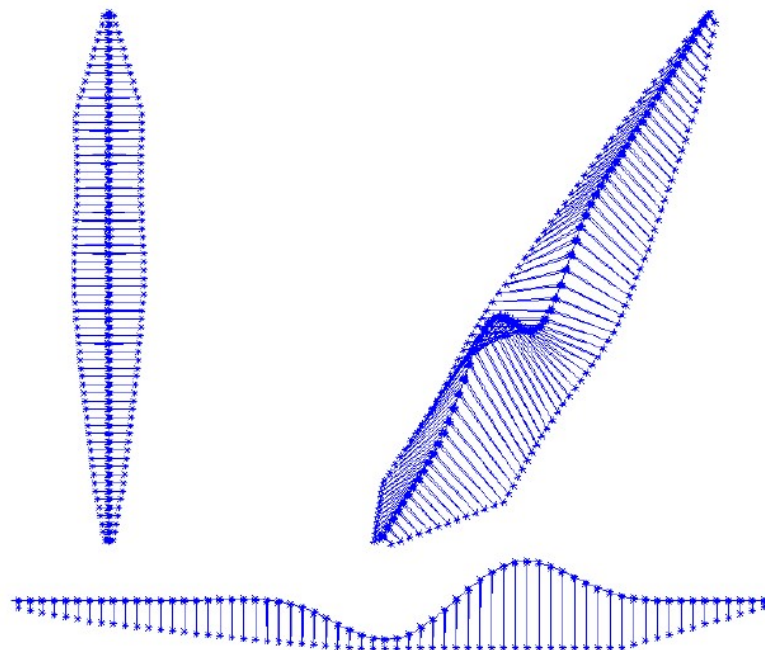
Figure 64 Sixth mode of the 3-D model

4.3 Conclusions

In this chapter, we have seen how to build the 2-D and 3-D models of our case-study Submerged Floating Tunnel under the Messina Strait.

Then we performed a preliminary Static and Modal Analysis to test the behaviour of our model mainly under static conditions and confronted the results obtained with theoretical theories and considerations.

With this model set-up, we are ready to enter the dynamic phase, apply hydrodynamic forces to the tunnel, and evaluate its response.

References Chapter 4

[4-1] Di Pilato, M., Perotti, F., Fogazzi, P. (2008), 3D dynamic response of submerged floating tunnels under seismic and hydrodynamic excitation, *Engineering Structures*, **30**, 268-281.

[4-2] Di Pilato, M., Feriani, A., Perotti, F. (2008), Numerical models for the dynamic response of submerged floating tunnels under seismic loading, *Earthquake Engineering and Structure Dynamics*, **37**,1203-1222.

[4-3] Moore P.J. (1985), Analysis and Design of Foundations for Vibrations, *A.A.Balkema Publishers: Rotterdam*.

[4-4] H. Max Irvine – Cable Structures, 1981

[4-5] Aspetti Geologici e di Stabilità per il Ponte sullo Stretto di Messina – Alessandro Guericchio, Maurizio Ponte – Università della Calabria, 2006

References Chapter 4

Chapter 5: Dynamic Analysis – SFT Subjected to Seaquake and Earthquake Excitations

In this chapter, we will focus on how to do a dynamic analysis of the structural models of the SFT obtained in the previous chapter. Our aim is to model seaquake forces on the tunnel taking into account the effects of flexible layers of soil overlapping the seabed.

The extension of the 3-D model does not allow a fast and clear examination of the results, for this reason, we performed the dynamic analysis only on three of the most significant sections: midspan, quarter-span and end. These are the same that we have implemented in the previous chapter.

In the figure below, the problem of earthquake and seaquake exitation on the tunnel is shown clearly. On the supports at the base we have the arthquake exitation ('eq'), meanwhile, for any point of the tunnel, we have seaquake exitaton, here indicated with 'sq'.
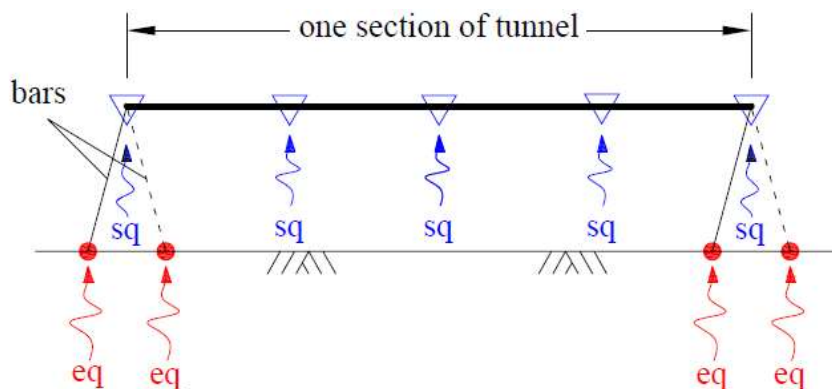
Figure 65 Seaquake and Earthquake forces on the SFT

For the aims of the dynamic analysis, some changes must be done to the model previously used for the static and modal analysis. These includes modelling damping and the added mass generated by the dynamic excitation of the tunnel.

5.1 Damping and Constraints Modelling

In transient analyses, Rayleigh damping is the most commonly used damping model to calculate the damping force. The damping matrix $[C]$ is defined as a combination of two matrixes that are already in the analysis, the mass matrix $[M]$ and the stiffness matrix $[K]$.

$$[C] = \alpha[M] + \beta[K] \tag{5.1}$$

Where α and β are chosen to give the desired fractions of critical damping at two specified frequencies.

$$\alpha = \frac{2\omega_1\omega_2(\omega_1\zeta_1 - \omega_2\zeta_2)}{\omega_1^2 - \omega_2^2} \tag{5.2}$$

$$\beta = \frac{2(\omega_1\zeta_1 - \omega_2\zeta_2)}{\omega_1^2 - \omega_2^2} \tag{5.3}$$

where:

- ω_1 , ω_2 are two natural frequencies which will be specified the amount of damping;
- ζ_1, ζ_2 are damping ratio, which supposed to have the same valueζ.

So equations change into

$$\alpha = \frac{2\omega_1\omega_2\zeta}{\omega_1 + \omega_2} \tag{5.4}$$

$$\beta = \frac{2\zeta}{\omega_1 + \omega_2} \tag{5.5}$$

In the work, according to the 3-D modal analysis results, ω_1 =0.628 rad/s and ω_2=11.21 rad/s are selected out and ζ =0.06. So α =0.0714 and β =0.0101.
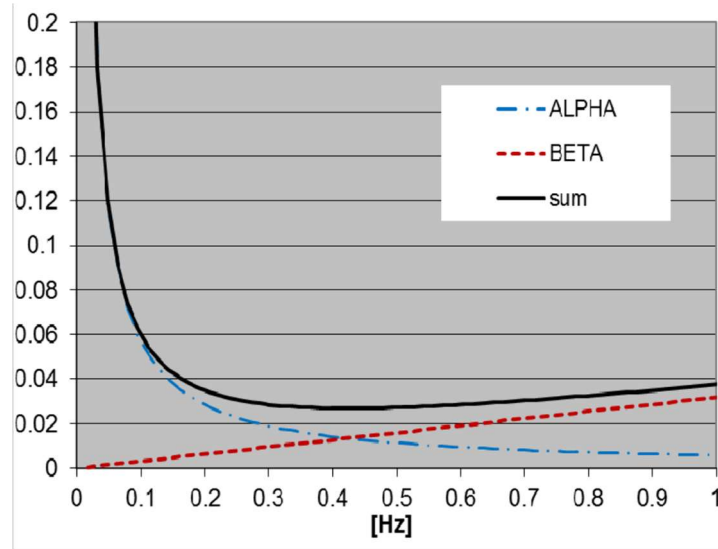
Figure 66 Rayleigh damping

Soil structure interaction cannot be neglected especially for heavy large structures standing on relatively soft soils. Due to the big scale of SFT and the deep location at sea bottom, soil structure interaction should be taken into account.

In the model, linear mechanical behaviour for soil is assumed. Soil-structure interaction is represented by three elastic springs and dashpots, located at each end of the anchor bars and at the shore abutments.

Accordingly, the dynamic equilibrium equations for the soil-structure system can be written in the partitioned form:

$$
\begin{bmatrix} M_{ss}^{(s)}+M_{ss}^{(h)} & M_{sc}^{(s)}+M_{sc}^{(h)} \\ M_{cs}^{(s)}+M_{cs}^{(h)} & M_{cc}^{(s)}+M_{cc}^{(h)} \end{bmatrix} \begin{Bmatrix} \ddot{q}_s \\ \ddot{q}_c \end{Bmatrix} + \begin{bmatrix} C_{ss}^{(s)}+C_{ss}^{(h)} & C_{sc}^{(s)}+C_{sc}^{(h)} \\ C_{cs}^{(s)}+C_{cs}^{(h)} & C_{cc}^{(s)}+C_{cc}^{(h)}+C_{cc}^{(g)} \end{bmatrix} \begin{Bmatrix} \dot{q}_s \\ \dot{q}_c \end{Bmatrix}
$$

$$
+ \begin{bmatrix} K_{ss}^{(s)} & K_{sc}^{(s)} \\ K_{cs}^{(s)} & K_{cc}^{(s)}+K_{cc}^{(g)} \end{bmatrix} \begin{Bmatrix} q_s \\ q_c \end{Bmatrix} = \begin{Bmatrix} R_s^{(s)} \\ R_c^{(s)} \end{Bmatrix} + \begin{Bmatrix} 0 \\ C_{CC}^{(g)}\dot{q}_c^{(f)} \end{Bmatrix} + \begin{Bmatrix} 0 \\ K_{cc}^{(g)} q_c^{(f)} \end{Bmatrix} + \begin{Bmatrix} Q_s \\ Q_c \end{Bmatrix}
$$

In this equation, the symbols represent:

-   q: the vector of Lagrangian coordinates, here represented by generalized absolute displacements;

- s, c: the subscripts denoting respectively the displacements q of structural nodes, and displacements q of 'contact' nodes, located at the ground-structure interface;

- (f): the subscript indicating free-field motion;

- M,C,K:- the inertia, damping and elastic stiffness matrices respectively;

- R: the vector of generalized non-linear restoring forces;

- (g), (s), (h): the superscript denoting respectively ground, structural and hydrodynamic (added mass and damping) contributions;

- Q: the vector of generalized components of external loads (wave loads, buoyancy, dead weights).

The computation of stiffness and damping constants is based upon the hypothesis of a six-pile foundation block. The block mass is assumed 2810 t. In the following table, the stiffness coefficient K and damping coefficient C of these elements are given.

Direction	K [kN/m]	C [kNs/m]
Horizontal	2.87×10^6	2.66×10^4
Vertical	1.72×10^7	1.14×10^5

Table 14 Coefficients of the Soil-Structure Interaction

* Horizontal stands for the transversal and longitudinal direction.
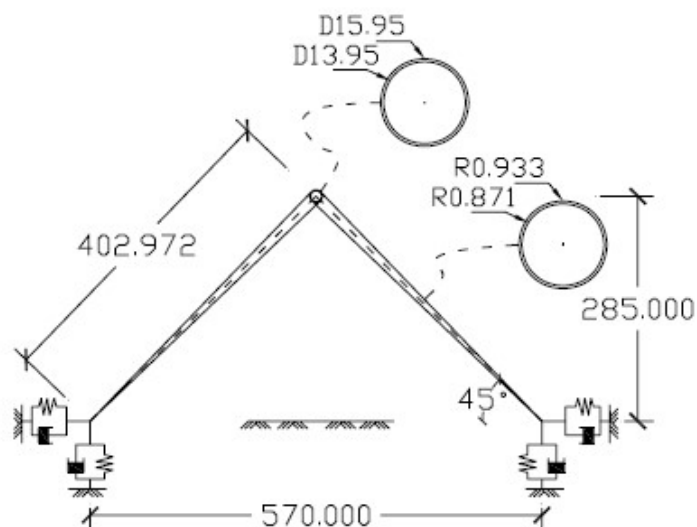
Figure 67 Real section 2-D geometrical model with two bars

On the basis of this theoretical premise, we modelled damping at the base of the tunnel adding three dampers for each anchorage point to the ground, respectively in direction x, y and z.

More in details, in the program ANSYS, we first defined the element COMBIN14 reproducing a Spring-Damper system. The ANSYS code for the definition is reported below:

```
!!! X !!!

et,3,combin14
keyopt,3,2,1
!keyopt,3,3,0
r,3,2.87e9,2.66e7

!!! Y !!!

et,4,combin14
keyopt,4,2,2
keyopt,4,3,0
r,4,1.72e10,1.14e8

!!! Z !!!

et,5,combin14
keyopt,5,2,3
!keyopt,5,3,0
r,5,2.87e9,2.66e7
```

Figure 68 Code ANSYS definition of the used elements
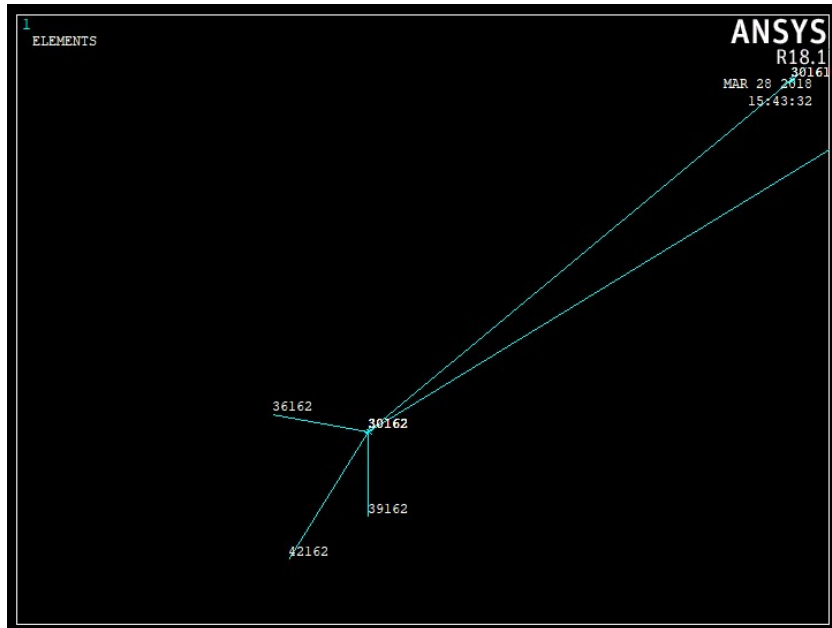
Figure 69 Dampers nodes of end section

This is an example of section 5, bars type C, in which you can see that the node 30162 was already defined before as a base constraint, whereas the nodes 36162, 39162 and 42162 where generated to define the elements corresponding to the dampers.

You can refer to the following table for an overview of the damper nodes for the three sections of the tunnel:

Section 35 - z = 2484m – Bars Type A

	Base Constraints	Damper X	Damper Y	Damper Z
Tunnel 1 Nodes	1302 1321	7302 7321	10302 10321	13302 13321
Tunnel 2 Nodes	31302 31321	37302 37321	40302 40321	43302 43321

Table 15 Number of the nodes of the bars type A

Section 15 - z = 1044m – Bars Type B

	Base Constraints	Damper X	Damper Y	Damper Z
Tunnel 1 Nodes	542 561	6542 6561	9542 9561	12542 12561
Tunnel 2 Nodes	30542 30561	36542 36561	39542 39561	42542 42561

Table 16 Number of the nodes of the bars type B

Section 5 - z = 324m – Bars Type C

	Base Constraints	Damper X	Damper Y	Damper Z
Tunnel 1 Nodes	162 181	6162 6181	9162 9181	12162 12181
Tunnel 2 Nodes	30162 30181	36162 36181	39162 39181	42162 42181

Table 17 Number of the nodes of the bars type C

Now the clamped edges will be the extremities of the dampers instead of the base constraints as in the previous model.

5.2 Modelling of Added Mass

Another important aspect to take into consideration in the dynamic model is the effect of the water displaced by the structure during motion, which phenomenon was extensively explained theoretically in Chapter 3. Now our aim is to understand how to insert this effect in our model.

Considering the fluid-structure interaction based on the Morison equation, the added mass on tunnel and bars is calculated with the following formula:

$$m_{add} = \rho_w * (C_m - 1) * A \hspace{3cm} (5.6)$$

where:

m_{add} = added mass per unit length of the tunnel

ρ_w = water density

A = area of the section

C_m = Inertial coefficient, here equal to 2

The results of the calculation of the added mass for the tunnel and the three different type of bars is reported in the table below:

Section Type	Section Area (m2)	Added Mass (kg/m)	L_{tot} (m)
Tunnel	46,96681017	203803,4014	72 (one section)
Bars Type A	0,351381	2789,416	403.051
Bars Type B	0,384924	3046,206	238.531
Bars Type C	0,42512	3392,976	116.883

Table 18 Added mass of the three type of bars

To apply the masses here calculated to the tunnel and bars, we defined the element MASS21, which corresponds to a point element to which you can assign a specific mass. Since the added mass has been calculated for an element of unit length and the mass must be added to the nodes, we have first to multiply the value of the added mass in the table for the length of the element and divide for the number of elements used in the model, that is 9 for the bars and 4 for the tunnels (that means each bar is composed of 9 elements and each tunnel of 4 in the ANSYS model). In this way we

obtain the value of the mass, in kg, to be added in each internal node of the element (in which two elements are converging); instead, for the extreme nodes, it will be applied half of the value, because in these nodes only one element converges.

Now, we have seen before that, thanks to the commend ACEL,,9.81, the program transforms the masses into forces applied to the structure. This was very useful in static analysis because it enabled to add automatically the self-weight of the elements in the model, without further calculations. In this case, instead, we have to cancel out the effect deriving from the transformation of the added masses here inserted into forces, so we applied, in each node of the tunnels and of the anchorage bars, a force directed upward equal to $m_{add}*g$, in order to balance the one directed downward generated by the program.

In short, you can find a summary of the elements used for the dynamic model and refer to Appendix D or to the ANSYS Help Manual for additional details.

No.	Component of SFT	Elements in ANSYS	Description
1	Tunnel	BEAM4	3-D Elastic
2	Anchoring bar	BEAM188	3-D Inelastic
3	Soil-Structure Interaction	COMBIN14	Spring-damper
4	Dissipation Device	COMBIN39, COMBIN14	Non Linear Spring
5	Added Mass	MASS21	Fluid-Structure Interaction

Table 19 Type elements used in transient analysis

All the aspects regarding dampers and added mass discusses above will be applied also to the 3-D model of the tunnel. Furthermore, for the 3-D model, it is necessary to add also dampers at the end of the tunnel.

The damper at the end of the tunnel were applied defining the element COMBIN39 that presents a non-linear spring, for modelling dampers in direction x and y. for the damper in z direction, it was used the previously defined element COMBIN14.

The input ANSYS code for the generation of such elements is here reported:

```
!!!NON LINEAR SPRING ELEMENTS!!!

et,9,combin39
keyopt,9,1,1
keyopt,9,2,0
keyopt,9,3,3
keyopt,9,6,1
r,9,0.1,280800000,4,323000000

!!!TUNNEL END DAMPER!!!

et,10,combin14
keyopt,10,2,3
r,10,0,5.0231e7
```

Figure 70 ANSYS code generation of the used elements

The nonlinear springs working as the passive control devices at the tunnel ends are used to limit the force transmitted and dissipate some energy. These structural elements have a displacement and a yield strength fixed respectively to 10 cm and 5% of the weight of a single tunnel.

5.3 Loading Condition – Modelling of Seaquake Forces

We have already discussed in Chapter 3 the meaning and the form assumed by the Morison equation, that we report below as a reminder:

$$f = \frac{1}{2}C_D\rho D|u - \dot{x}|(u - \dot{x}) + C_M\rho\frac{\pi}{4}D^2(\dot{u} - \ddot{x}) + \rho\frac{\pi}{4}D^2\ddot{x} \qquad (5.7)$$

where:

C_D , C_M = drag coefficient and inertia coefficient, $C_M = C_A + 1$;

C_A = added mass coefficient;

ρ= water density;

D = cylinder diameter;

u , u = instantaneous water particle velocity and acceleration;

$\dot{x}$, $\ddot{x}$ = structure move velocity and acceleration;

$u - \dot{x}, \dot{u} - \ddot{x}$ = relative velocity and acceleration.

It provides the hydrodynamic force to be applied to a structure immersed in a fluid in motion. To use this equation, we need the velocity and acceleration of water near the structure. These values can be obtained through an artificial generation of time-histories at the seabed to take into account the spatial stochastic variation of the seismic input, and then filter this generated excitation applying the transfer function from bedrock to water. So, the approach consists in gathering data and processing them on the basis of an assumed stochastic model and can be regarded as a quite empirical approach since rigorous physical solutions are unattainable.

In this way, we will obtain the velocity and acceleration of water near the tunnel taking into consideration the modification of the seismic input due to the passage of the waves through one (or more layers) of different flexible soil strata, which will better represent the real geology of the Messina Strait.

At this point, the transient analysis was set up in the file *analysis_transient.txt*. Here we introduced the seismic and hydrodynamic forces on the tunnel for each load step

to perform the dynamic analysis. First of all, we defined the constant parameters for the writing of the Morison Equation:

```
Diameter=15.95                          !External diameter of the tunnel
CD=1.2                                  !Drag coefficient
WD=1020                                 !Water density
CM=2                                    !Mass coefficient of Morison equation
Volume=WD*3.14156*Diameter*Diameter/4   !Total volume of water displaced byt the tunnel
```

Figure 71 ANSYS code definition of parameters for Morison equation

Then we entered the solution processor specifying the type of analysis as Transient (TRANS). Then we implement the first load step in which we applied only static forces, the same that have been defined in the static model seen above. In this way, we will obtain a first load step in the analysis in which the static displacement of the structure is displayed. Then we go on with the second load step in which we apply again static forces along with seismic and hydrodynamic ones.

The seismic forces were applied at the base of the bars with the formula:

```
!!! ACHORAGE POINTS TO THE GROUND OF BARS OF TUNNEL 1 !!!!

!We have two anchorage points to the ground for each tunnel and for each of them we apply seismic forces in the x,y,z directions

f,1302,fx,2.87e9*g*shi265r03gs137(t-btime,1)+2.66e7*g*shi265r03gv137(t-btime,1)
f,1302,fy,1.72e10*g*shi265r01gs137(t-btime,1)+1.14e8*g*shi265r01gv137(t-btime,1)
f,1302,fz,2.87e9*g*shi265r01gs85137(t-btime,1)+2.66e7*g*shi265r01gv85137(t-btime,1)

f,1321,fx,2.87e9*g*shi265r03gs137(t-btime,1)+2.66e7*g*shi265r03gv137(t-btime,1)
f,1321,fy,1.72e10*g*shi265r01gs137(t-btime,1)+1.14e8*g*shi265r01gv137(t-btime,1)
f,1321,fz,2.87e9*g*shi265r01gs85137(t-btime,1)+2.66e7*g*shi265r01gv85137(t-btime,1)
```

Figure 72 Seismic force formula

where we recall the files '*shi265r01gs%*', which contain the ground displacements calculated from the artificial generation of time-histories.

Then we apply seaquake forces to the nodes of tunnel and linkage:

```
*do,eq,39,43,1                          !39-43 are the numer of nodes of the tunnel considered, 1 is the increment

    seave=shi265r01sv%eq%(t-btime,1)     !Derive the sea velocity for each load step
    seaac=shi265r01sac%eq%(t-btime,1)    !Derive the sea acceleration for each load step


    tsv=node_sv%eq%(jnum)
    tsa=node_ac%eq%(jnum)


    !!! IDRODINAMIC FORCES ON TUNNEL 1 !!!


    tdampingforceve=node_tdampingv%eq%(jnum)
    hypar=(CD*WD*Diameter/2)*g*tun1/ntunnel


    f,18100+eq,fx,hypar*(hydrve-tdampingforceve)*abs(hydrve-tdampingforceve)        !Idrodinamic force in direction x
    f,18100+eq,fy,par1*(seave-tsv)*abs(seave-tsv)+par2*(seaac-tsa)+Volume*g*tsa*tun1/ntunnel   !Idrodinamic force in direction y
```

Figure 73 Seaquake force formula

Which implements the Morison equation into the model. As you can see, in the parameters *seave* and *seaac* we insert in the model the files containing the time histories of seaquake velocities and accelerations that we have generated for different layers of flexible soil strata. Refer to the following paragraph for the detailed practical generation of these time-histories.

The seismic and hydrodynamic forces added in this step are contained in a loop of time to reproduce their variation in time. For every value of the time t that goes from an initial time BTIME of 0 s to an end time ETIME of 40 s, with a step DTIME that varies depending on the precision you want to achieve in the analysis and on the time at your disposal, you applied hydrodynamic and seismic forces to the tunnel deriving the results. Remember that the smaller is the time step, the slower the analysis will be. For the final analysis we chose a time step of 0.01 s, that is the minimum allowed since the time histories generated have this time step, but, for testing the model, you can use a bigger one, such as 0.05 or even 0.5 in order to obtain the result in a very short time.

5.3.1 Artificial Generation of Time-Histories

We implemented the procedure to generate the artificial time-histories with one and two flexible layers upon sea-bed. For this purpose, we started from a Fortran90 code that previously generated the time-histories for rigid-bed and modified it in order to consider the additional effects of the flexible layer.

The theoretical procedure for the generation follows what has been explained in Chapter 2. The spatial variability of ground motion is described by means of the so-called coherency function that is defined in terms of cross-power spectral density (PSD) of ground accelerations between two station i and j and their separation distance ξ. Then Fourier Transform of this coherency function $\Gamma(k, \omega)$ is necessary to calculate the discretization of the frequency-wave-number spectrum, F-K Spectrum as follows:

$$S(k,\omega) = S(\omega) * \Gamma(k, \omega) \tag{5.8}$$

Analysis of SFT Resting on Flexible Soil Strata Subjected to Seaquake Excitation

where $S(\omega)$ is the Kanai-Tajimi power spectral density (PSD) modified by Ruiz and Penzien, adopted to describe the seismic motion at a single point.

At this point, the F-K Spectrum $S(k,\omega)$ can be used to calculate the Fast Fourier Transform (FFT) from which the artificial time-histories will be generated:

$$f(x,t) = \sqrt{2} \sum_{\eta=\pm 1} \sum_{J=0}^{J-1} \sum_{n}^{N-1} \left[S(k_j, \omega_n) \Delta k \Delta \omega \right]^{1/2} \cdot \cos \left[\eta k_j x + \omega_n \left(t - \frac{x}{v_{app}} \right) + \varphi^{(\eta)}_{jn} \right] \qquad (5.9)$$

The procedure can be schematically summarized as follows:

Kanai-Tajimi PSD for seismic motion at a single point
$S(\omega)$

↓

Coherency Function of Luco & Wong
$\gamma(\xi,\omega)$

↓

Fourier Transform of Coherency Function
$\Gamma(k,\omega)$

↓

F-K Spectrum
$S(k,\omega) = S(\omega) * \Gamma(k,\omega)$

↓

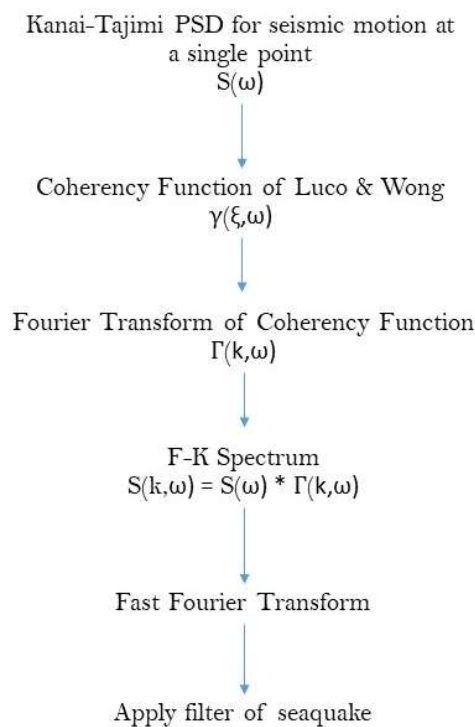Fast Fourier Transform

↓

Apply filter of seaquake

Figure 74 Procedure for generation of time-histories

The Fortran source code implemented for the time-histories generation is composed of different files, each of them performing a step discussed in the scheme above. The file genero is called *seno.f90* and connects all the files of the directory. Here you can find a summary of the generation procedure.

calcpar.f90 calculates the parameters for the definition of the spectrum of Kani-Tajimi modified by Clough-Penzien.

spcp.f90 derives the spectrum of Kanai-Tajimi modified by Clough-Penzien.

Analysis of SFT Resting on Flexible Soil Strata Subjected to Seaquake Excitation

gamma.f90 defines the Fourier Transform of the coherency function.

fft.f90 defines the Fast Fourier Transform.

integr.f90 is the file in which the integration in the frequency domain is performed.

waterfiltervp is the file in which it is inserted the velocity potential of seaquake, necessary to generate acceleration of water.

waterfiltersv contains the function expressing seaquake velocity, calculated as the derivative of the velocity potential.

seaq.f90 recalls the functions corresponding to seaquake velocity and acceleration in order to apply the filter corresponding to seaquake.

invil-times.f90 is the file that contains the generation of seaquake velocities and accelerations. This file will be then recalled in the file *writedata.f90* that writes and generates the .txt files with the resulting time-histories of acceleration and velocity of seaquake necessary to run the ANSYS analysis with flexible sea-bed. First, an envelope of the values of acceleration is performed, multiplying the acceleration for an envelope function. Then, it is imposed that the mean value of this acceleration is equal to zero. Subsequently, the file FFT is recalled to transform the accelerations from the time domain to the frequency domain. Then, in the frequency domain, the velocities and displacements are computed, recalling the file *integr.f90* in which the integral is defined. In the last part, the generation of seaquake is performed recalling the file *seaq.f90* in which the filter was generated, then the impulse response function of the water filter is computed. Next, we go back to accelerations and velocities in the time domain with the inverse Fourier Transform and, in the end, a convolution integral of the ground velocity is performed in the time domain to obtain the water velocity.

The results were derived for 265 stations all along the tunnel. Here, as an example, the results of the first three stations with a single flexible layer of thickness of 100m will be reported.

Station 1

It is the one at the tunnel end corresponding to zero distance from the seabed to the tunnel (z = 0). The ground velocity time history obtained is shown below:
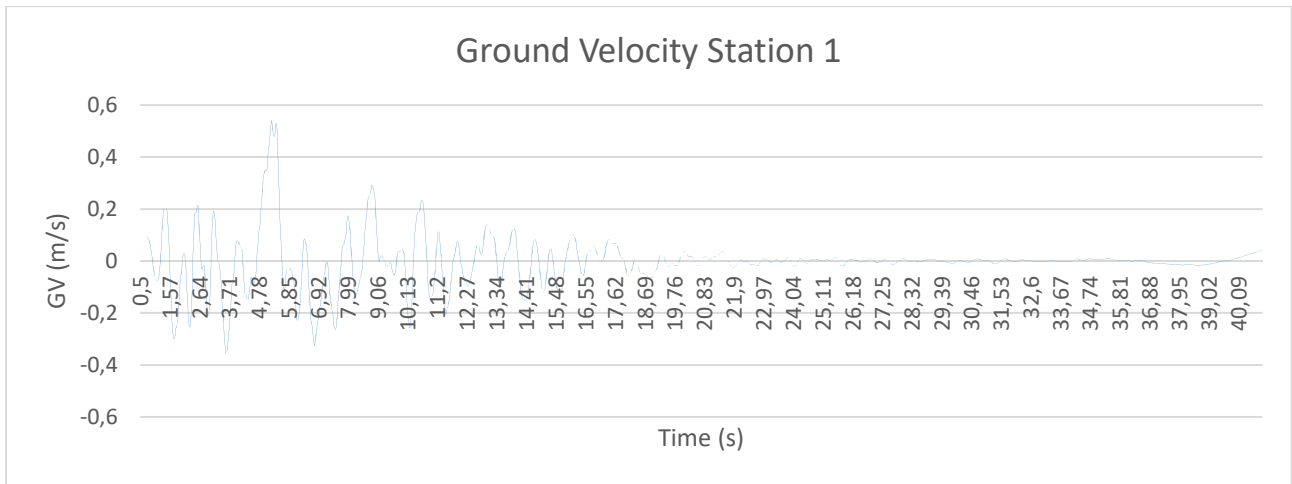
Figure 75 Ground velocity of station 1 with a single flexible layer

To make a quick check of the results obtained, we put a thin layer of 10cm of very rigid soil and we obtained a seaquake velocity time history quite coincident with the ground velocity at seabed, as shown below.
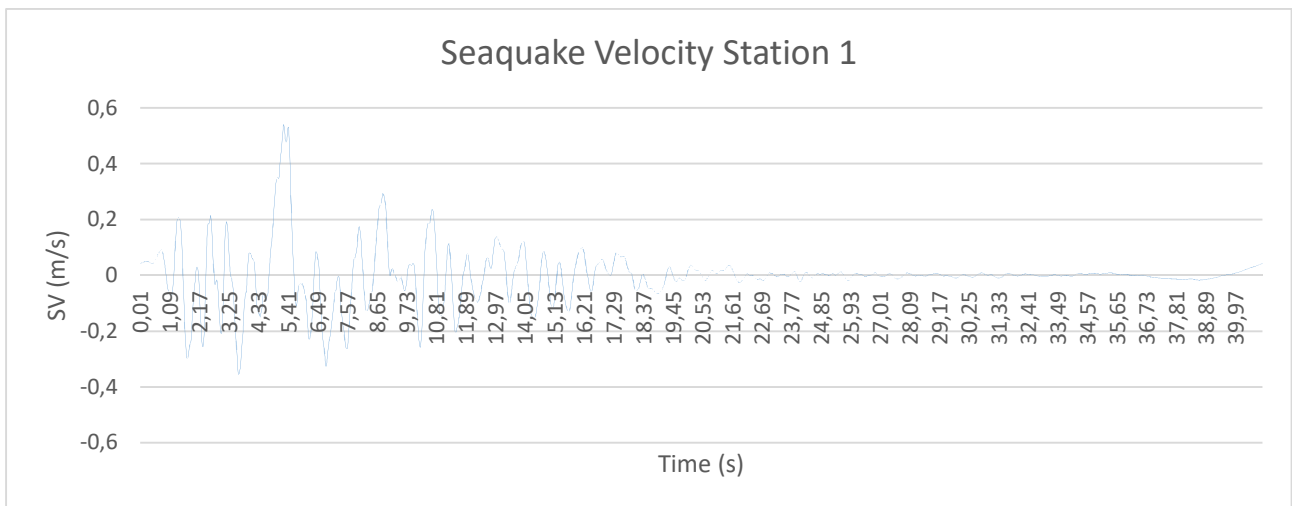

Figure 76 Seaquake velocity of station 1 with a single flexible layer

This happens because in station 1 we are at the sea floor and, considering the soil very rigid, we should retrieve the results obtained for rigid seabed.

Then, with the aid of an EXCEL spreadsheet, we calculated the Fast Fourier Transforms of the above signals. The version of the program used is EXCEL 2013.

First thing to do if you want to obtain a FFT of these time-histories using EXCEL is make sure that you have installed the *Analysis Toolpack*. You can go to *Data* and check at

the extreme right part of the bar if it appears. If it is not there, go to *File* → *Options* → *Add-ins* and add the package. Then it will be displayed in the *Data* section.

Step 1: Label Columns

Label five columns in EXCEL as follows: Time, SV, Frequencies, Complex Fourier Coefficient SV, Coefficient columns.

These will correspond to columns from A to E in the excel spreadsheet.

Step 2: Import data, determine sampling frequency, adjust number of samples to 2n

Import the sampled data of time and Seaquake Velocity from the time histories generated. Let D correspond to the number of rows of data. Therefore, in our case we have sa = 4096.

Determine the time interval subtracting the time value of the second cell with the one of the first, in this case we have that the time step is t = 0.01s. The duration total is:

$$D = t * sa = 40{,}96 \text{ s}$$

Determine the sampling frequency, fs as:

$$fs = \frac{1}{t} = 100 \text{ Hz}$$

In the next step, one of the limitations of using the FFT function in Excel is that the number of data point operated must be a number that is a power of two. In our case we have 4096 data points which corresponds to 2^{12}, so they are ok for the determination. In case they are not, you can simply add zeros at the end to reach a number that is a power of two.

$$sa = 4096$$

Step 3: Fill the Column of Complex Fourier Coefficients

Using *Data* → *Data Analysis* → *Fourier Analysis* you will get the following window:

Analysis of SFT Resting on Flexible Soil Strata Subjected to Seaquake Excitation
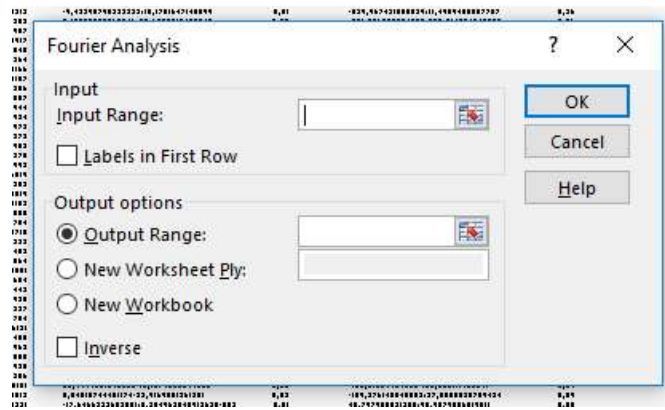

Figure 77 Fourier analysis window

In which you have to select the input range that is our Seaquake Velocity at the station considered and the output range that is the column in which you want the results to be displayed. Then click OK.

Step 4: Fill the column called Coefficient Column

Calculate the FFT magnitude by finding the absolute value of the column of the Complex Fourier Coefficients. So you have to insert the formula:

=IMABS(D2)

And you can drag it to all the cells of the column.

Step 5: Fill the Column C of Frequencies

The first cell of the frequencies is always zero.

The second cell of the FFT frequency is 1 x 1 / D = 0.02, where D is the total duration of the signal.

In the next cell you have 2 x 1 / D and so on.

Instead of manually filling the column, we can automatically do it using the Excel Series function. Leave the first value always zero. In the second, put 2 x 1 / D and then go to *Fill → Series* and insert following values:

Step value: 1/D

Analysis of SFT Resting on Flexible Soil Strata Subjected to Seaquake Excitation

<u>Stop Value</u>: 50

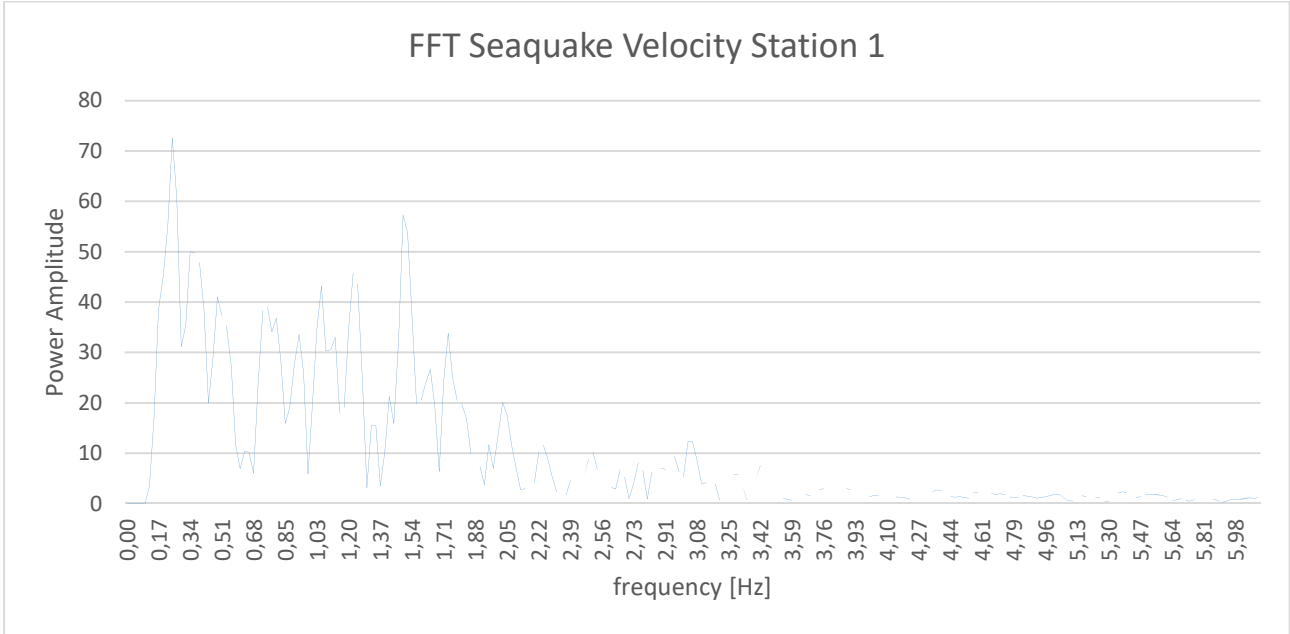Now you just have to plot the frequency vs FFT of Seaquake Velocity to obtain the spectrum shown below:

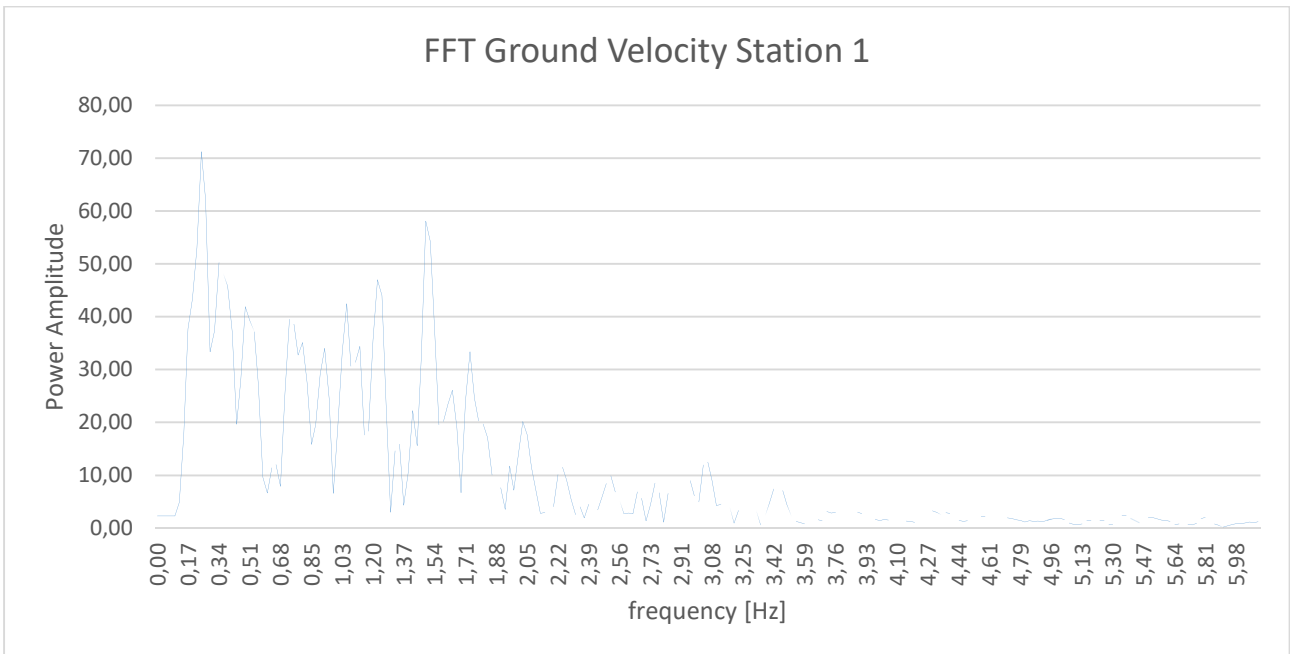*Figure 78 Fast Fourier Transform of seaquake velocity at station 1*

Figure 79 Fast Fourier Transform of ground velocity at station 1

Analysis of SFT Resting on Flexible Soil Strata Subjected to Seaquake Excitation

Station 2

Its position is defined by a 125 m distance from the seabed to the tunnel, with 165 m depth of the water apart from Station 1. The obtained ground velocity and seaquake velocity time histories are shown in the figures below.
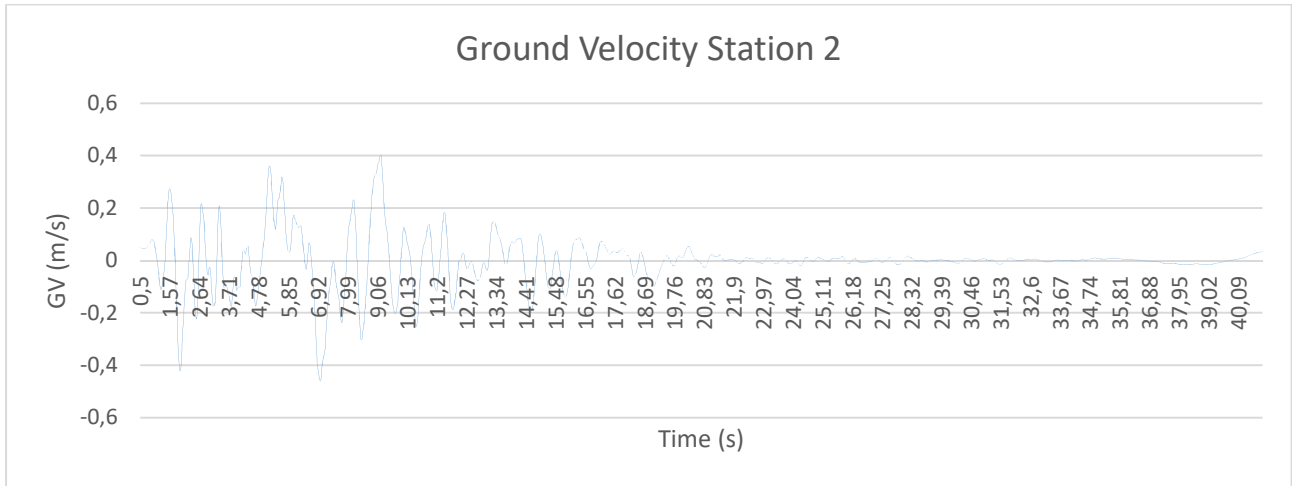
Figure 80 Ground velocity of station 2 with a single flexible layer
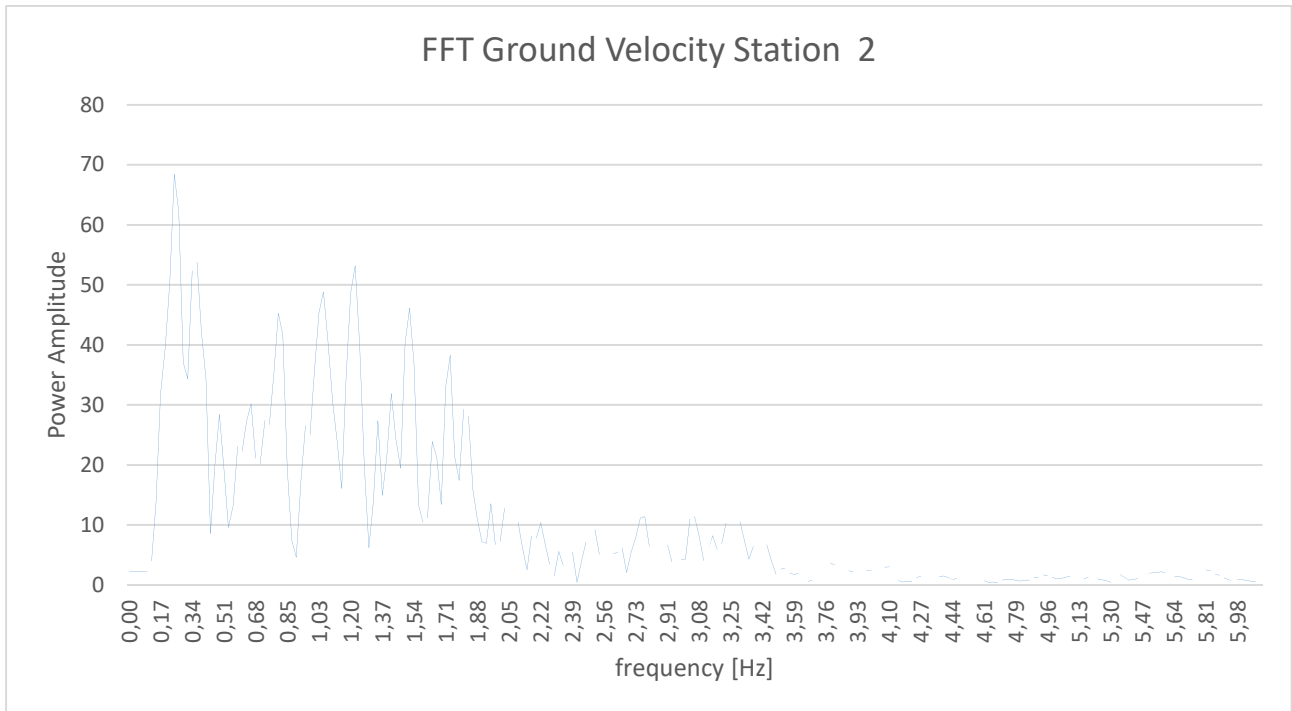

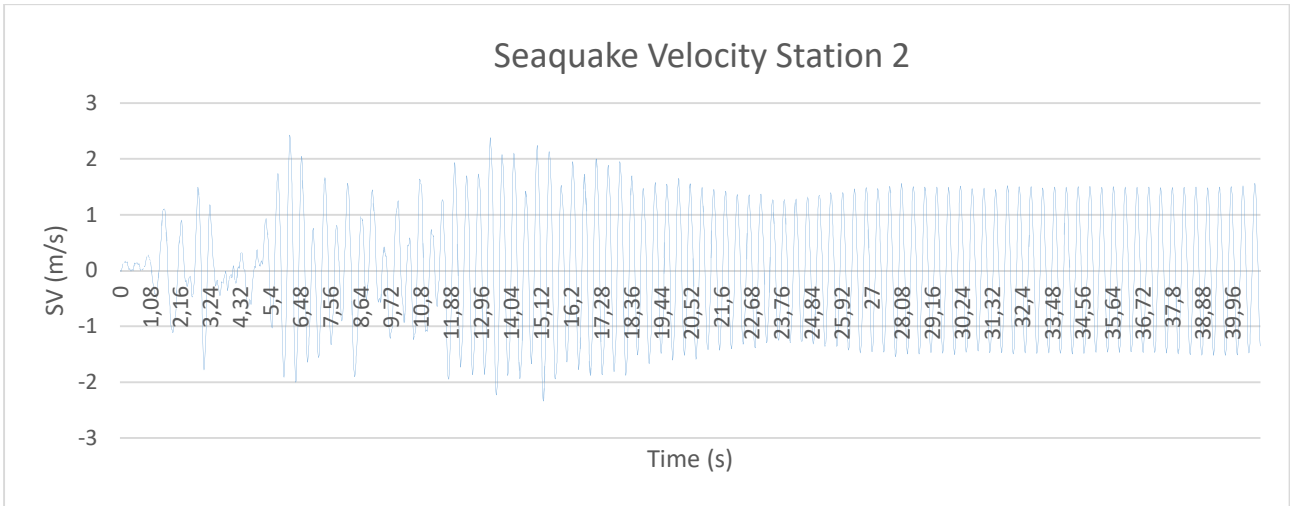*Figure 81 Fast Fourier Transform of ground velocity at station 2*

Figure 82 Seaquake velocity of station 2 with a single flexible layer
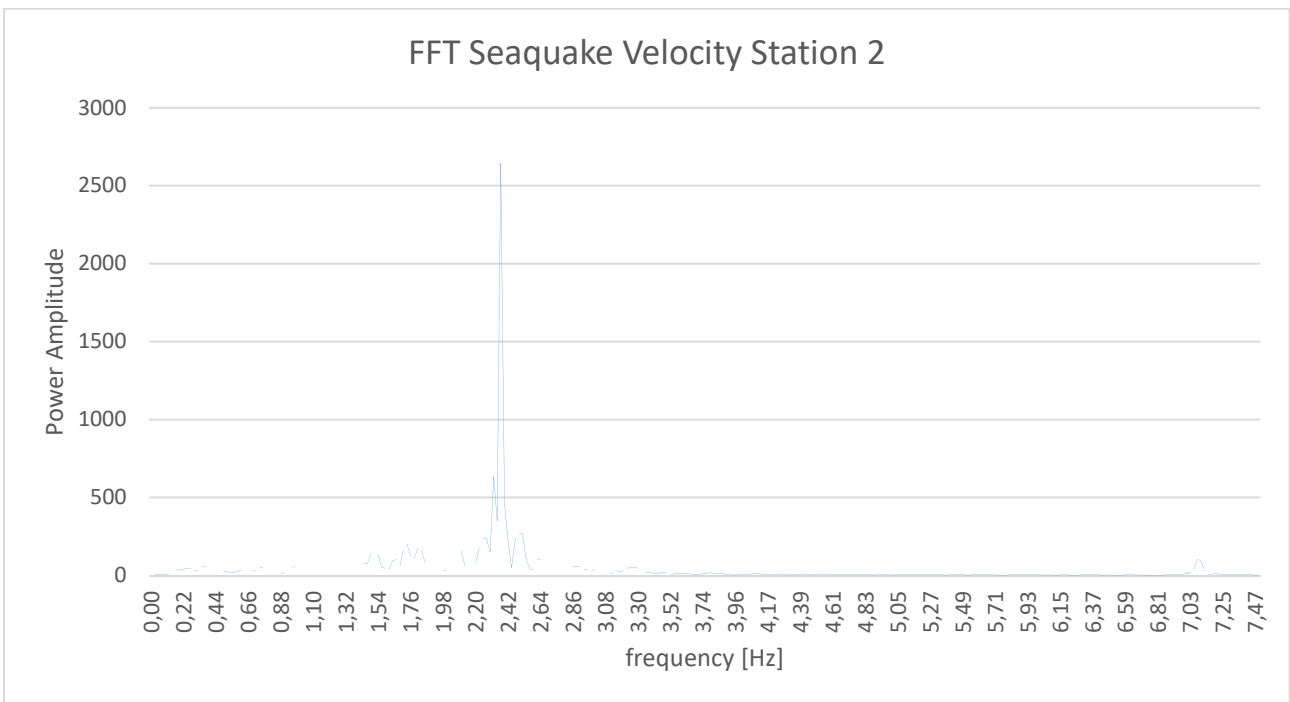

Figure 83 Fast Fourier Transform of seaquake velocity at station 2

From the seaquake velocity time history, we can detect a quasi-harmonic behavior and we can assess the convenience in working in the frequency domain, since in time domain, as can be seen from the graph above, at the end you have a residual velocity that should be considered as initial condition for another generation. Moreover, in the seaquake's velocity power spectrum we can guess that a resonance might occur at a frequency of 2,39 Hz and there is another similar peak at around 7 Hz.

Station 3

Station 3 corresponds to the middle-span of the tunnel with a 285 m distance from the seabed to the tunnel body and 325 m in depth. The obtained ground velocity and seaquake velocity time histories are shown above.
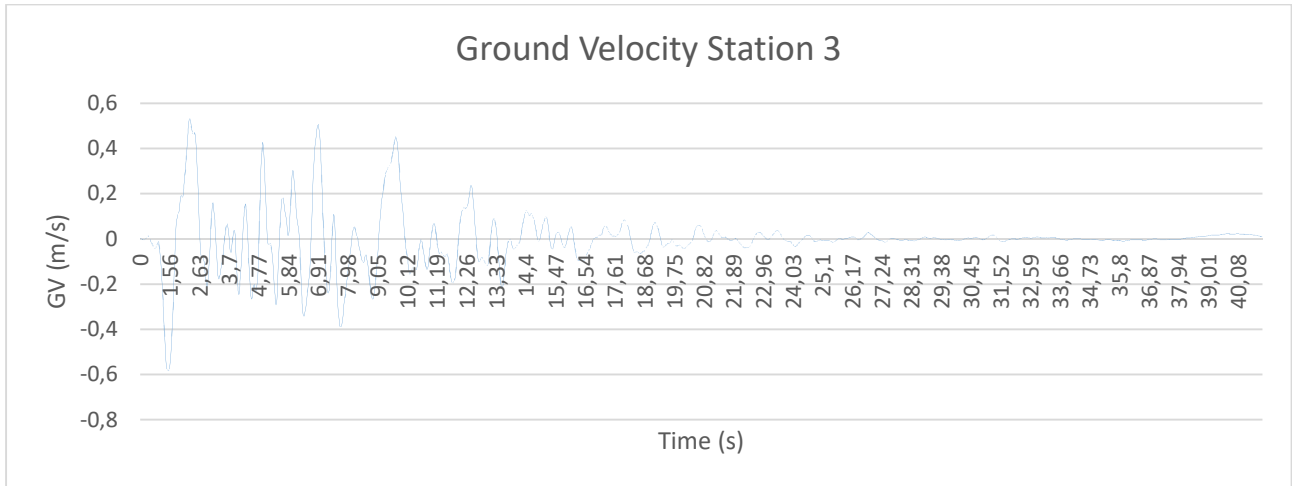

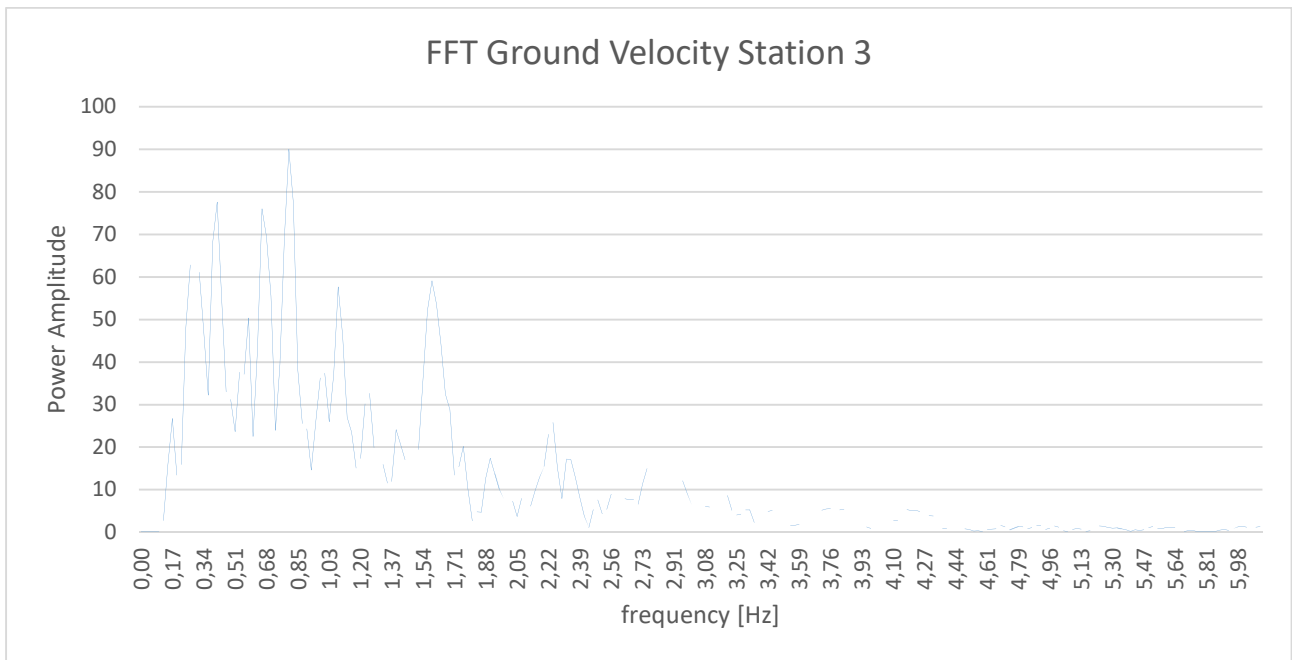*Figure 84 Ground velocity of station 3 with a single flexible layer*

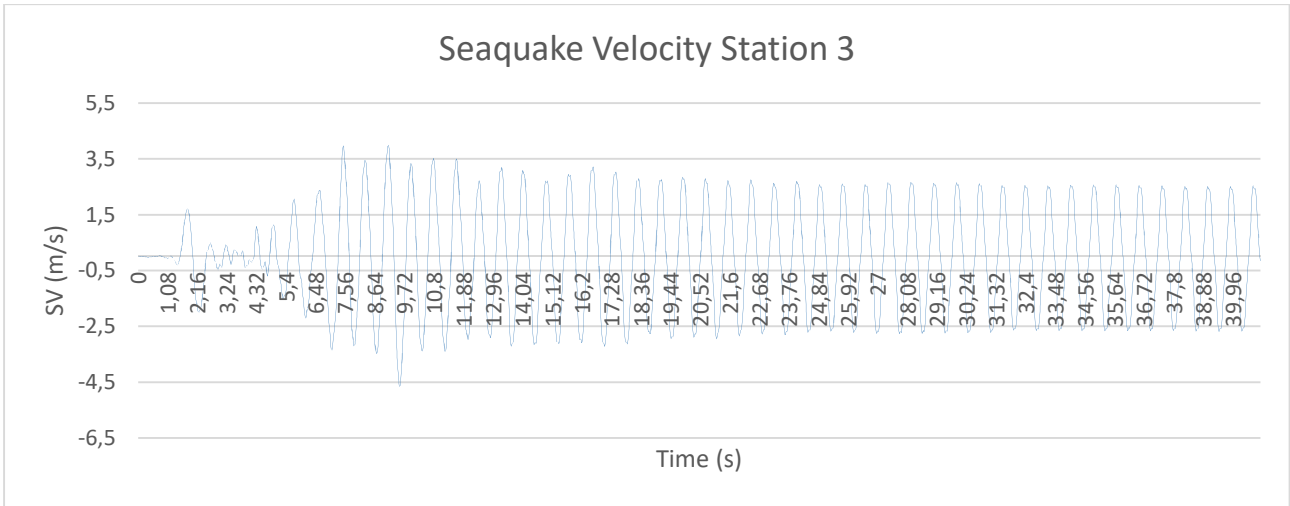*Figure 85 Fast Fourier Transform of ground velocity at station 3*

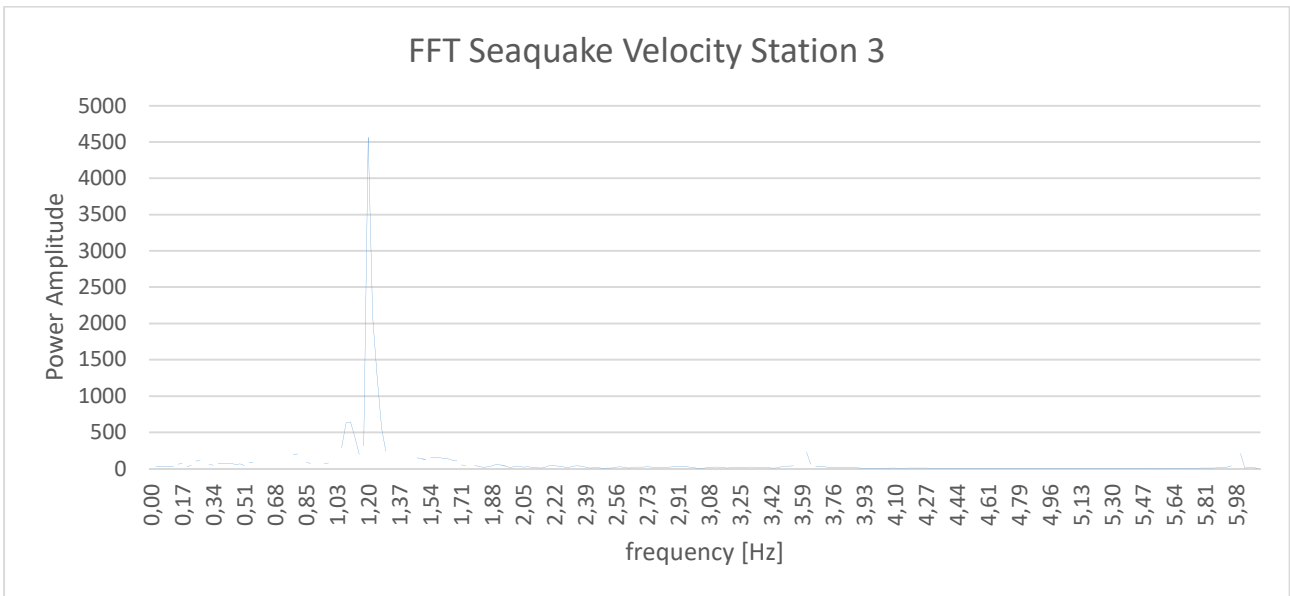*Figure 86 Seaquake velocity of station 3 with a single flexible layer*

Figure 87 Fast Fourier Transform of seaquake velocity at station 3

There can be made the same considerations for .

5.3.2 Resonance frequency

As we know, the frequency of waves transmitted in water f_{water} is:

$$f_{water} = \frac{c}{\lambda} \tag{5.10}$$

Where λ is the propagation wavelength. From the theory of axial waves in rods we know that, with the boundary conditions here enforced, resonance occurs when the rod length is equal to an odd multiple of one quarter of the wavelength.
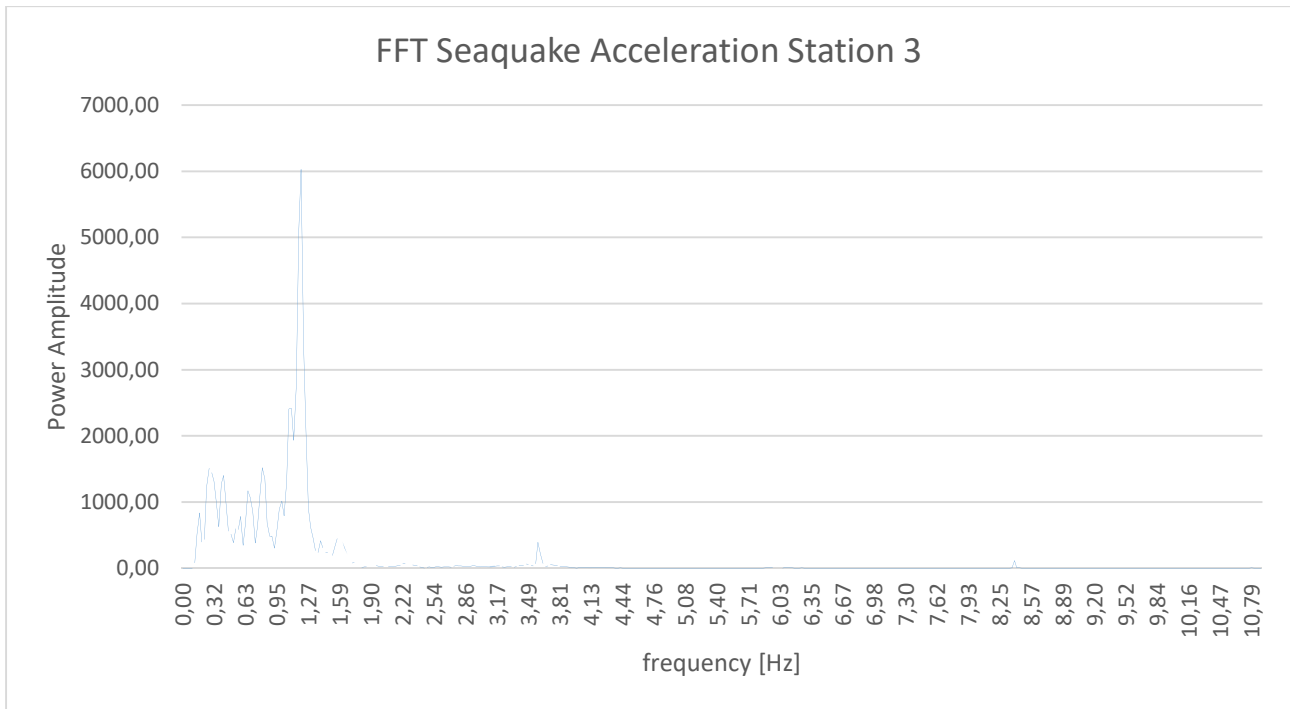
144

Figure 88 Seaquake acceleration power spectrum at station 3 (d = 325m)

The resonance frequencies of acceleration correspond to 1.27 Hz, 3.5 Hz, 6Hz, 8.3 Hz.

For the analysis of the 2-D model of the tunnel, 3 station have been chosen. These are station 21 which is the one near the end of the tunnel with diameter of bars type C, station 61 which corresponds to a quarter span of the tunnel with bars diameter type B and a third station corresponding to midspan with bars type A.

The time histories obtained for the 3 stations aforementioned, that will be used to run the dynamic analysis of the 3 sections subjected to seaquake excitation, are shown above. Two layers of flexible layer were considered with the aim of better reproducing the real geology of the Messina Strait.

Referring to the geological model shown in the previous chapter, the analysis is carried out considering a soil composed of two flexible layers and a layer of bedrock. The mechanical characteristics are shown in the following table.

Layers	Thickness (m)	Density (kg/m³)	Vp (m/s)	Vs (m/s)	Shear Modulus G (Mpa)	Lamda, Lame's constant
Terraced deposits	42	2200	625	450	51750	76983.35
"Messina" gravel	107	1900	625	450	384750	27321500
Bedrock	-	2900	5500	3500	27869000	31987000000

Table 20 Mechanical parameters

The mechanical parameters of the various layers of soil were obtained from the propagation velocities of the P and S waves in these; in fact, the ways with which a wave propagates in the medium depends on the characteristics of this.

$$V_s = \sqrt{\frac{G}{\rho}}$$ (5.11)

$$V_p = \sqrt{\frac{\lambda + 2G}{\rho}}$$ (5.12)

The points excited by the earthquake support motion ('eq') and by the lumped seaquake force ('sq') on each section of the SFT between anchor bars are presented, where the circle represents the support point at the end of each anchor bar while the '∇' symbolizes the five points loaded by the transmitted seaquake forces.
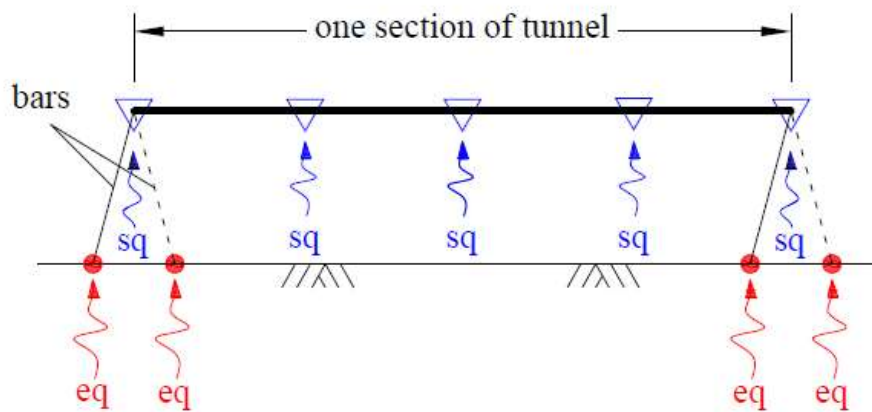

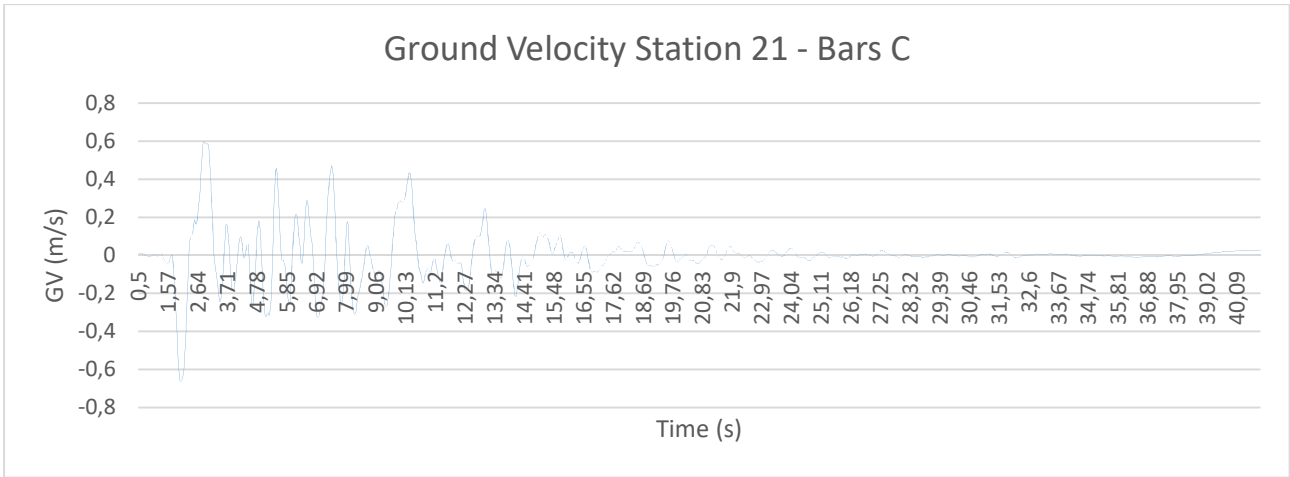*Figure 89 Seaquake force and ground earthquake force on SFT tunnel*

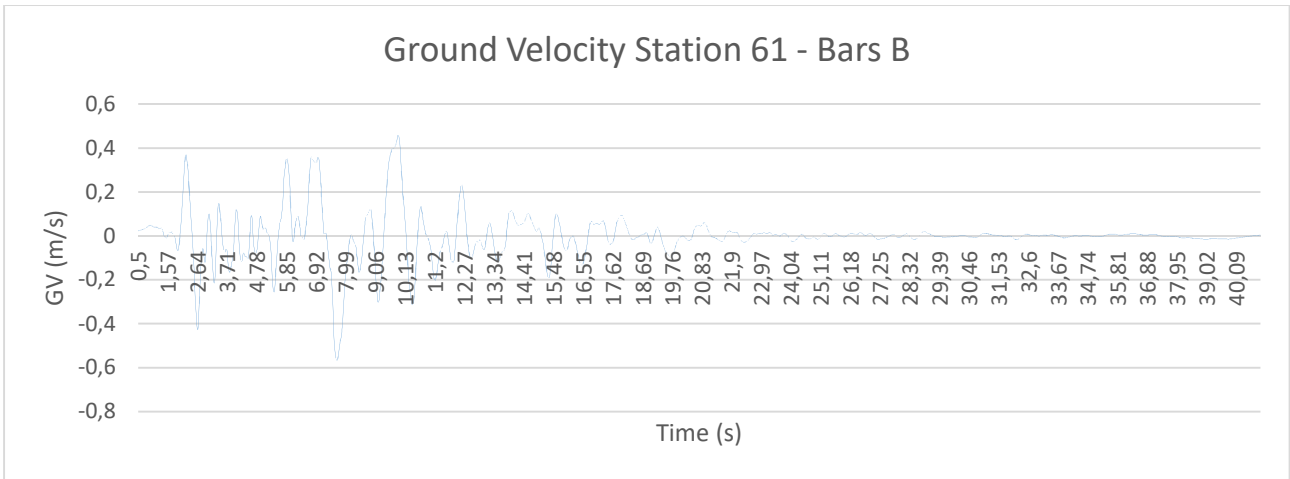*Figure 90 Ground velocity at station 21 for 2 flexible layers*

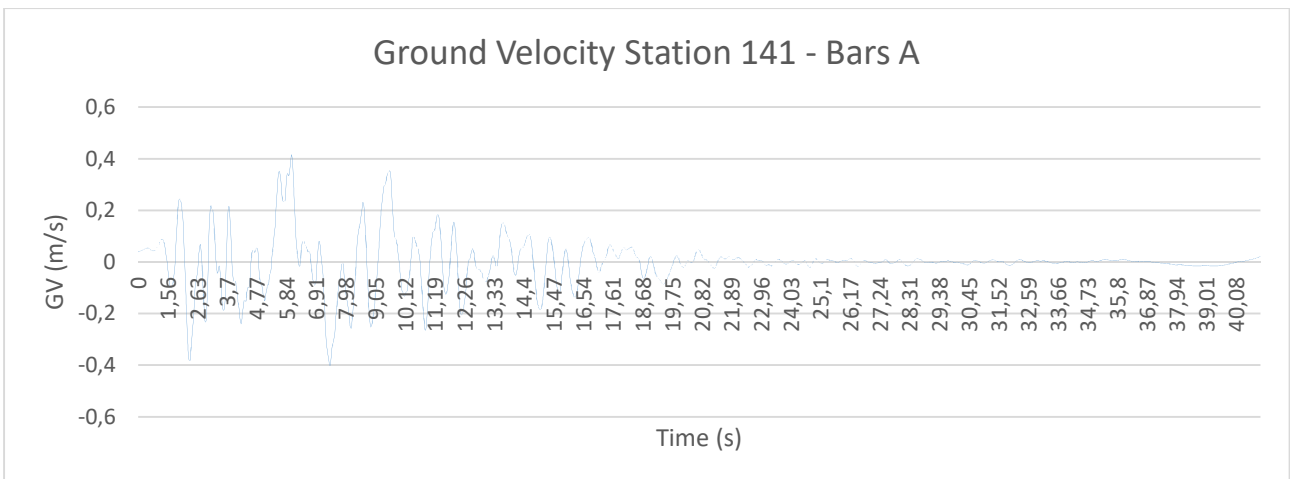*Figure 91 Ground velocity at station 61 for 2 flexible layers*

Figure 92 Ground velocity at station 141 for 2 flexible layers
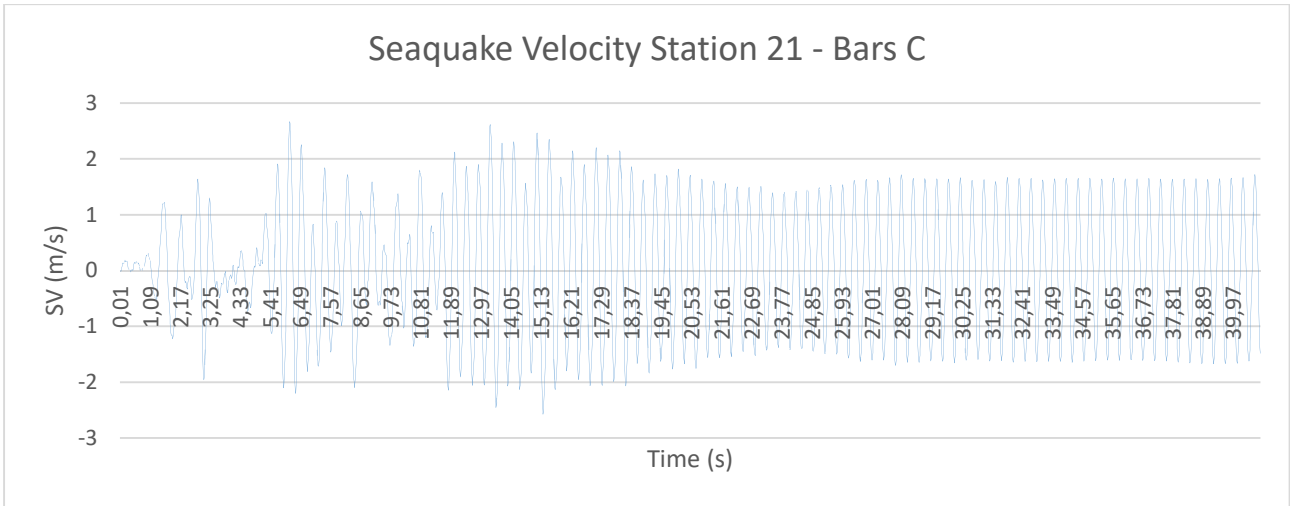
Figure 93 Seaquake velocity at station 21 of 2 soil layers
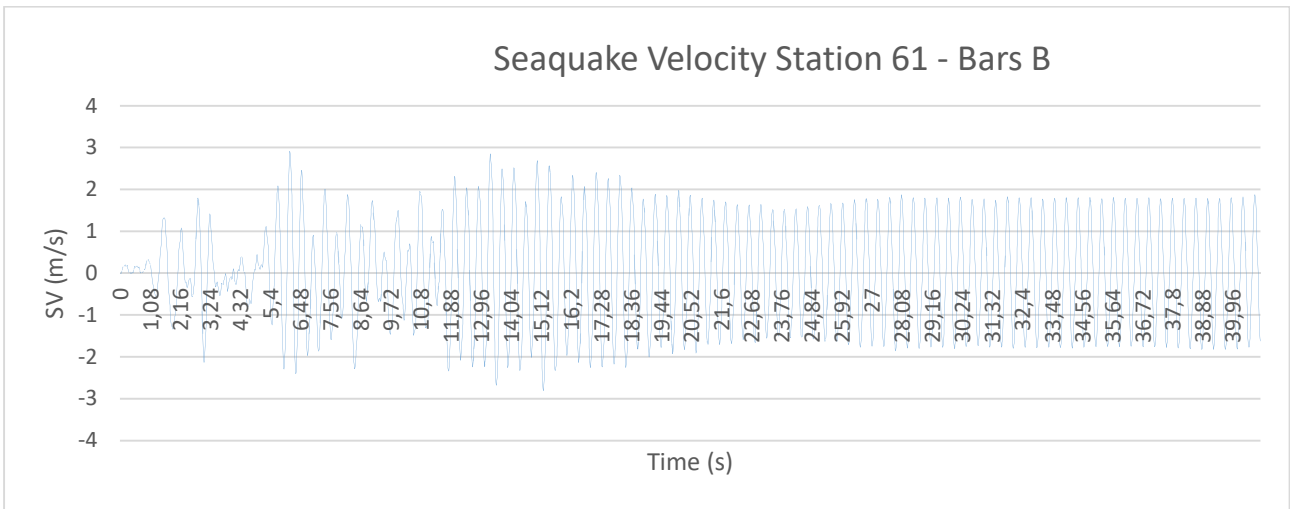
Figure 94 Seaquake velocity at station 61 of 2 soil layers
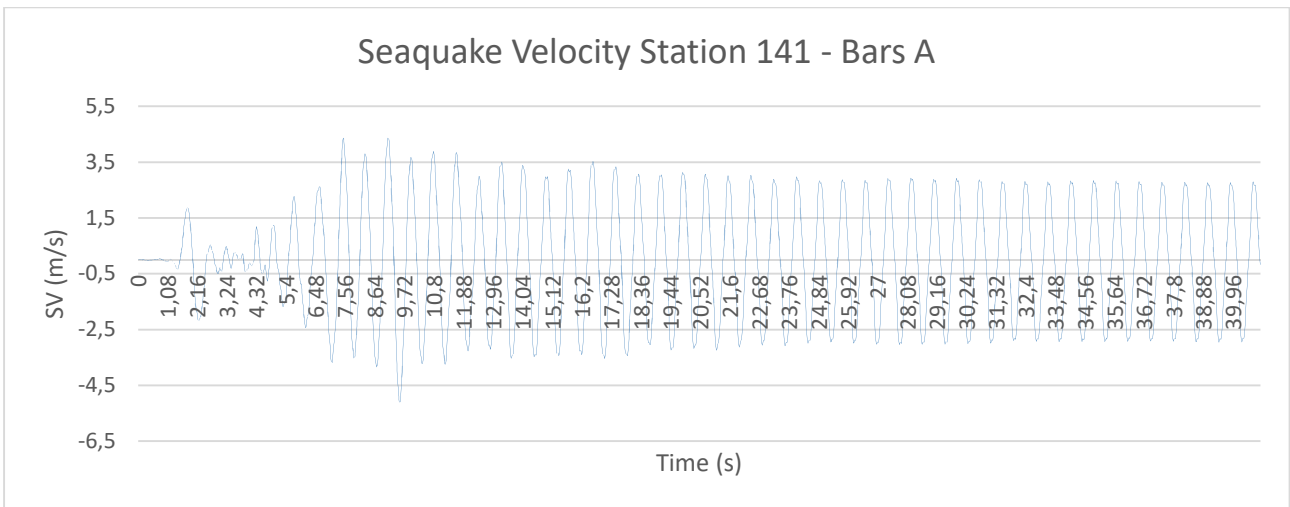
Figure 95 Seaquake velocity at station 141 of 2 soil layers

Analysis of SFT Resting on Flexible Soil Strata Subjected to Seaquake Excitation

We report also the FFT of seaquake velocity, ground velocity and seaquake acceleration for the station 141 (midspan section).
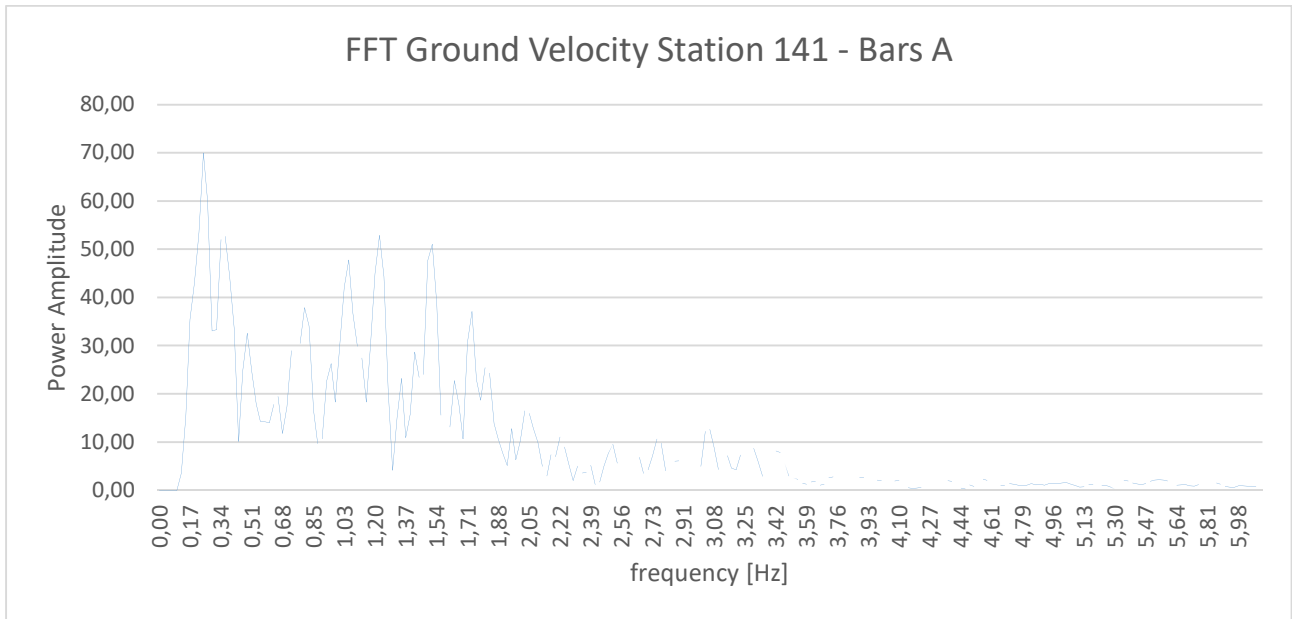
Figure 96 Fast Fourier Transform of ground velocity at station 141 for 2 flexible strata
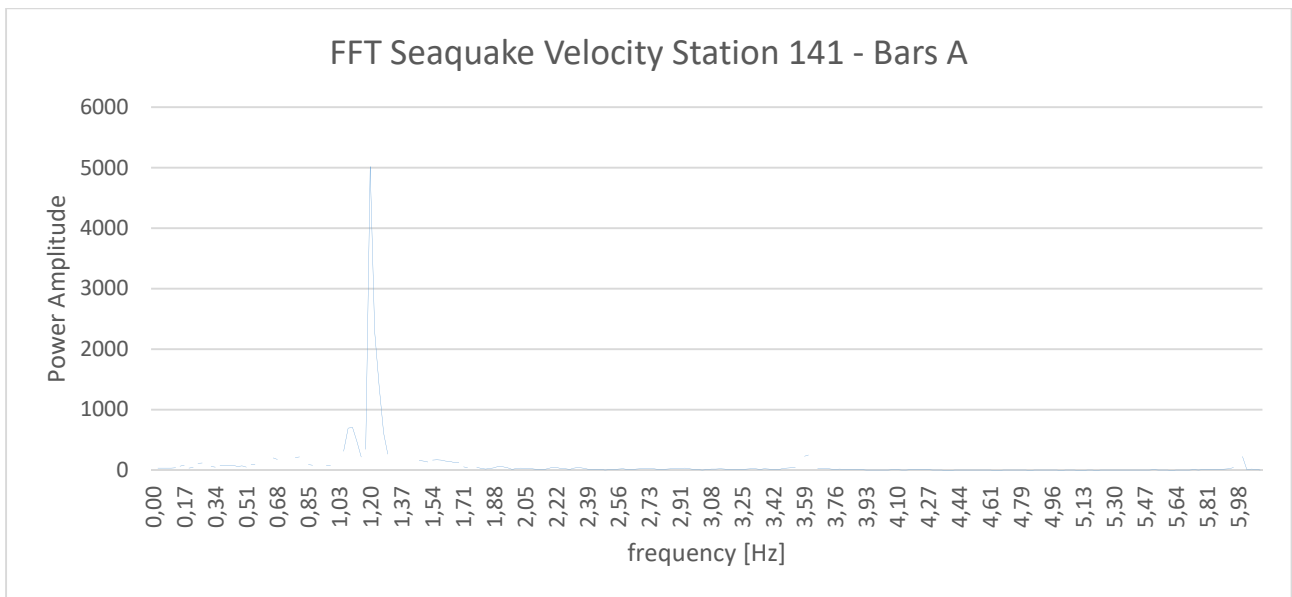
Figure 97 Fast Fourier Transform of seaquake velocity at station 141 for 2 flexible strata

Figure 98 Fast Fourier Transform of seaquake acceleration at station 141 for 2 flexible strata

Analysis of SFT Resting on Flexible Soil Strata Subjected to Seaquake Excitation

To better understand the relation between ground velocity and seaquake velocity, the difference between the phase angles of these two have also been calculated for station 141.
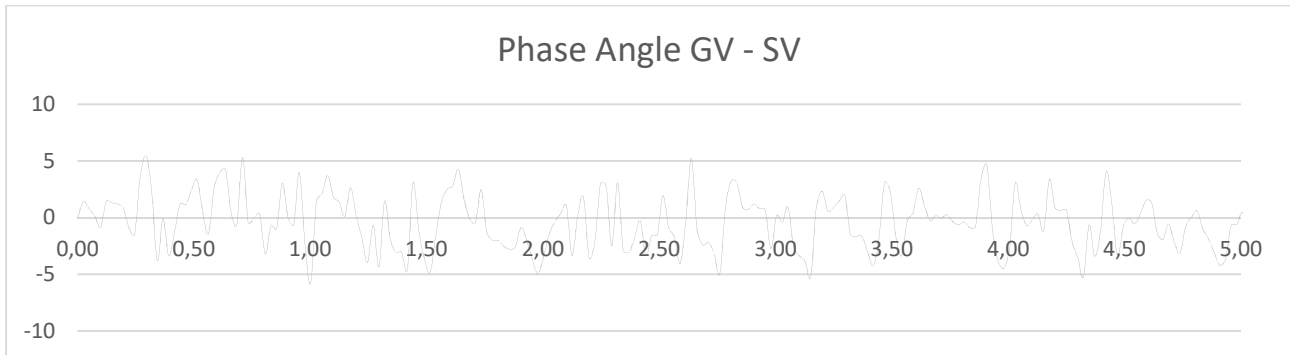
Figure 99 Phase angles of ground velocity and seaquake velocity at station 141 with 2 flexible layers
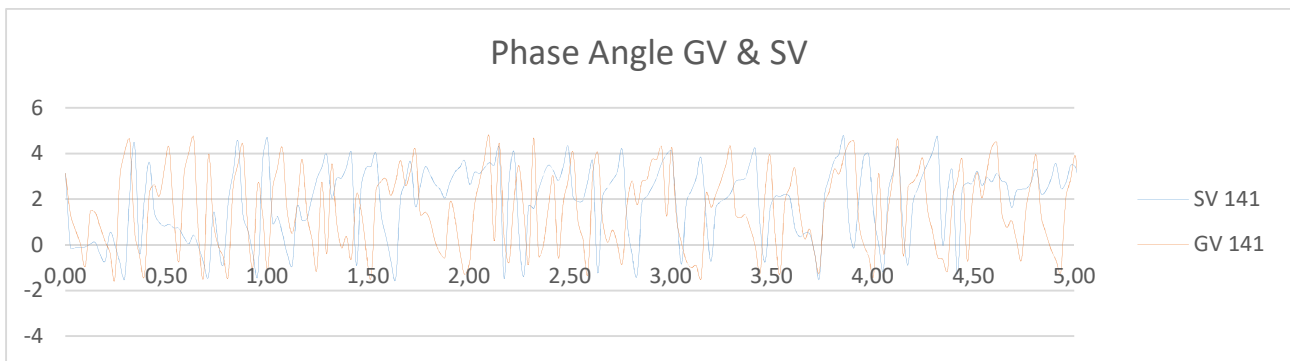
Figure 100 Difference of phase angles of ground velocity and seaquake velocity at station 141 with 2 flexible layers

The results show that the interaction between the two is very variable, leading to in phase and out of phase behaviour.

5.4 Results of Dynamic Analysis

Inserting the time histories determined for two layers of flexible strata over seabed and considering different thicknesses and mechanical characteristics of the strata, we analysed the displacements in Y direction (vertical direction in the section of the tunnel) with elastic bars and inelastic bars.

5.4.1 Results of 2-D Model with Elastic Anchoring Bars

The first analysis has been made with elastic behaviour of the anchoring bars and with the following strata:

| Layers	Thickness (m)	Density (kg/m³)	Vp (m/s)	Vs (m/s)	Shear Modulus G (Mpa)	Lamda, Lame's constant
Terraced deposits	42	2200	625	450	51750	76983.35
"Messina" gravel	107	1900	625	450	384750	27321500
Bedrock	-	2900	5500	3500	27869000	31987000000

Table 21 Characteristics of the soil strata considered

The resulting displacement in direction Z (longitudinal axis) and X (transversal axis along the section) were of very limited entity compared to the much more prevalent displacement in the Y direction. Therefore, this has become our primal parameter of analysis.

Hereafter you can find a comparison of the results obtained with the 3 sections subjected to time histories generated for rigid seabed and the one obtained for the flexible soil strata with the aforementioned characteristics.

Figure 101 Vertical displacement of tunnel master node with rigid seabed for section 141 with elastic

bars

Figure 102 Vertical displacement of tunnel master node with two flexible soils strata with

characteristics of table 18 for section 141 with elastic bars

Figure 103 Vertical displacement of tunnel master node with rigid seabed for section 61 with elastic bars

Figure 104 Vertical displacement of tunnel master node with two flexible soils strata with characteristics of table 18 for section 61 with elastic bars
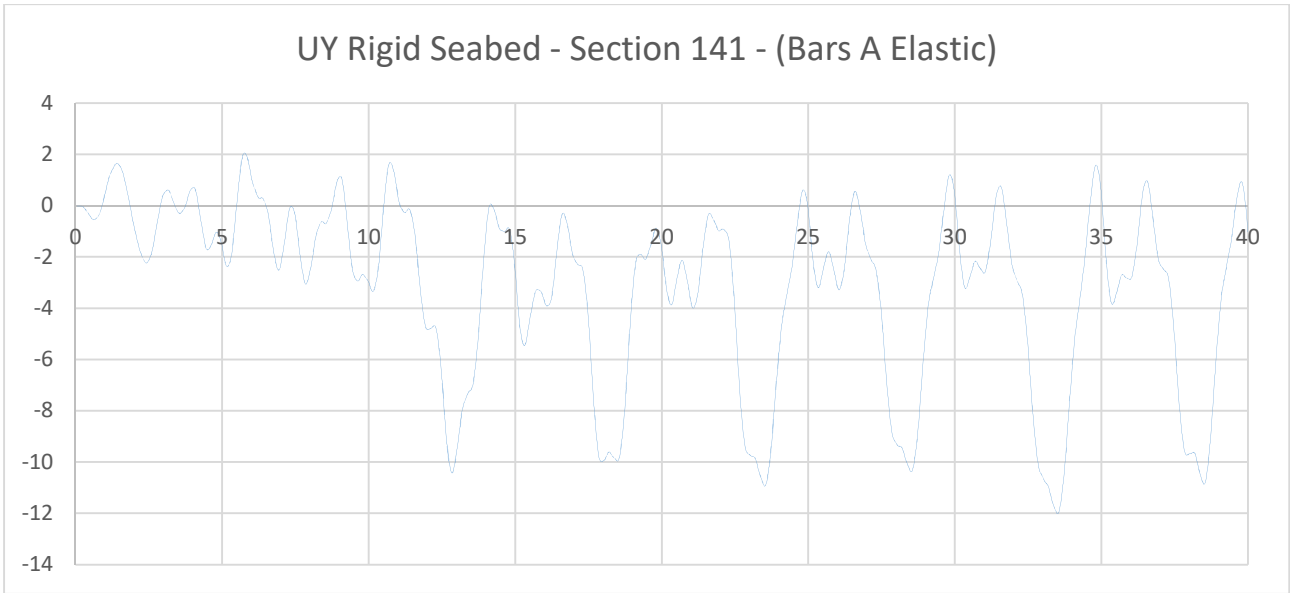
Figure 105 Vertical displacement of tunnel master node with rigid seabed for section 21 with elastic bars

Figure 106 Vertical displacement of tunnel master node with two flexible soils strata with characteristics of table 18 for section 21

Analysis of SFT Resting on Flexible Soil Strata Subjected to Seaquake Excitation

We can observe that the results for rigid seabed and flexible layers are not so different of the section at one-quarter and at midspan but there is an accentuation of the vertical displacement for section 21, that is the section near the end of the tunnel. This can signify that the seaquake excitation becomes more important as the tunnel approaches the shore.

To make everything more clear, we made another analysis changing the characteristics of the soil strata.

Layers	Thickness (m)	Density (kg/m³)	Vp (m/s)	Vs (m/s)	Shear Modulus G (Mpa)	Lamda, Lame's constant
Silty deposits	42	1700	500	300	153000	11900000
"Messina" gravel	107	1900	625	450	384750	27321500
Bedrock	-	2900	5500	3500	27869000	31987000000

Table 22 Characteristics of the soil strata considered

Again, the resulting displacement in direction Z (longitudinal axis) and X (transversal axis along the section) were of very limited entity compared to the much more prevalent displacement in the Y direction, so we report only the last one.
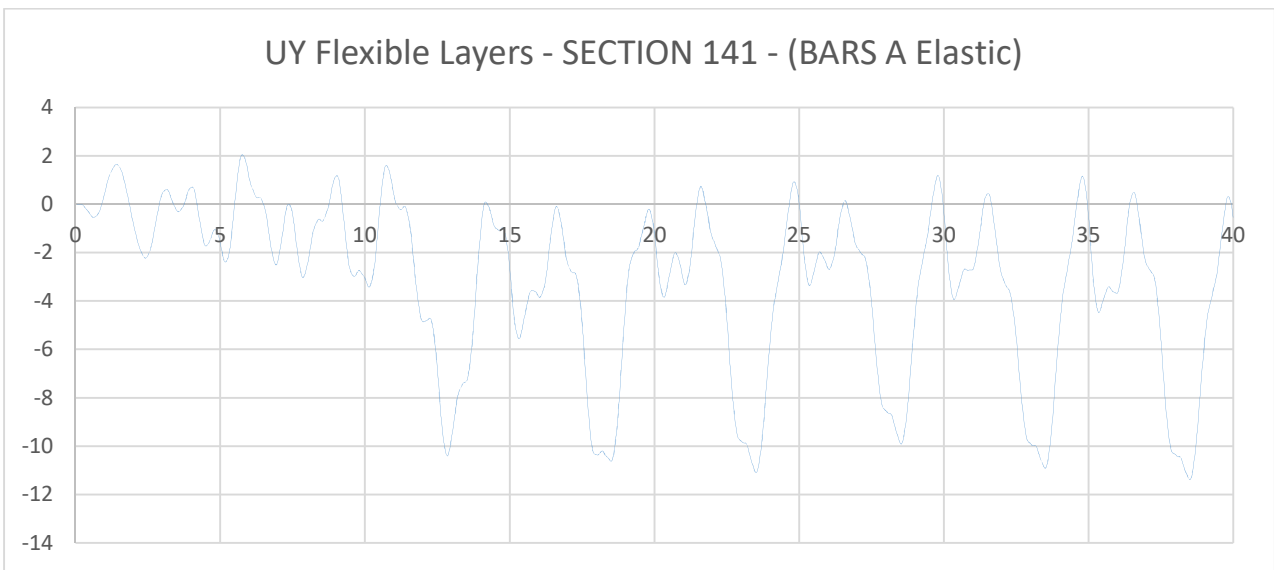
Figure 107 Vertical displacement of tunnel master node with two flexible soils strata with characteristics of table 21 for section 141 with elastic bars
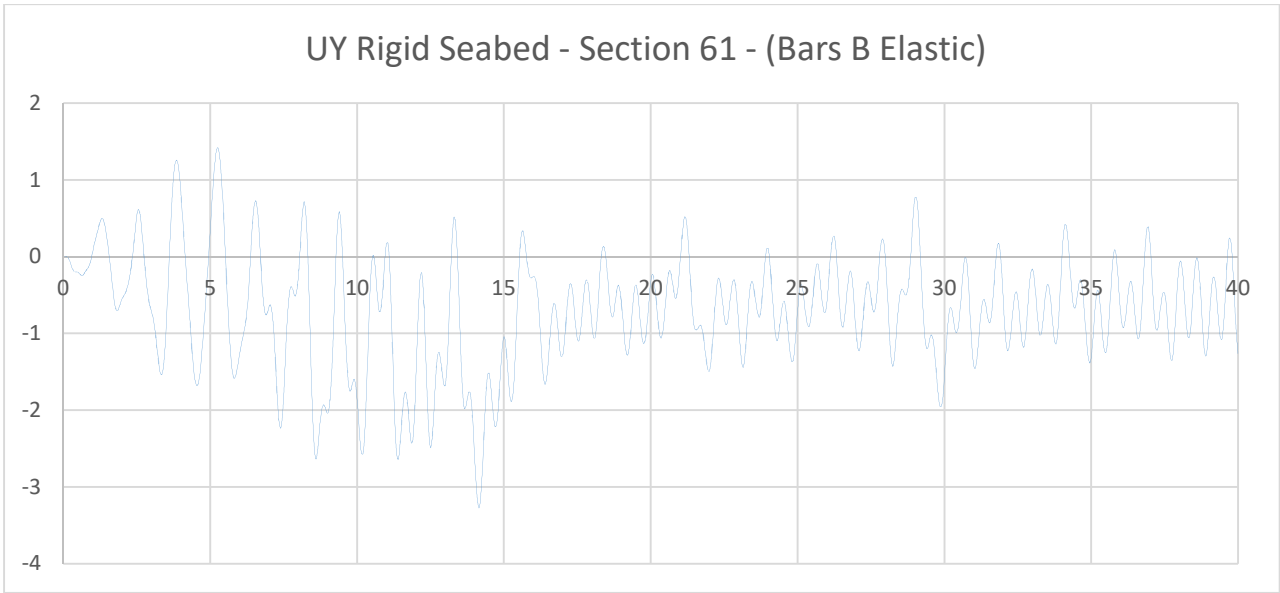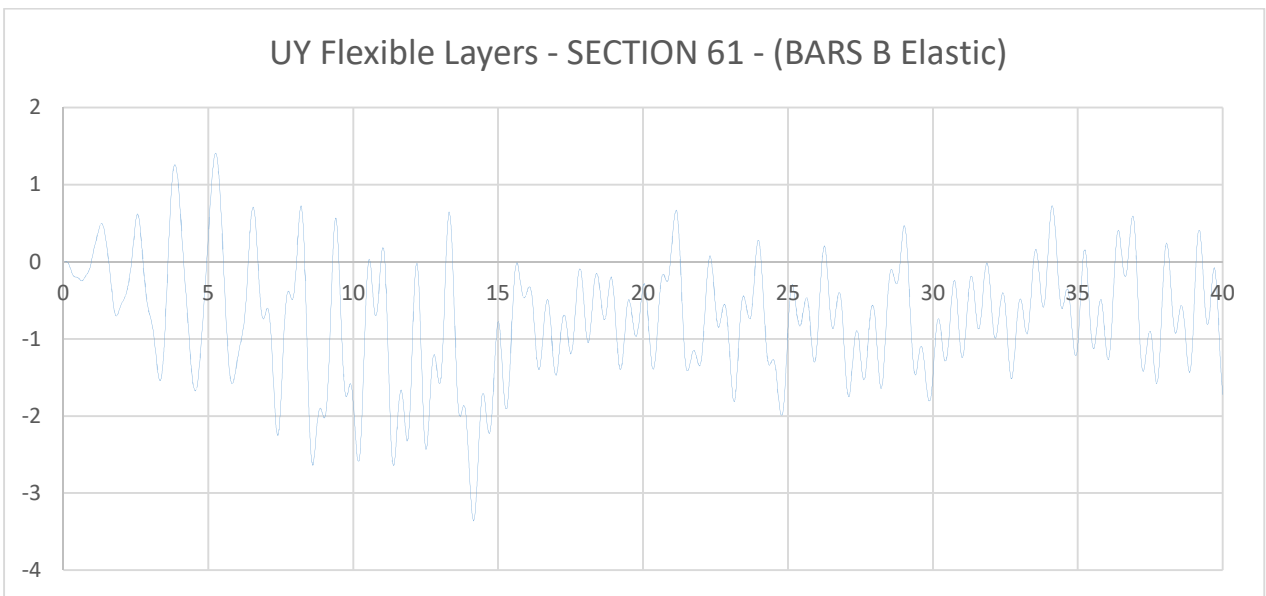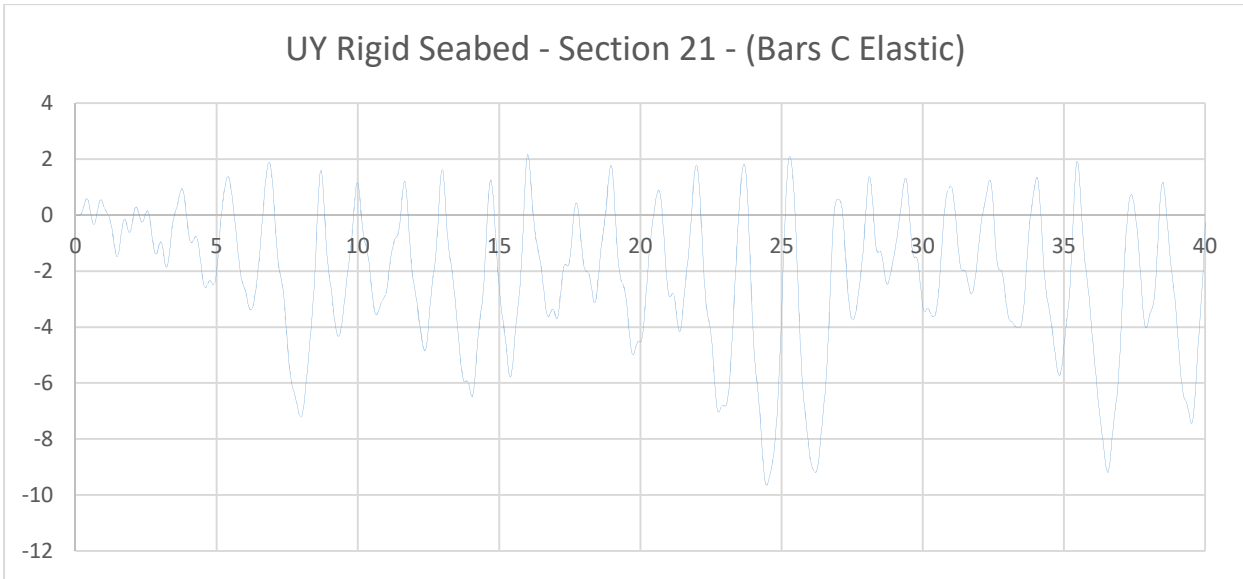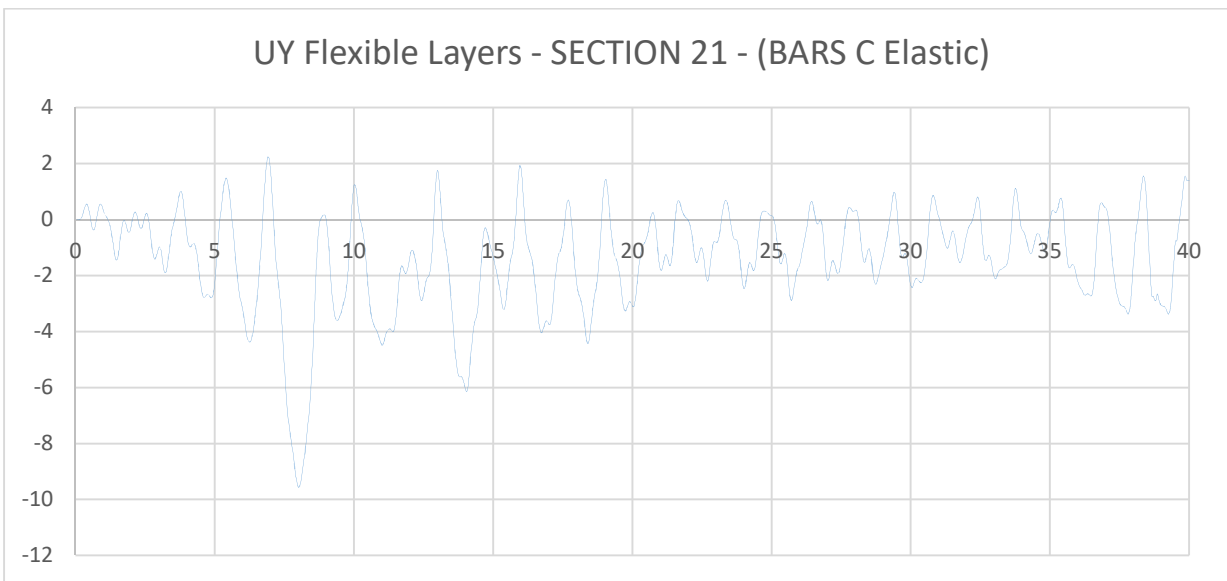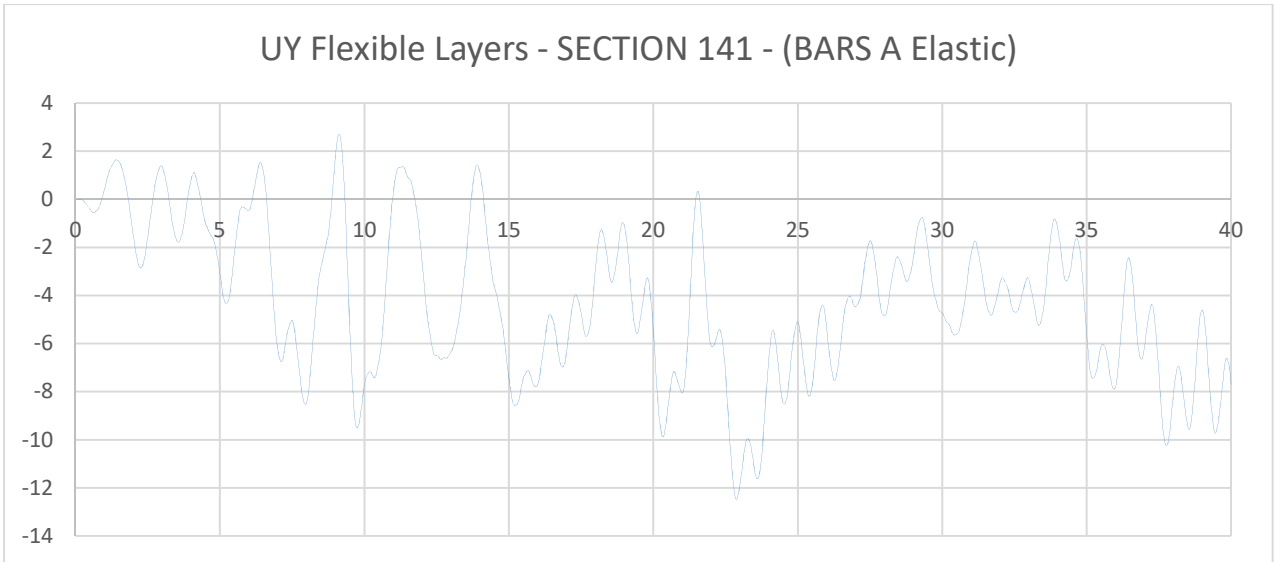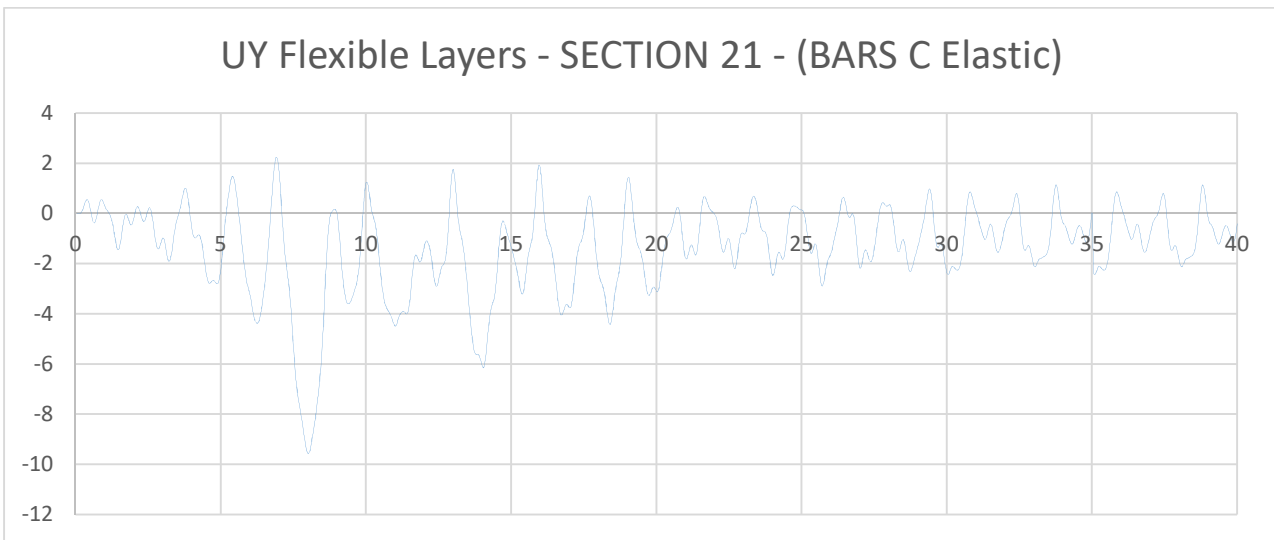

Figure 108 Vertical displacement of tunnel master node with two flexible soils strata with characteristics of table 21 for section 21

As can be seen from the results obtained above, the displacements in the vertical direction increase in the presence of a more compressible layer, with respect to the previous case (Stretto di Messina soil strata). In fact, the presence of a layer with these mechanical characteristics amplifies the effects going to increase both the speed of the soil and water. This phenomenon is more emphasized in the midspan section (section 161), where there is a greater overlying water column and it is gradually decreasing towards the end sections, where the vertical displacements are close to those obtained with a more rigid strata.

5.4.2 Results of 2-D Model with Inelastic Anchoring Bars

To take into account possible yielding of anchoring bars, we performed also a dynamic analysis with the same models and cases that we have developed above, but changing the behaviour of the bars from elastic to inelastic.

To implement this characteristic in ANSYS, it is necessary to change the characteristics of the bar element BRAM188 in order to take into account the yield stress and tangent modulus of the material.

The code above was added at the end of the definition of the element 188 in the file "elements_section_constraints.txt" and was used to add the characteristics of the material beyond the elastic range:

```
tb,bkin,1,1
tbtemp,0.0
tbdata,1,210e6,2.06e11*0.02
```

Figure 109 ANSYS code for the definition of inelastic properties of bars

The values in the last line represent the yield stress and tangent modulus of the material respectively.

The results for the vertical displacement obtained for both rigid bed and the two flexible soil strata of table 19 are the following:
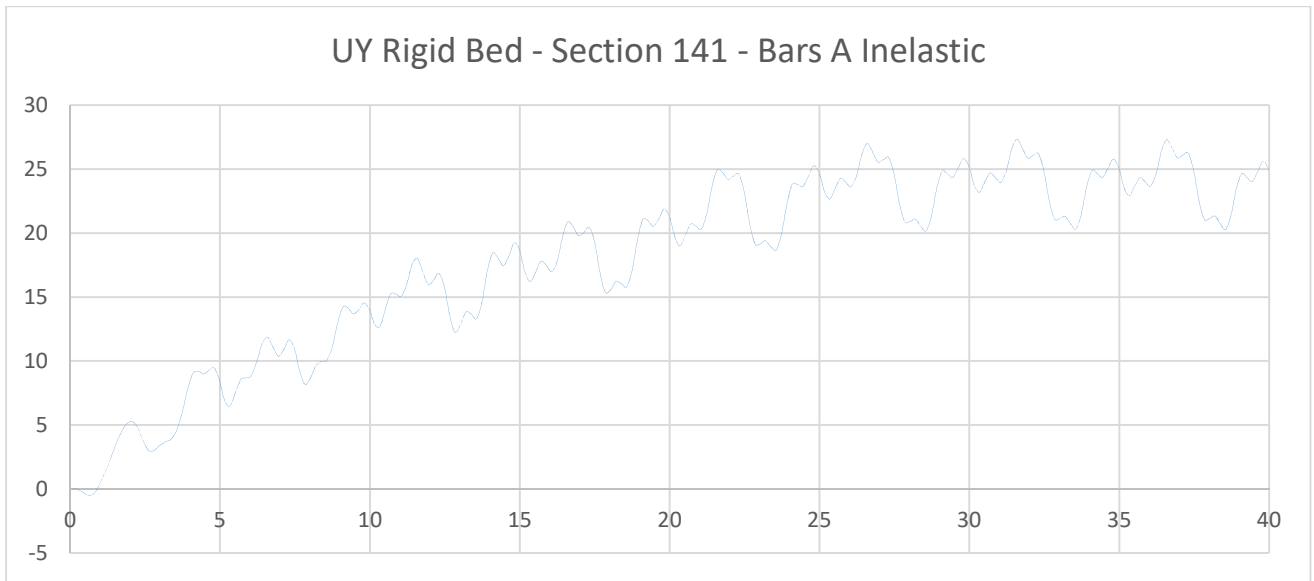
Figure 110 Vertical displacement of midspan section with inelastic bars on rigid seabed
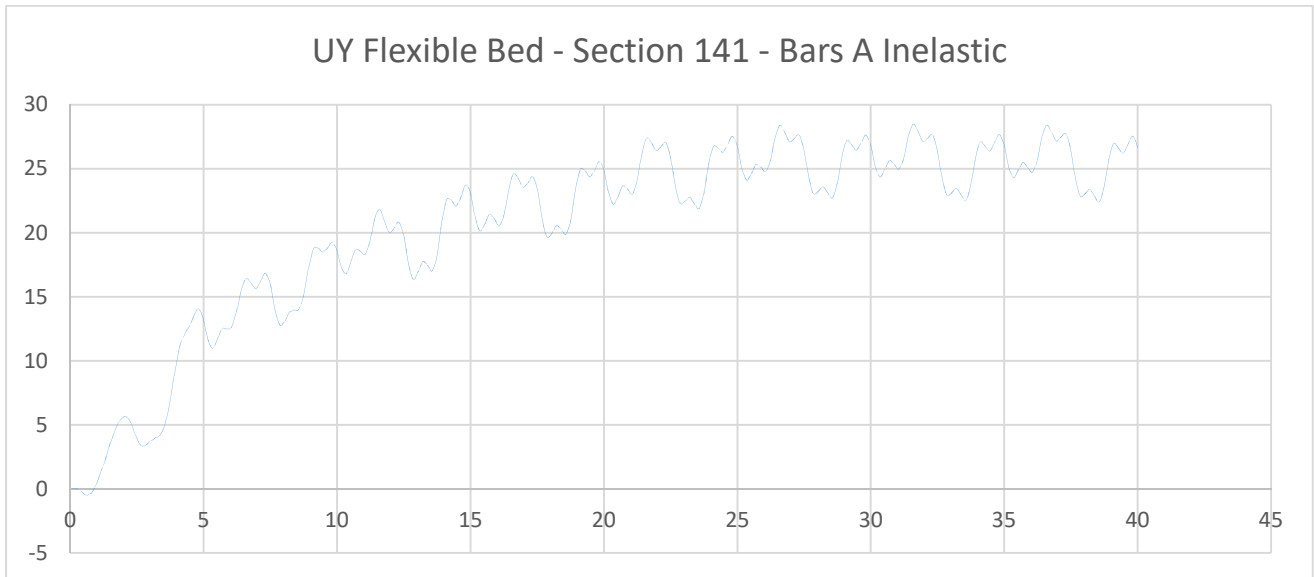
Figure 111 Vertical displacement of midspan section with inelastic bars on flexible soil strata of table 19

Analysis of SFT Resting on Flexible Soil Strata Subjected to Seaquake Excitation

Making a comparison, we can see that, as we expected, the displacements considering also the non-linear behaviour of the material are much bigger that the ones obtained with elastic bars.
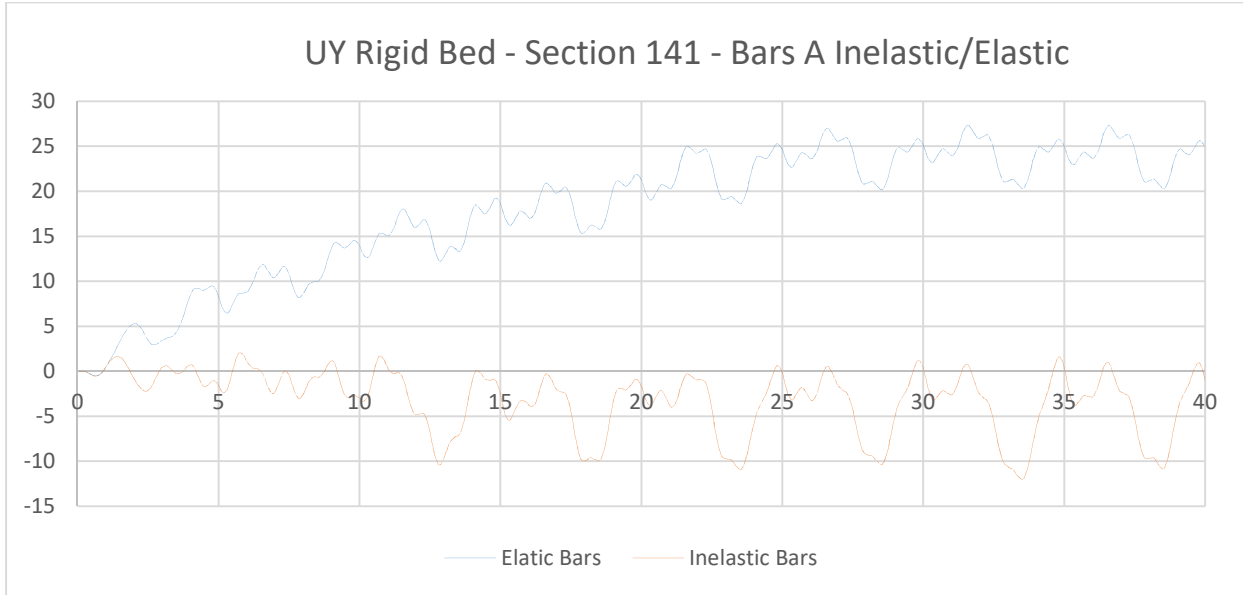
Figure 112 Vertical displacement for rigid bed with elastic and inelastic bars
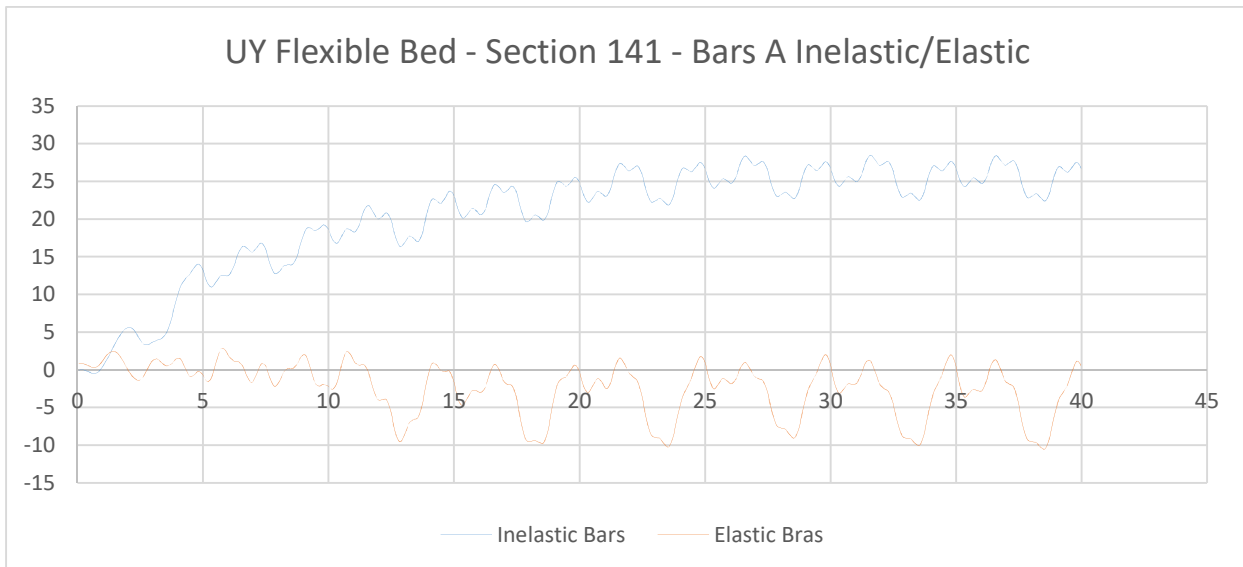
Figure 113 Vertical displacement for flexible layers of table 19 with elastic and inelastic bars

5.5 Conclusion

The conclusion that we can draw for the different cases here considered is that seaquake affects remarkably the response of the submerged floating tunnel but, adding different soil strata of various thickness, is not so critical for the behaviour of the structure with respect to the case of rigid seabed.

Moreover, we observed that the displacements are generally higher at the midspan and become gradually smaller approaching the shore. This means that we should expect higher internal forces at the extreme points of the tunnel and this is why, in the preliminary project, bigger bars were assigned to the sections near to the end, since we already expected such behaviour.

References Chapter 5

[5-1] Frequency Domain Using Excel – Larry Klingenberg – San Francisco State University, School of Engineering – April 2005

CONCLUSION

In this work of thesis, we tried to study the problem of the Submerged Floating Tunnel subjected to seaquake excitation in all its aspects, trying to understand how the different ground and structural conditions can affect the behaviour of this unusual type of construction.

As we have seen, the Messina Strait has very peculiar characteristics regarding geology, position and conformation. Its minimum length of 3km and the deepness of the seabed of nearly 400m makes it very difficult to cross using traditional constructions.

To study the whole model, that has a length of 4680 km, would have been very difficult and time consuming so, although we have also implemented a 3-D model on which we performed static and modal analyses, we concentrated on the dynamic study of three peculiar sections of the tunnel, in order to make more analyses and generate a various preliminary study of the behaviour of the tunnel.

The problems that we faced and solved were very different.

We started from the analytical generation of the transfer function relative to the passage of waves from seabed into two generic flexible soil strata.

Then, we implemented a program to construct the non-synchronous time histories to be applied to the tunnel that takes into consideration the filter due to the flexible strata.

In a second phase, we started the generation of the model, 2-D and 3-D, with the aid of the finite element program for structural analysis ANSYS, in which we represented the structure with nodes and different type of elements. We started to perform a simple static and modal analyses to test our model and understand its main characteristics in term of displacements. We have seen that, the tunnel moves upward in static condition in order to put the anchoring bars in tension and avoid unwanted instability of this ones that would lead to the sinking of the tunnel. This part of the work was the most time consuming, because we tried to build a model as much clear

and precise as possible, to take into account the most important aspects affecting the tunnel without creating a complex and unmanageable model.

All this was preliminary to the true aim of the thesis, the study of the tunnel under seaquake forces. But was also necessary due to the complexity of the model.

The dynamic analysis has been carried out only on the three most significant sections of the tunnel: the section at midspan, the one at a quarter span and one near the end.

The first analysis we made is inserting in the model the time-histories related to rigid seabed, considering the anchoring bars in the elastic range. This was a reference point for us, since, from previous studies, we learnt the importance of seaquake on the structural behaviour of a submerged floating tunnel. But we wanted to understand deeper how the behaviour changes inserting different soil strata upon bedrock.

So we made a second analysis generating the time histories for a sea floor in which there are two flexible layers upon the rigid rock. This leads to a slight increase of the displacement of the tunnel, that seemed to state that seaquake amplifies the response of the structure, especially at the end section, if there are flexible layers placed between rigid bed and water.

To validate even more our model, we interposed two layers more flexible than the ones used in the previous analysis between rigid bed and water and we noticed that, in this case, the displacements were still increasing, this time with an higher rate in the midspan section.

We repeated the above analysis with inelastic behaviour of the anchoring bars, detecting, as expected, a significant increasing of the displacement of the structure due to the overcome of the yielding of the material.

On this topic there is still much work to do, but it is certain that seaquake is a phenomenon that cannot be neglected in the study of a complex, extensive and innovative structure as the submerged floating tunnel.

Our aim is also to give a direction for future researches for continuing studying the effect of seaquake excitation generated by a signal that passes thought different layers

of flexible soil. In particular, we encourage the research in studying the effect of more than two layers, trying to reproduce real geologies and analyse the effects.

APPENDIX A – Derivation Of Seaquake Velocity Potential For Rigid Seabed

A.1 Seaquake wave equation and boundary conditions

The following derivation has been taken from Shi Chunxia PhD Program Thesis "Problems Related to the Seismic Behaviour of a Submerged Floating Tunnel", 2013.
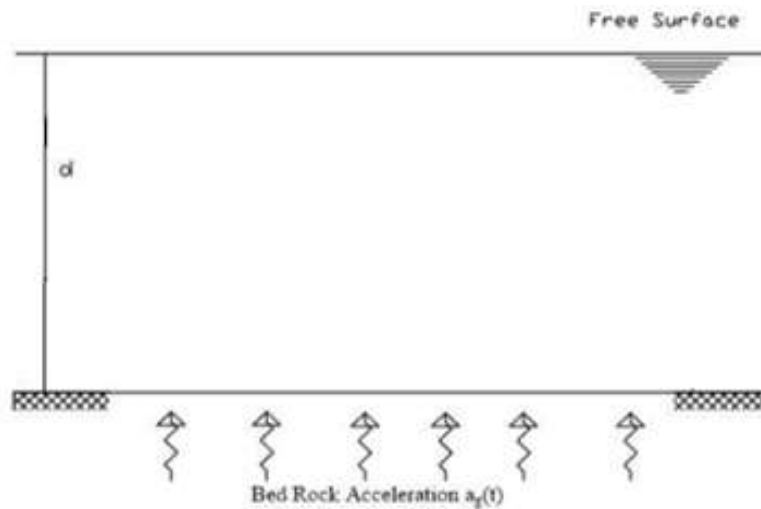
Figure 114 Schematization of rigid bedrock under a column of water d

For sake of simplicity, we recall here the equation and the boundary conditions to be solved to derive the velocity potential function ϕ:

Linearized wave equation:

$$\nabla^2 \Phi = \frac{1}{c^2}\frac{\partial^2 \Phi}{\partial t^2} \tag{A.1}$$

Free surface boundary condition 1,

$$\frac{\nabla \Phi}{\partial z} + \frac{1}{g}\frac{\partial^2 \Phi}{\partial t^2} = 0 \ \text{ at z=d} \tag{A.2}$$

Seabed boundary condition 2,

$$\frac{\nabla \Phi}{\partial z} = \frac{\partial U_g(t)}{\partial t} \ \text{ at z=0} \tag{A.3}$$

A.2 Mathematical solution

The solution will be found using the method of separation of variables. Suppose that the function ϕ can be decomposed into two separate factors. The first is function of time t, T(t) and the second is function of the vertical location, Z(z),

$$\phi(t,z) = T(t)Z(z)$$

(A.4)

The input (A.4) into eq. (A.1) gives the relation:

$$\frac{T''(t)}{c^2 T(t)} = \frac{Z''(z)}{Z(z)} = \text{constant}$$

(A.5)

From this and denoting the constant with $-\lambda$, two conditions are derived in the following form:

$$T''(t) + \lambda c^2 T(t) = 0$$

(A.6)

$$Z''(z) + \lambda Z(z) = 0$$

(A.7)

A.2.1 Solution of space function Z(z)

First step is to solve the differential equation (A.7):

$$\text{r}^2 + \lambda = 0, r = \pm i\sqrt{\lambda}$$

$$Z(z) = m \cos \sqrt{\lambda} z + n \sin \sqrt{\lambda} z$$

(A.8)

$$Z'(z) = -m\sqrt{\lambda} \sin \sqrt{\lambda} z + n\sqrt{\lambda} \cos \sqrt{\lambda} z$$

(A.9)

$$Z''(z) = -m\lambda \cos \sqrt{\lambda} z - n\lambda \sin \sqrt{\lambda} z$$

(A.10)

Substituting (5-4) into (5-2), the boundary condition 1 can be simplified to the relation function of z as follows:

$$\frac{\partial \phi}{\partial Z} + \frac{1}{g}\frac{\partial^2 \phi}{\partial t^2} = T(t)Z'(z) + \frac{1}{g}c^2 \nabla^2 \phi$$

$$= T(t)Z'(z) + \frac{c^2}{g}T(t)Z''(z) = 0\big|z = d$$

$$= Z'(z) + \frac{c^2}{g}Z''(z) = 0\big|z = d \tag{A.11}$$

Then by inserting (A.9) and (A.10) into (A.11) we can get:

$$(-m\lambda \cos\sqrt{\lambda}z - n\lambda\sin\sqrt{\lambda}z) + \frac{g}{c^2}(-m\sqrt{\lambda}\sin\sqrt{\lambda}z + n\sqrt{\lambda}\cos\sqrt{\lambda}z) = 0\big|z = d$$

$$(-\lambda\cos\sqrt{\lambda}d - \frac{g}{c^2}\sqrt{\lambda}\sin\sqrt{\lambda}d)\ m + (-\lambda\sin\sqrt{\lambda}d + \frac{g}{c^2}\sqrt{\lambda}\cos\sqrt{\lambda}d)\ n = 0$$

$$m = \frac{(-\lambda\sin\sqrt{\lambda}d + \frac{g}{c^2}\sqrt{\lambda}\cos\sqrt{\lambda}d)}{(\lambda\cos\sqrt{\lambda}d + \frac{g}{c^2}\sqrt{\lambda}\sin\sqrt{\lambda}d)}n \tag{A.12}$$

Now input (A.12) into (A.8), the function of the vertical location can be derived in (A.13):

$$Z(z) = m\cos\sqrt{\lambda}z + n\sin\sqrt{\lambda}z$$

$$= \frac{(-\lambda\sin\sqrt{\lambda}d + \frac{g}{c^2}\sqrt{\lambda}\cos\sqrt{\lambda}d)}{(\lambda\cos\sqrt{\lambda}d + \frac{g}{c^2}\sqrt{\lambda}\sin\sqrt{\lambda}d)}n \times \cos\sqrt{\lambda}z + n\sin\sqrt{\lambda}z$$

$$= \frac{(-\lambda\sin\sqrt{\lambda}d\cos\sqrt{\lambda}z + \frac{g}{c^2}\sqrt{\lambda}\cos\sqrt{\lambda}d\cos\sqrt{\lambda}z) + \sin\sqrt{\lambda}z\lambda\cos\sqrt{\lambda}d + \sin\sqrt{\lambda}z\frac{g}{c^2}\sqrt{\lambda}\sin\sqrt{\lambda}d}{(\lambda\cos\sqrt{\lambda}d + \frac{g}{c^2}\sqrt{\lambda}\sin\sqrt{\lambda}d)}n$$

$$= \frac{-\lambda\sin\sqrt{\lambda}(d-z) + \frac{g}{c^2}\sqrt{\lambda}\cos\sqrt{\lambda}(d-z)}{(\lambda\cos\sqrt{\lambda}d + \frac{g}{c^2}\sqrt{\lambda}\sin\sqrt{\lambda}d)}n$$

$$= \frac{-c^2\sqrt{\lambda}\sin\sqrt{\lambda}(d-z) + g\cos\sqrt{\lambda}(d-z)}{\left(c^2\sqrt{\lambda}\cos\sqrt{\lambda}d + g\sin\sqrt{\lambda}d\right)}n$$

$$= \frac{-c^2\mu\sin\mu(d-z) + g\cos\mu(d-z)}{(c^2\mu\cos\mu d + g\sin\mu d)}n$$

$$Z(z) = \frac{-c^2\mu\sin\mu(d-z) + g\cos\mu(d-z)}{(c^2\mu\cos\mu d + g\sin\mu d)}n$$

(A.13)

Note that $\sqrt{\lambda} = \mu$ has been assumed in the course of the derivation.

A.2.2 Solution of time function T(t)

Simplify the boundary condition equation (A.3) in the left and right one separately.

$$right = \frac{\partial U_g(t)}{\partial t} = \dot{U}_g(t)$$

$$left = \frac{\partial \phi}{\partial Z} = T(t)\dot{Z}(z)$$

$$= T(t)\frac{c^2\mu^2\cos\mu(d-z) + g\mu\sin\mu(d-z)}{(c^2\mu\cos\mu d + g\sin\mu d)}n\Big|z = 0$$

$$= T(t)\mu n$$

So we can get:

$$T(t) = \dot{U}_g(t)/n\mu\Big|z = 0$$

(A.14)

The ground acceleration function can be written in terms of power spectral density function seen in Chapter 2. The related symbols can be found in the aforementioned Chapter.

$$\overset{(2)}{\ddot{U}_g}(t) = \sum_{\eta=\pm1}\sum_{j=0}^{J-1}\sum_{n}^{N-1}\sqrt{2S(w_n)\times\Gamma(k_j,w_n)\ \Delta k\Delta w}\times\cos\left[\eta k_j x + w_n(t - \frac{x}{v_{app}}) + \phi_{jn}^{(\eta)}\right]$$

(A.15)

Considering the boundary condition 2, inserting (A.14) into (A.4), we get:

$$T''(t) + \lambda c^2 T(t) = 0$$

$$\overset{(3)}{\dddot{U}_g}(t)/(n\mu) + \lambda c^2 \overset{(1)}{\dot{U}_g}(t)/(n\mu) = 0$$

$$\overset{(4)}{\dddot{U}_g}(t) + \lambda c^2 \overset{(2)}{\ddot{U}_g}(t) = 0 \overset{known}{\Longleftarrow}$$

$$\overset{(2)}{U}_g(t) = \sum_{\eta=\pm1}\sum_{j=0}^{J-1}\sum_{n}^{N-1}\sqrt{2S(w_n)\times\Gamma\ (k_j,w_n)\ \Delta k\Delta w}\times\cos\left[\eta k_j x + w_n(t-\frac{x}{v_{app}})+\phi_{jn}^{(\eta)}\right]$$

$$\overset{(4)}{U}_g(t) = -\sum_{\eta=\pm1}\sum_{j=0}^{J-1}\sum_{n}^{N-1}(w_n)^2\sqrt{2S(w_n)\times\Gamma\ (k_j,w_n)\ \Delta k\Delta w}\times\cos\left[\eta k_j x + w_n(t-\frac{x}{v_{app}})+\phi_{jn}^{(\eta)}\right]$$

$$-\sum_{\eta=\pm1}\sum_{j=0}^{J-1}\sum_{n}^{N-1}(w_n)^2\sqrt{2S(w_n)\times\Gamma\ (k_j,w_n)\ \Delta k\Delta w}\times\cos\left[\eta k_j x + w_n(t-\frac{x}{v_{app}})+\phi_{jn}^{(\eta)}\right]$$

$$+\lambda c^2\sum_{\eta=\pm1}\sum_{j=0}^{J-1}\sum_{n}^{N-1}\sqrt{2S(w_n)\times\Gamma\ (k_j,w_n)\ \Delta k\Delta w}\times\cos\left[\eta k_j x + w_n(t-\frac{x}{v_{app}})+\phi_{jn}^{(\eta)}\right]=0$$

First suppose that λ is a constant:

$$\sum(iw_n)^2 + \lambda c^2 = 0$$
$$\lambda = -\frac{\sum(iw_n)^2}{c^2} = \frac{\sum w_n^2}{c^2}$$

Since λ is not a constant, actually is a relation of wₙ, we write:

$$\sum(iw_n)^2 + \sum\lambda c^2 = 0$$
$$(iw_n)^2 + \lambda c^2 = 0$$
$$-w_n^2 + \lambda c^2 = 0$$
$$\lambda = \frac{w_n^2}{c^2} = \mu^2$$

From the upper deduction, we can get:

$$\mu = \frac{w_n}{c} \tag{A.16}$$

As a result:

$$T(t) = \dot{U}_g(t)/(n\mu) = \frac{\int \ddot{U}_g(t)dt}{(n\mu)}$$

$$= \frac{\int \sum_{\eta=\pm 1} \sum_{j=0}^{J-1} \sum_{n}^{N-1} \sqrt{2S(w_n) \times \Gamma\ (k_j, w_n)\ \Delta k \Delta w} \times \cos\left[\eta k_j x + w_n(t - \frac{x}{v_{app}}) + \phi_{jn}^{(\eta)}\right] dt}{n\mu}$$

$$= \sum_{\eta=\pm 1} \sum_{j=0}^{J-1} \sum_{n}^{N-1} \frac{\sqrt{2S(w_n) \times \Gamma\ (k_j, w_n)\ \Delta k \Delta w} \times \cos\left[\eta k_j x + w_n(t - \frac{x}{v_{app}}) + \phi_{jn}^{(\eta)}\right]}{\mu n \times (w_n)} \qquad \text{(A.17)}$$

$$= \sum_{\eta=\pm 1} \sum_{j=0}^{J-1} \sum_{n}^{N-1} \frac{\sqrt{2S(w_n) \times \Gamma\ (k_j, w_n)\ \Delta k \Delta w} \times (\sin\left[\eta k_j x + w_n(t - \frac{x}{v_{app}}) + \phi_{jn}^{(\eta)}\right])}{\mu n \times (w_n)}$$

A.2.3 Solution of velocity potential □

Finally, putting (A.13), (A.16), and (A.17) into (A.3):

$$\phi = T(t) * Z(z)$$

$$= \sum_{\eta=\pm 1} \sum_{j=0}^{J-1} \sum_{n}^{N-1} \frac{\sqrt{2S(w_n) \times \Gamma\ (k_j, w_n)\ \Delta k \Delta w} \times (\sin\left[\eta k_j x + w_n(t - \frac{x}{v_{app}}) + \phi_{jn}^{(\eta)}\right])}{(w_n)}$$
$$\times \frac{-c^2 \mu \sin \mu(d-z) + g \cos \mu(d-z)}{\mu \times (c^2 \mu \cos \mu d + g \sin \mu d)}$$

$$\Leftarrow V_0 = A_0 / w_n, \ A_0 = \sqrt{2S(w_n) \times \Gamma\ (k_j, w_n)\ \Delta k \Delta w}$$

$$\phi = \sum_{\eta=\pm 1} \sum_{j=0}^{J-1} \sum_{n}^{N-1} \frac{V_0}{\mu} \frac{-c^2 \mu \sin \mu(d-z) + g \cos \mu(d-z)}{(c^2 \mu \cos \mu d + g \sin \mu d)}$$
$$\times \sin\left[\eta k_j x + w_n(t - \frac{x}{v_{app}}) + \phi_{jn}^{(\eta)}\right]$$

So, the velocity potential function can be written as:

$$\phi = \sum_{\eta=\pm 1} \sum_{j=0}^{J-1} \sum_{n}^{N-1} \frac{V_0}{\mu} \frac{-c^2 \mu \sin \mu(d-z) + g \cos \mu(d-z)}{(c^2 \mu \cos \mu d + g \sin \mu d)}$$
$$\times (\sin\left[\eta k_j x + w_n(t - \frac{x}{v_{app}}) + \phi_{jn}^{(\eta)}\right]) \qquad \text{(A.18)}$$

Transferring equation (A.18) into full expression in frequency domain:

$$\phi = \sum_{\eta=\pm 1} \sum_{j=0}^{J-1} \sum_{n}^{N-1} \sqrt{2S(w_n) \times \Gamma\ (k_j, w_n)\ \Delta k \Delta w} \times \frac{-c^2 w_n \sin\frac{w_n}{c}(d-z) + cg\cos\frac{w_n}{c}(d-z)}{cw_n^{\,3}\cos\frac{w_n}{c}d + w_n^{\,2}g\sin\frac{w_n}{c}d} \qquad (A.19)$$

$$\times (\sin\left[\eta k_j x + w_n(t - \frac{x}{v_{app}}) + \phi_{jn}^{(\eta)}\right])$$

APPENDIX B – Derivation of Seaquake Velocity Potential for Flexible Layer

B.1 Seaquake wave equation and boundary conditions

For sake of simplicity, we recall here the equation and the boundary conditions to be solved to derive the velocity potential function φ for flexible seabed.
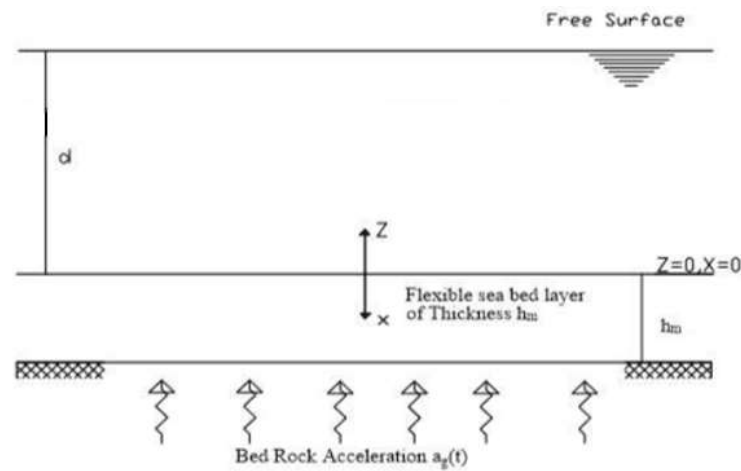
Figure 115 Schematic representation of flexible sea bed with one elastic layer

Wave 1-D equation:

$$\frac{\partial^2 u}{\partial x^2} = \frac{1}{\alpha^2}\frac{\partial^2 u}{\partial t^2}$$
(B.1)

where

$$\alpha = \left(\frac{\lambda + 2\mu}{\rho_s}\right)^{1/2}$$

B.c. 1: Compatibility between the motion of the elastic layer and bedrock acceleration

$a_g(t) = a_g * e^{(i\omega t)}$

$$a_g e^{i\omega t} + \frac{\partial^2 u}{\partial t^2} \quad \text{at x=}h_m$$
(B.2)

B.c. 2: Compatibility between flexible layer velocity and water velocity

$$\frac{du}{dt} + \frac{d\Phi}{dz} = 0 \quad \text{at x=0 and z=0}$$
(B.3)

B.c. 3: Equilibrium equation at the interface between water and soil layer

$$\frac{\rho_s \left(\frac{\partial u}{\partial x}\right) \omega^2}{k_s^2} - \rho_w \frac{\partial \Phi}{\partial t} = 0 \text{ at x=0 and z=0} \tag{B.4}$$

B.2 Setting of Solution

An important factor to be considered in the analysis is the loss of energy during the propagation of waves. The phenomenon is usually referred as *material damping*. For most soils, the mechanism of damping is not sufficiently well understood to allow for explicit modelling. For the purposes of viscoelastic wave propagation, soils are usually modelled as materials whose resistance to shearing deformation is the sum of an elastic part and a viscous part, which is represented in the equation below:

$$\rho \frac{\partial^2 u}{\partial t^2} = (\lambda + 2\mu)\frac{\partial^2 u}{\partial x^2} + \eta \frac{\partial^3 u}{\partial x^2 \partial t} \qquad\qquad \text{(B.5)}$$

The harmonic displacement with frequency ω, solution of the equation above, can be written as the product of a term function of time and a term function of space (separation of variables):

$$u(x,t) = U(x)e^{i\omega t} \qquad\qquad \text{(B.6)}$$

Substituting equation (B.6) in (B.5), we get:

$$\left((\lambda + 2\mu) + i\omega\eta\right)\frac{\partial^2 u}{\partial x^2} = \rho \omega^2 U \qquad\qquad \text{(B.7)}$$

Which general solution is:

$$U(x) = E e^{ik_s x} + F e^{-ik_s x} \qquad\qquad \text{(B.8)}$$

where:

$$k_s = \frac{\rho_s \omega^2}{(\lambda + 2\mu) + i\omega\eta} = \frac{\rho_s \omega^2}{E^*}$$

k_s = complex wave number

The critical damping ratio, β, is related to viscosity, η by the relation:

$$\omega\eta = 2(\lambda + 2\mu)\beta$$

Experiments on many soil materials indicate that G and β are nearly constant over the frequency range which is of main interest in the analysis. It is convenient to express the complex shear modulus in the terms of the critical damping ratio, equation mention below:

$$E^* = (\lambda + 2\mu) + i\omega\eta \tag{B.9}$$

The Critical Damping ratio β and viscosity constant η are related by the following:

$$\eta = \frac{2\beta(\lambda+2\mu)}{\omega}$$

Equations (B.8) and (B.9) give the solution of the displacement field in the ground:

$$u(x,t) = Ee^{i(k_s x+\omega t)} + Fe^{-(ik_s x-\omega\ )} \tag{B.10}$$

where the first term represents the incident wave travelling in the negative x-direction and second term represents the reflected wave travelling in the positive x-direction.

The velocity potential of water considering only rigid seabed can also be written in the following form

$$\Phi = \frac{A_s g\cos\big(\mu(d-z)\big)-c^2\mu\sin\big(\mu(d-z)\big)*e^{i\omega t}}{g\sin(d\mu)+c^2\mu\omega\cos(d\mu)} \tag{B.11}$$

Or, alternatively

$$\Phi = \frac{A_s e^{i\omega t}[cg\cos\left(\frac{(d-z)\omega}{c}\right)-c^2\omega\sin\left(\frac{(d-z)}{c}\right)}{\omega\left(g\omega^2\sin\left(\frac{d\omega}{c}\right)+c^2\mu\omega\,\cos\left(\frac{d\omega}{c}\right)\right)} \tag{B.12}$$

B.3 Derivation of the solution

Our aim is now to solve equation (5) with the three boundary conditions seen above, taking in mind that the general solution of eq. (5) is given by eq. (10) and exploiting the velocity potential in water considering rigid seabed of eq. (11) and (12) (given by Shi Chunxia PhD Program Thesis "Problems Related to the Seismic Behaviour of a Submerged Floating Tunnel", 2013).

In b.c. 1 we substitute the general expression of u given by eq. (10) and evaluating this expression at x = h, i.e. at the interface between flexible layer and rigid rock, we obtain the following equation:

$$-E\omega^2 e^{i(t\omega+hk)} - F\omega^2 e^{-i(t\omega+hk)} + a_g e^{it\omega} = 0 \qquad (B.13)$$

In b.c. 2 we substitute the expressions given by eq. (10) and (11) and we evaluate it at x=0 and z=0, i.e. at the interface between the top surface of the flexible layer and water, obtaining the equation as follows:

$$\frac{A_s e^{i\omega t}\left(g\omega \sin\left(\frac{d\omega}{c}\right)+c\omega^2 \cos\left(\frac{d\omega}{c}\right)\right)}{\omega\left(g\omega^2 \sin\left(\frac{d\omega}{c}\right)+c\omega^3 \cos\left(\frac{d\omega}{c}\right)\right)} + E\omega e^{it\omega} + F\omega e^{it\omega} = 0 \qquad (B.14)$$

In b.c 3, as before, we substitute expressions (10) and (11) and evaluate everything at x=0 and z=0:

$$\frac{\rho_s\omega^2(E\omega e^{it\omega}-F\omega e^{it\omega})}{k_s} - \frac{A_s\rho_w e^{i\omega t}\left(cg\cos\left(\frac{d\omega}{c}\right)-c^2\omega\sin\left(\frac{d\omega}{c}\right)\right)}{g\omega^2\sin\left(\frac{d\omega}{c}\right)+c\omega^3\omega\cos\left(\frac{d\omega}{c}\right)} = 0 \qquad (B.15)$$

Solving the system given by the three boundary conditions of equations (13), (14) and (15) with unknowns E, F and A_s (=a_g), we derive the values of E, F and A_s that substituted in eq. (10) and (12) give:

Motion at bedrock from motion in the soil layer:

(%o14)   u=

$$\frac{\%e^{\%i\left(t\omega+hk\right)}\left(\left(a_g\,c^2\,k\,\%e^{\%i\,h\,k}\,\rho_v-\%i\,a_g\,g\,\%e^{\%i\,h\,k}\,\rho_s\right)\omega\sin\left(\frac{d\,\omega}{c}\right)+\left(-\%i\,a_g\,c\,\%e^{\%i\,h\,k}\,\rho_s\,\omega^2-a_g\,c\,g\,k\,\%e^{\%i\,h\,k}\,\rho_v\right)\cos\left(\frac{d\,\omega}{c}\right)\right)}{\left(\left(c^2\,k\,\%e^{2\,\%i\,h\,k}-c^2\,k\right)\rho_v+\left(-\%i\,g\,\%e^{2\,\%i\,h\,k}-\%i\,g\right)\rho_s\right)\omega^3\sin\left(\frac{d\,\omega}{c}\right)+\left(\left(-\%i\,c\,\%e^{2\,\%i\,h\,k}-\%i\,c\right)\rho_s\,\omega^4+\left(c\,g\,k-c\,g\,k\,\%e^{2\,\%i\,h\,k}\right)\rho_v\,\omega^2\right)\cos\left(\frac{d\,\omega}{c}\right)}$$

$$-\frac{\%e^{-\%i\left(h\,k-t\,\omega\right)}\left(\left(a_g\,c^2\,k\,\%e^{\%i\,h\,k}\,\rho_v+\%i\,a_g\,g\,\%e^{\%i\,h\,k}\,\rho_s\right)\omega\sin\left(\frac{d\,\omega}{c}\right)+\left(\%i\,a_g\,c\,\%e^{\%i\,h\,k}\,\rho_s\,\omega^2-a_g\,c\,g\,k\,\%e^{\%i\,h\,k}\,\rho_v\right)\cos\left(\frac{d\,\omega}{c}\right)\right)}{\left(\left(c^2\,k\,\%e^{2\,\%i\,h\,k}-c^2\,k\right)\rho_v+\left(-\%i\,g\,\%e^{2\,\%i\,h\,k}-\%i\,g\right)\rho_s\right)\omega^3\sin\left(\frac{d\,\omega}{c}\right)+\left(\left(-\%i\,c\,\%e^{2\,\%i\,h\,k}-\%i\,c\right)\rho_s\,\omega^4+\left(c\,g\,k-c\,g\,k\,\%e^{2\,\%i\,h\,k}\right)\rho_v\,\omega^2\right)\cos\left(\frac{d\,\omega}{c}\right)}$$

(10)

And the velocity potential for motion in water:

(%o15) $\Phi=-\left(\%e^{\%i\,t\,\omega}\left(2\,a_g\,g\,\%e^{\%i\,h\,k}\,\rho_s\,\omega^2\sin\left(\frac{d\,\omega}{c}\right)+2\,a_g\,c\,\%e^{\%i\,h\,k}\,\rho_s\,\omega^3\cos\left(\frac{d\,\omega}{c}\right)\right)\left(c\,g\cos\left(\frac{(d-z)\,\omega}{c}\right)-c^2\,\omega\sin\left(\frac{(d-z)\,\omega}{c}\right)\right)\right)$

$/\left(\omega\left(\left(\left(c^2\,k\,\%e^{2\,\%i\,h\,k}-c^2\,k\right)\rho_v+\left(-\%i\,g\,\%e^{2\,\%i\,h\,k}-\%i\,g\right)\rho_s\right)\omega\sin\left(\frac{d\,\omega}{c}\right)+\left(\left(-\%i\,c\,\%e^{2\,\%i\,h\,k}-\%i\,c\right)\rho_s\,\omega^2+\left(c\,g\,k-c\,g\,k\,\%e^{2\,\%i\,h\,k}\right)\rho_v\right)\right.$

$\left.\cos\left(\frac{d\,\omega}{c}\right)\right)\left(g\,\omega^2\sin\left(\frac{d\,\omega}{c}\right)+c\,\omega^3\cos\left(\frac{d\,\omega}{c}\right)\right)\right)$

(11)

That, with some assumptions, can be written in a more compact form as eq. (5-13) seen in chapter 3.

Dividing eq. (11) by the expression of acceleration at bedrock $a_g*exp^{(i*\omega*t)}$, we obtain the transfer function from acceleration at bedrock and velocity potential:

$$\frac{2\,c^2\,\rho_s\,\omega\,\%e^{2\,\%i\,t\,\omega+\%i\,h\,k}\sin\left(\frac{(z-d)\,\omega}{c}\right)+2\,c\,g\,\rho_s\,\%e^{2\,\%i\,t\,\omega+\%i\,h\,k}\cos\left(\frac{(z-d)\,\omega}{c}\right)}{\left(\left(c^2\,k\,\%e^{2\,\%i\,h\,k}-c^2\,k\right)\rho_v+\left(-\%i\,g\,\%e^{2\,\%i\,h\,k}-\%i\,g\right)\rho_s\right)\omega^2\sin\left(\frac{d\,\omega}{c}\right)+\left(\left(-\%i\,c\,\%e^{2\,\%i\,h\,k}-\%i\,c\right)\rho_s\,\omega^3+\left(c\,g\,k-c\,g\,k\,\%e^{2\,\%i\,h\,k}\right)\rho_v\,\omega\right)\cos\left(\frac{d\,\omega}{c}\right)}$$

Deriving the function ϕ of equation (11) with respect to z, we obtain the velocity of water:

(%o23) $\frac{d}{d\,z}\Phi=-\left(\%e^{\%i\,t\,\omega}\left(2\,a_g\,g\,\%e^{\%i\,h\,k}\,\rho_s\,\omega^2\sin\left(\frac{d\,\omega}{c}\right)+2\,a_g\,c\,\%e^{\%i\,h\,k}\,\rho_s\,\omega^3\cos\left(\frac{d\,\omega}{c}\right)\right)\right.$

$\left(g\,\omega\sin\left(\frac{(d-z)\,\omega}{c}\right)+c\,\omega^2\cos\left(\frac{(d-z)\,\omega}{c}\right)\right))/\left(\omega\left(\left(\left(c^2\,k\,\%e^{2\,\%i\,h\,k}-c^2\,k\right)\rho_v+\left(-\%i\,g\,\%e^{2\,\%i\,h\,k}-\%i\,g\right)\rho_s\right)\omega\sin\left(\frac{d\,\omega}{c}\right)+\right.$

$\left.\left(\left(-\%i\,c\,\%e^{2\,\%i\,h\,k}-\%i\,c\right)\rho_s\,\omega^2+\left(c\,g\,k-c\,g\,k\,\%e^{2\,\%i\,h\,k}\right)\rho_v\right)\cos\left(\frac{d\,\omega}{c}\right)\right)\left(g\,\omega^2\sin\left(\frac{d\,\omega}{c}\right)+c\,\omega^3\cos\left(\frac{d\,\omega}{c}\right)\right)\right)$

APPENDIX C – Derivation of Seaquake Velocity Potential for Multiple Flexible Layers

C.1 Seaquake wave equation and boundary conditions

For sake of simplicity, we recall here the equation and the boundary conditions to be solved to derive the velocity potential function ϕ for flexible seabed.
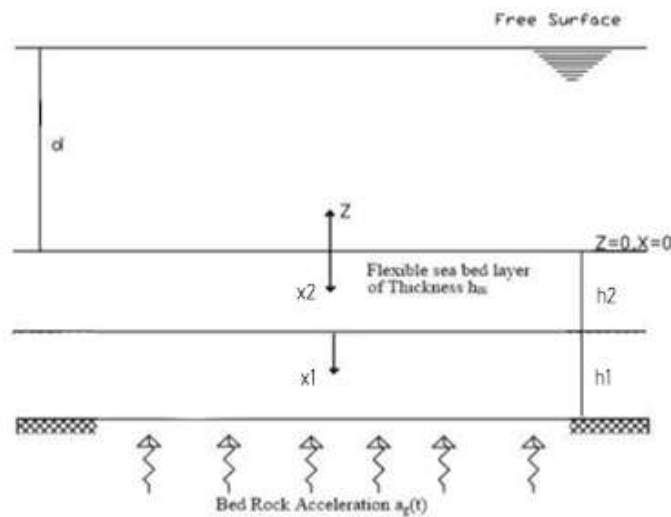

Figure 116 Schematic representation of flexible sea bed with two elastic layers

Wave 1-D equation:

$$\frac{\partial^2 u}{\partial x^2} = \frac{1}{\alpha^2}\frac{\partial^2 u}{\partial t^2} \tag{C.1}$$

where

$$\alpha = \left(\frac{\lambda + 2\mu}{\rho_s}\right)^{1/2}$$

Bc1: compatibility between the motion of the second layer with the first ones

$$\frac{d^2 u_2}{dt^2} + \frac{d^2 u_1}{dt^2} = 0 \text{ at x=h}_2 \tag{C.2}$$

Bc2: compatibility of water velocity and ground layer velocity

$$\frac{du_2}{dt} + \frac{d\Phi}{dz} = 0 \text{ at z=0 and x=0} \tag{C.3}$$

Bc3: equilibrium in the vertical direction at water soil layer

$$\frac{\rho_{s2}\left(\frac{\partial u_2}{\partial x}\right)\omega^2}{k_{s2}^2} - \rho_w \frac{\partial \Phi}{\partial t} = 0 \text{ at z=0 and x=0} \tag{C.4}$$

Where:

ρ_w - Density of water

ϕ - Velocity Potential

$k_s = \rho_s \omega^2 / E^*$

$k_{s2} = \rho_{s2} \omega^2 / E_2{}^*$

$E^* = (\lambda + 2\mu) + i\omega\,\eta$ The complex modulus.

$E_2{}^* = (\lambda_2 + 2\mu_2) + i\omega\,\eta_2$ The complex modulus.

η - viscosity constant.

u2 - Ground displacement of layer 2

u1 - Ground displacement of layer 1

C.2 Setting of Solution

The equation of waves to be solved is the one above, that is composed of an elastic part and a viscoud part, to take into account damping of material.

$$\rho \frac{\partial^2 u}{\partial t^2} = (\lambda + 2\mu) \frac{\partial^2 u}{\partial x^2} + \eta \frac{\partial^3 u}{\partial x^2 \partial t}$$

(C.5)

The harmonic displacement with frequency ω, solution of the equation above, can be written as the product of a term function of time and a term function of space (separation of variables):

$$u2(x, t) = U2(x)e^{i\omega t}$$

(C.6)

Substituting equation (B.6) in (B.5), we get:

$$\left((\lambda + 2\mu) + i\omega\eta\right) \frac{\partial^2 u}{\partial x^2} = \rho\omega^2 U2$$

(C.7)

Which general solution is:

$$U2(x) = Ee^{ik_{s2}x} + Fe^{-ik_{s2}x}$$

(C.8)

where:

$$k_{s2} = \frac{\rho_2 \omega^2}{(\lambda 2 + 2\mu 2) + i\omega\eta} = \frac{\rho_2 \omega^2}{E2^*}$$

k_{s2} = complex wave number

The critical damping ratio, β, is related to viscosity, η by the relation:

$$\omega\eta = 2(\lambda + 2\mu)\beta$$

Experiments on many soil materials indicate that G and β are nearly constant over the frequency range which is of main interest in the analysis. It is convenient to express the complex shear modulus in the terms of the critical damping ratio, equation mention below:

$$E^* = (\lambda + 2\mu) + i\omega\eta$$

(C.9)

The Critical Damping ratio β and viscosity constant η are related by the following:

$$\eta = \frac{2\beta(\lambda + 2\mu)}{\omega}$$

Equations (C.8) and (C.9) give the solution of the displacement field in the ground:

$$u2(x,t) = E e^{i(k_s x+\omega)} + F e^{-(ik_s x-\omega t)} \tag{C.10}$$

where the first term represents the incident wave travelling in the negative x-direction and second term represents the reflected wave travelling in the positive x-direction.

The velocity potential of water considering only rigid seabed can also be written in the following form

$$\Phi = \frac{A_s g \cos(\mu(d-z)) - c^2 \mu \sin(\mu(d-z)) * e^{i\omega t}}{g \sin(d\mu) + c^2 \mu \omega \cos(d\mu)} \tag{C.11}$$

Or, alternatively

$$\Phi = \frac{A_s e^{i\omega t} [cg\cos\left(\frac{(d-z)\omega}{c}\right) - c^2 \omega \sin\left(\frac{(d-z)}{c}\right)}{\omega\left(g\omega^2 \sin\left(\frac{d\omega}{c}\right) + c^2 \mu \omega \cos\left(\frac{d\omega}{c}\right)\right)} \tag{C.12}$$

While the motion of soli layer 1 with respect to bedrock is the one for 1 flexible layer derived in Appendix B:

(C.13)

C.3 Derivation of the solution

Our aim is now to solve equation (1) with the three boundary conditions seen above, taking in mind that the general solution of eq. (1) is given by eq. (4) and exploiting the velocity potential in water considering rigid seabed of eq. (5) and (6) (given by Shi Chunxia PhD Program Thesis "Problems Related to the Seismic Behaviour of a Submerged Floating Tunnel", 2013).

In b.c. 1 we substitute the general expression of u_1 and u_2 given by eq. (10) and (13) and evaluating this expression at x = h_2, i.e. at the interface between flexible layer and rigid rock, we obtain the following equation:

$$\frac{\omega^2\,\%e^{-\%i\left(hk-t\,\omega\right)}\left(\left(a_g\,c^2\,k\,\%e^{\%i\,hk}\rho_\nu+\%i\,a_g\,g\,\%e^{\%i\,hk}\rho_1\right)\omega\sin\left(\frac{d\omega}{c}\right)+\left(\%i\,a_g\,c\,\%e^{\%i\,hk}\rho_1\,\omega^2-a_g\,cgk\,\%e^{\%i\,hk}\rho_\nu\right)\cos\left(\frac{d\omega}{c}\right)\right)}{\left(\left(c^2\,k\,\%e^{2\,\%i\,hk}-c^2\,k\right)\rho_\nu+\left(-\%i\,g\,\%e^{2\,\%i\,hk}-\%i\,g\right)\rho_1\right)\omega^3\sin\left(\frac{d\omega}{c}\right)+\left(\left(-\%i\,c\,\%e^{2\,\%i\,hk}-\%i\,c\right)\rho_1\,\omega^4+\left(cgk-cgk\,\%e^{2\,\%i\,hk}\right)\rho_\nu\,\omega^2\right)\cos\left(\frac{d\omega}{c}\right)}-$$

$$\frac{\omega^2\,\%e^{\%i\left(t\,\omega+hk\right)}\left(\left(a_g\,c^2\,k\,\%e^{\%i\,hk}\rho_\nu-\%i\,a_g\,g\,\%e^{\%i\,hk}\rho_1\right)\omega\sin\left(\frac{d\omega}{c}\right)+\left(-\%i\,a_g\,c\,\%e^{\%i\,hk}\rho_1\,\omega^2-a_g\,cgk\,\%e^{\%i\,hk}\rho_\nu\right)\cos\left(\frac{d\omega}{c}\right)\right)}{\left(\left(c^2\,k\,\%e^{2\,\%i\,hk}-c^2\,k\right)\rho_\nu+\left(-\%i\,g\,\%e^{2\,\%i\,hk}-\%i\,g\right)\rho_1\right)\omega^3\sin\left(\frac{d\omega}{c}\right)+\left(\left(-\%i\,c\,\%e^{2\,\%i\,hk}-\%i\,c\right)\rho_1\,\omega^4+\left(cgk-cgk\,\%e^{2\,\%i\,hk}\right)\rho_\nu\,\omega^2\right)\cos\left(\frac{d\omega}{c}\right)}-E\,\omega^2$$

$$\%e^{\%i\left(t\,\omega+h2\,k_2\right)}-F\,\omega^2\,\%e^{-\%i\left(h2\,k_2-t\,\omega\right)}=0$$

(C.14)

In b.c. 2 we substitute the expressions given by eq. (12) and (13) and we evaluate it at x=0 and z=0, i.e. at the interface between the top surface of the second flexible layer and water, obtaining the equation as follows:

$$\frac{A_S e^{i\omega t}\left(g\omega\sin\left(\frac{d\omega}{c}\right)+c\omega^2\cos\left(\frac{d\omega}{c}\right)\right)}{\omega\left(g\omega^2\sin\left(\frac{d\omega}{c}\right)+c\omega^3\cos\left(\frac{d\omega}{c}\right)\right)}+E\omega e^{it\omega}+F\omega e^{it\omega}=0 \qquad\qquad\text{(C.15)}$$

In b.c 3, as before, we substitute expressions (12) and (13) and evaluate everything at x=0 and z=0:

$$\frac{\rho_s\omega^2\left(E\omega e^{it\omega}-F\omega e^{it\omega}\right)}{k_s}-\frac{A_s\rho_w e^{i\omega t}\left(cg\cos\left(\frac{d\omega}{c}\right)-c^2\omega\sin\left(\frac{d\omega}{c}\right)\right)}{g\omega^2\sin\left(\frac{d\omega}{c}\right)+c\omega^3\omega\cos\left(\frac{d\omega}{c}\right)}=0 \qquad\qquad\text{(C.16)}$$

Solving the system given by the three boundary conditions (14), (15), (16), with unknowns E, F and A_s (=a_g), we derive the values of E, F and A_s that substituted in eq. (12) and (13) give the expressions of u_2, motion in the second flexible layer, and Φ, velocity potential for motion of water that is the expression seen in chapter 3.

APPENDIX D – Elements Characteristics Used in ANSYS Implementation

The following table schematically presents the type of elements used in the implementation of the model in ANSYS for each part of the tunnel:

No.	Component of SFT	Elements in ANSYS	Description
1	Tunnel	BEAM4	3-D Elastic
2	Anchoring bar	BEAM188	3-D Inelastic
3	Soil-Structure Interaction	COMBIN14	Spring-damper
4	Dissipation Device	COMBIN39, COMBIN14	Non Linear Spring
5	Added Mass	MASS21	Fluid-Structure Interaction

Here you will find the detailed characteristics of each element. For more details, you can refer to ANSYS Library.

BEAM 4, a uniaxial elastic beam element having tension, compression, torsion and bending capabilities with 6 degrees of freedom at each node, is used to simulate the tunnel section.
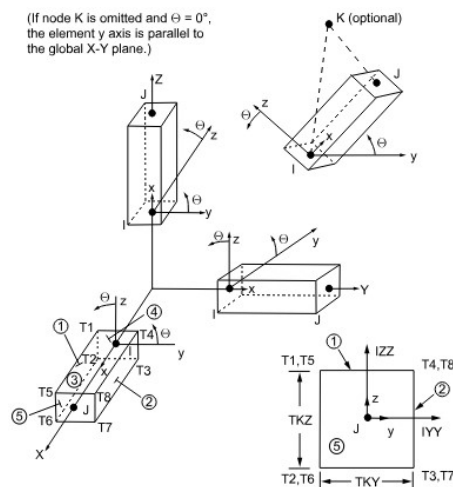

Figure 117 BEAM 4 ANSYS element

BEAM188, a 3-D beam element with 6 degrees of freedom at each node which is well-suited for linear, larger deflection and nonlinear applications, is applied to build the anchoring system. Due to the thin thickness of the bars compared with the diameters and the nonlinear analysis, a real section shape is asked to be imitated, which BEAM188 meets with this kind of requirement. The shape function along the length is cubic.
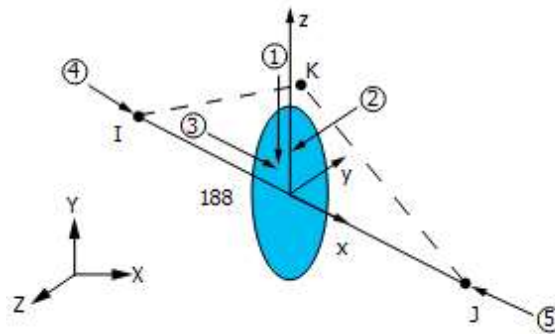

Figure 118 BEAM 188 ANSYS element

COMBIN14, a spring-damper element with longitudinal or torsional capability in 1-D, 2-D or 3-D applications, is adopted to model the soil structure interaction. The foundation weight is considered as a lumped mass at the connection between soil and structure in the form in ANSYS as the element MASS21, which is a point element having up to six degrees of freedom to consider the structural mass in the model.
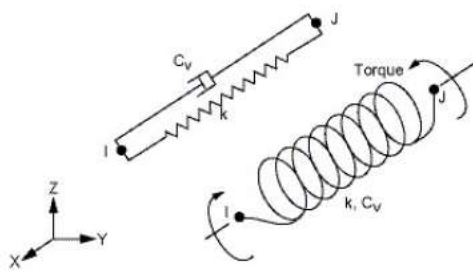
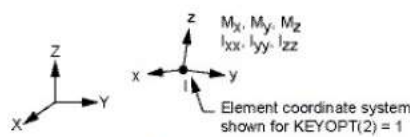2-D elements must lie in a z = constant plane

Figure A-1. COMBIN14 geometry

Figure A-2. MASS21 geometry

Figure 119 COMBIN14 ANSYS element

COMBIN39, a unidirectional element with nonlinear generalized force-deflection capability that can be used in any analysis, is utilized as the dissipation device in the form of nonlinear spring which is located at the ends of the tunnel to dissipate the energy due to the transient loading.
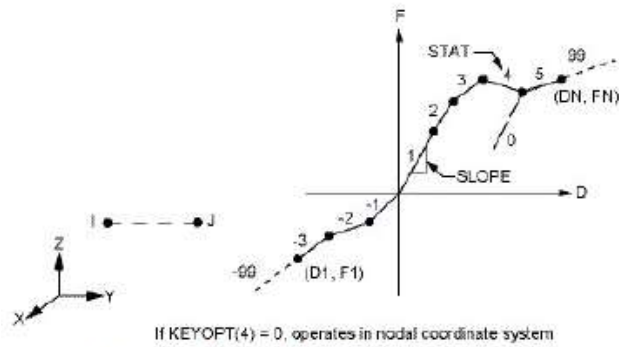

Figure A-3. COMBIN39 geometry

Figure 120 COMBIN39 ANSYS element

MASS21, is a point element having up to six degrees of freedom: translations in the nodal x, y, and z directions and rotations about the nodal x, y, and z axes. A different mass and rotary inertia may be assigned to each coordinate direction.
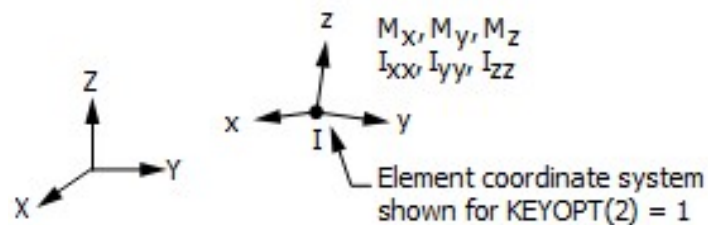

Figure 121 MASS21 ANSYS element